Physical Layer Security for Visible Light Communication Systems Subject to Eavesdropper Location Uncertainty



Sunghwan Cho

Wolfson College

Department of Engineering Science, University of Oxford

Supervised by Professor Justin P. Coon

A thesis submitted to the University of Oxford for the degree of Doctor of Philosophy in Engineering Science

Trinity 2020

Abstract

Thesis Title: Physical Layer Security for Visible Light Communication Systems Subject to Eavesdropper Location Uncertainty
Name: Sunghwan Cho
College: Wolfson College
Degree: Doctor of Philosophy
Term and Year of Submission: Trinity 2020

The past few decades have witnessed the acceleration in the development of groundbreaking information technology applications, such as smartphones/tablets, Internet of Things devices, virtual reality devices, etc. These new applications require a significant amount of data traffic to be conveyed wirelessly. Furthermore, the growing number of devices imposes a big challenge of providing seamless and low-delay communication. To satisfy these requirements, visible light communication (VLC) systems have gained considerable popularity thanks to its inherent advantages, such as unlicensed wide bandwidth, high area spectral efficiency, and high security. At the same time, in VLC systems, network security remains a significant challenge. Even with the inherent wireless communication security of VLC systems, there is still a possibility that an eavesdropper can wiretap important/private information in large open spaces. Therefore, this research investigates physical layer security (PLS) to secure the VLC indoor transmission in the presence of randomly located eavesdroppers, proposing three different beamforming and jamming strategies for different VLC system scenarios. PLS is a set of techniques that enable a transmitter and a legitimate receiver to securely transmit and receive important data, eliminating the possibility of eavesdropping by utilizing the randomness of a channel between transmitter and receiver. Dealing with the random locations of eavesdroppers by using tools from stochastic geometry, the proposed PLS schemes do not require precise locations or channel state information of eavesdroppers. Numerical and Monte Carlo simulation results are provided to verify the performances of the proposed schemes.

Acknowledgements

First and foremost, I would like to express sincerest thanks to my supervisor, Prof. Justin P. Coon, who always encouraged me with insightful advice and guidance. He has ever modeled for me the genuine attitude and practices of the ideal advisor. Without his support, it would not be possible to begin and finish this research.

Also, I especially thank Dr. Gaojie Chen, who helped me to obtain a broader understanding of this research. His detailed and constructive comments were vital to the development of this thesis. In addition, I appreciate all of my colleagues, Dr. Mihai-Alin Badiu, Mr. Dene A. Hedges, Ms. Arta Cika, Ms. Tanmayee Deshprabhu, Mr. Ferhat Yarkin, Ms. Zijing Wang, Mr. Tianxiong Wang, and Mr. Martin Wafula. They were always open for discussion and conversation, providing me an opportunity to broaden my horizon. Furthermore, I would like to say 'thank you' to the reviewers of my publications and the examiners of my works. They provided indispensable comments to improve the quality of my research.

I would also like to thank the Republic of Korea Army, who allowed and funded me to study in Oxford. Moreover, I would like to extend my appreciation to the faculty members, Dr. Yeongyoon Choi, Dr. Wonwoo Lee, and Dr. Yongchul Kim, at the Korea Military Academy for their continuing encouragement and support.

Most importantly, to my loved wife, sons, parents, and brother, I thank you all for your unconditional support and encouragement throughout my study. I love you so much.

List of Publications

Journal Publication

1. **S. Cho**, G. Chen, and J. P. Coon, "Zero-Forcing Beamforming for Active and Passive Eavesdropper Mitigation in Visible Light Communication Systems," in *IEEE Transactions on Information Forensics and Security*, vol. 16, pp. 1495-1505, 2021.

2. **S. Cho**, G. Chen, and J. P. Coon, "Enhancement of physical layer security with simultaneous beamforming and jamming for visible light communication systems," in *IEEE Transactions on Information Forensics and Security*, vol. 14, no. 10, pp. 2633-2648, Oct. 2019.

3. **S. Cho**, G. Chen, and J. P. Coon, "Physical layer security in visible light communication systems with randomly located colluding eavesdroppers," in *IEEE Wireless Communications Letters*, vol. 7, no. 5, pp. 7768-771, Oct. 2018.

4. **S. Cho**, G. Chen, and J. P. Coon, "Securing visible light communication systems by beamforming in the presence of randomly distributed eavesdroppers," in *IEEE Transactions on Wireless Communications*, vol. 17, no. 5, pp. 2918-2931, May 2018.

Conference Publication

1. **S. Cho**, G. Chen and J. P. Coon, "Enhancing Security in VLC Systems Through Beamforming," in *2020 IEEE Globecom in Taipei, Taiwan*, pp. 1–6, Dec. 2020.

2. **S. Cho**, G. Chen, and J. P. Coon, "Physical layer security in multiuser VLC systems with a randomly located eavesdropper," in *IEEE Globecom in Waikoloa, HI, USA*, pp. 1-6, Dec. 2019.

3. **S. Cho**, G. Chen, and J. P. Coon, "Securing visible light communications with spatial jamming," in *IEEE ICC in Shanghai, China*, pp. 1-6, May 2019.

4. **S. Cho**, G. Chen, H. Chun, J. P. Coon, and D. O'Brien, "Impact of multipath reflections on secrecy in VLC systems with randomly located eavesdroppers," in *IEEE WCNC in Barcelona, Spain*, pp. 1-6, Apr. 2018.

5. **S. Cho**, G. Chen, and J. P. Coon, "Secrecy analysis in visible light communication systems with randomly located eavesdroppers," in *IEEE ICC Workshops in Paris, France*, pp. 475-480, May 2017.

Acronyms

5G	5th generation
AED	Active eavesdropper
AWGN	Additive white Gaussian noise
BPP	Binomial point process
CCP	Concave-convex procedure
CDF	Cumulative distribution function
CSI	Channel state information
DC	Direct-current
ED	Eavesdropper
FoV	Field-of-view
JEITA	Japan Electronics and Information Technology Industries Association
LD	Laser diode
LED	Light-emitting diode
LoS	Line-of-sight
MIMO	Multiple-input multiple-output
MISO	Multiple-input single-output
OFDM	Orthogonal frequency division multiplexing
PAM	Pulse-amplitude modulation
PD	Photodiode
PDF	Probability density function
PED	Passive eavesdropper
PGFL	Probability generating functional
PLS	Physical layer security
PPP	Poisson point process
RF	Radiofrequency
SINR	Signal-to-interference-plus-noise ratio
SISO	Single-input single-output
SNR	Signal-to-noise ratio
SOP	Secrecy outage probability
SQP	Sequential quadratic programming
TDMA	Time-division multiple access
TS	Tabu search
UE	User equipment or Legitimate user
VLC	Visible Light Communication
ZF	Zero-forcing

Contents

Abstract i

Acknowledgements ii

List of Publications iii

Acronyms v

List of Figures ix

List of Tables xiii

List of Mathematical Notations xiv

1 Introduction 1
- 1.1 Overview . . . 1
  - 1.1.1 Visible Light Communication: A Future Wireless Network . . . 1
  - 1.1.2 Secure Communications in VLC . . . 2
- 1.2 Motivation . . . 3
- 1.3 Thesis Organization and Contribution . . . 4

2 Background 8
- 2.1 Visible Light Communication . . . 8
  - 2.1.1 What Is VLC? . . . 8
  - 2.1.2 Recent Achievements . . . 10
  - 2.1.3 Modulation Scheme . . . 12
  - 2.1.4 Optical Channel Gain . . . 14
  - 2.1.5 Beamforming for the MISO VLC Channel . . . 15
  - 2.1.6 Channel Capacity Under Amplitude Constraints . . . 16
- 2.2 Physical Layer Security . . . 18
  - 2.2.1 The Wiretap Channel and the Secrecy Capacity . . . 18
  - 2.2.2 Wiretap Code . . . 20
- 2.3 PLS for VLC . . . 21
  - 2.3.1 Differences in the RF and VLC Security Environments . . . 21
  - 2.3.2 Existing PLS Schemes for VLC . . . 24
  - 2.3.3 The Secrecy Capacity Bounds for VLC . . . 25

2.4 Stochastic Geometry . . . 28
2.4.1 BPP . . . 28
2.4.2 PPP . . . 29
2.5 Summary . . . 30

3 Beamforming and LED Selection **31**
3.1 System Framework . . . 33
3.1.1 Data Transmission . . . 33
3.1.2 Performance Measures . . . 35
3.2 Beamforming . . . 37
3.2.1 Beamforming Based on SNR . . . 37
3.2.1.1 Minimizing Average Eavesdropper SNR . . . 37
3.2.1.2 Maximizing User SNR . . . 41
3.2.2 Beamforming Based on Rate . . . 42
3.2.2.1 Minimizing Eavesdropper Average Rate . . . 42
3.2.2.2 Maximizing User Rate . . . 43
3.2.3 Comparing MISO Beamforming to LED Selection . . . 44
3.3 LED Selection . . . 46
3.3.1 SNR and Transmission Rate Analysis . . . 47
3.3.2 Secrecy Outage Probability . . . 48
3.4 Numerical Results . . . 53
3.4.1 Signal-to-Noise Ratio . . . 55
3.4.2 Secrecy Outage Probability . . . 61
3.5 Summary . . . 63
3.A Appendices . . . 64
3.A.1 Proof of the Lemma 1 . . . 64
3.A.2 Proof of the Lemma 2 . . . 66

4 Simultaneous Beamforming and Jamming **68**
4.1 System Framework . . . 71
4.1.1 Data Transmission and Jamming . . . 71
4.1.2 Performance Measures . . . 73
4.2 The Joint Strategy of Beamforming and Jamming . . . 76
4.2.1 Optimization of the Joint Strategy Based on SINR . . . 76
4.2.2 Beamforming and Jamming Characteristics . . . 80
4.3 The Ternary Strategy Based on SINR . . . 81
4.4 Optimization Based on Secrecy Rate with the Continuum Model . . . 85
4.4.1 Received Optical Power Density Analysis . . . 86
4.4.2 SINR and Secrecy Rate Analysis . . . 88
4.4.3 Optimization Based on Average Secrecy Rate . . . 88
4.4.4 Link Between the Continuum and Discrete Cases . . . 89
4.5 Numerical Results . . . 92
4.5.1 Signal-to-Interference-plus-Noise Ratio . . . 93
4.5.2 Secrecy Rate with the Continuum Model . . . 97
4.6 Summary . . . 105

4.A Appendices . . . 106
4.A.1 Secrecy Rate with the Joint Technique of Beamforming and Jamming . . . 106
4.A.2 Secrecy Rate with the SISO channel . . . 107

5 Zero-Forcing Beamforming for Active and Passive Eavesdroppers Mitigation 109
5.1 System Framework . . . 112
5.1.1 Data Transmission . . . 112
5.1.2 Performance Measures . . . 114
5.2 Zero-Forcing Beamforming . . . 116
5.2.1 Maximizing the Legitimate User's SNR . . . 116
5.2.2 Minimizing the Average SNR of Passive Eavesdroppers . . . 120
5.3 Relaxed Zero-Forcing Beamforming . . . 121
5.3.1 Sampling the SNR Space . . . 123
5.3.2 Optimizing Over the Sampled Space . . . 125
5.4 Numerical Results . . . 128
5.5 Summary . . . 136

6 Conclusion 138
6.1 Thesis Summary . . . 138
6.2 Future Directions . . . 140
6.2.1 Enhanced Jamming . . . 140
6.2.2 Reduced Complexity . . . 142
6.3 Conclusions . . . 143

Bibliography 146

List of Figures

2.1 The electromagnetic spectrum. 9
2.2 Simplified block diagram of a PAM VLC system. 13
2.3 Current-power response of a typical LED. 14
2.4 Rectangular room configuration for VLC systems. 15
2.5 Simplified block diagram of a MISO beamforming of VLC. 16
2.6 Wyner's wiretap channel 18
2.7 Nested structure of a wiretap code. 20

3.1 Rectangular room configuration for VLC systems. W and L are the room's width and length, and H denotes the height from the ceiling to the work plane. Dots denote LED transmitters. 33
3.2 The average SNR of EDs for different UE locations plotted against beamforming weights. Two transmitters T_1 and T_2 are located at $(2.5, 0)$ and $(-2.5, 0)$, respectively. The room size is $L = 8$ m, $W = 8$ m, and $H = 3$ m. $\rho_U = 40$ dB is applied. 44
3.3 The room configuration for LED selection. 46
3.4 The average SNR of EDs as a function of the UE location. The full-color surfaces in (a) and (b) denote the results for the beamforming (identical). The monochromatic mesh surfaces denote LED selection and repetition coding, respectively. In (c), the ratio of the average SNRs of EDs are given in which the monochromatic mesh surface denotes the ratio of repetition coding and beamforming, and the full-color surface denotes the ratio of LED selection and beamforming, respectively. $\lambda_E = 0.05$ and $\rho_U = 20$ dB are used. Four LED transmitters are symmetrically located at $(\pm 1, \pm 1)$. 55
3.5 The average SNR of EDs as a function of the UE location. The full-color surfaces in (a) and (b) denote the results for the beamforming (identical). The monochromatic mesh surfaces denote LED selection and repetition coding, respectively. In (c), the ratio of the average SNRs of EDs are given in which the monochromatic mesh surface denotes the ratio of repetition coding and beamforming, and the full-color surface denotes the ratio of LED selection and beamforming, respectively. $\lambda_E = 0.05$ and $\rho_U = 20$ dB are used. Four LED transmitters are symmetrically located at $(\pm 3, \pm 3)$. 56

3.6 The SNR of the UE as a function of the UE locations. The monochromatic mesh surfaces in (a) and (b) denote the result for the beamforming (identical). The full-color surfaces denote LED selection and repetition coding, respectively. In (c), the ratio of the SNRs of UE are given in which the monochromatic mesh surface denotes the ratio of beamforming and repetition coding, and the full-color surface denotes the ratio of beamforming and LED selection, respectively. $\lambda_E = 0.05$ and $\overline{\rho}_{PE} = 30$ dB are used. Four LED transmitters are symmetrically located at $(\pm 1, \pm 1)$. 57
3.7 The average SNR of the UE as a function of the UE locations. The monochromatic mesh surfaces in (a) and (b) denote the result for the beamforming (identical). The full-color surfaces denote LED selection and repetition coding, respectively. In (c), the ratio of the SNRs of UE are given in which the monochromatic mesh surface denotes the ratio of beamforming and repetition coding, and the full-color surface denotes the ratio of beamforming and LED selection, respectively. $\lambda_E = 0.05$ and $\overline{\rho}_{PE} = 30$ dB are used. Four LED transmitters are symmetrically located at $(\pm 3, \pm 3)$. 58
3.8 The upper and lower bounds on the SOP with LED selection for different C_{th} according to different intensities of EDs λ_E, where $N = 4 \times 4$, $g = 1$ m, $\hat{a} = 1$ m, $\hat{k} = 1.25$, $L = 10$ m, $W = 12$ m, and $H = 3$ m. 61
3.9 A comparison of the upper bound on the SOP between LED selection and beamforming for different numbers of transmitters according to different intensities of EDs λ_E, where $C_{\text{th}} = 0.5$ bit/Hz/s, $g = 1$ m, $L = 10$ m, $W = 12$ m, and $H = 3$ m. 62
3.10 An example of $\hat{D}(d)$ for $\hat{a} = 4$ m, $\hat{k} = 1.5$. Note $\hat{a}\hat{k} = 6$ m and $\hat{a}\sqrt{\hat{k}^2 + 1} = 7.21$ m. $\hat{a}\hat{k} = 6$ m and $\hat{a}\sqrt{\hat{k}^2 + 1} = 7.21$ m 64

4.1 Rectangular room configuration for VLC systems. W and L are the room's width and length, and H denotes the height from the ceiling to the work plane. Dots denote LED transmitters. 71
4.2 The values of beamforming weights and jamming intensities according to the locations of different LED transmitters. They are obtained from the optimization problem (4.13). The UE is located at $(7, 7, 0)$. The 6×6 LED transmitters are located at (x_T, y_T, H) for $x_T, y_T \in \{\pm 2.5, \pm 7.5, \pm 12.5\}$. $L = 30$ m, $W = 30$ m, $H = 2.2$ m, $\phi_{1/2} = 60^\circ$ and $\overline{\rho}_{PE} = 0.15$ are used. 81
4.3 Examples of tier groups. The move of the TS changes the roles of transmitters in a tier group. 83
4.4 The beamforming and jamming vectors with the ternary scheme obtained from the assignment optimization problem (4.17). the UE is located at $(7, 7, 0)$. The 6×6 LED transmitters are located at (x_T, y_T, H) for $x_T, y_T \in \{\pm 2.5, \pm 7.5, \pm 12.5\}$. $L = 30$ m, $W = 30$ m, $H = 2.2$ m, $\phi_{1/2} = 60^\circ$ and $\overline{\rho}_{PE} = 0.15$ are used. 84

4.5 Geometry of the ternary scheme with the continuous LED model. The blue shaded circular plane centered at the UE denotes the LEDs that act as the information transmitters, while the yellow annulus denotes the jammers. 85
4.6 An example of the role selection of the discrete transmitters. For the continuum model, $\mathcal{R}_T = 3$ m, $\mathcal{R}_{J_1} = 8$ m and $\mathcal{R}_{J_2} = 9$ m are assumed. For the discrete model, the 20×20 discrete LED transmitters are assumed to be uniformly distributed on a square lattice in the 30×30 m^2 room. 91
4.7 The comparison of the SINRs of the UE between the joint strategy and the ternary strategy. $\overline{\rho}_{PE} = 0.3$ is used for the optimizations. 94
4.8 The comparison for the SINRs of PE between the joint strategy and the beamforming according to the different locations of PE. In both figures, U is equipped with $A_{\mathrm{PD},U} = 1$ cm^2, while PE has a larger PD $A_{\mathrm{PD},E} = 100$ cm^2 in (b). 95
4.9 The optimized average secrecy rates of the continuum model and its corresponding discrete model for the different number of transmitters $N = N_r \times N_r$. $\overline{R}^{\star}_{s,\mathrm{cont.}}$ and $\overline{R}^{\star}_{s,\mathrm{disc.}}$ correspond to (4.23) and (4.29), respectively. 97
4.10 The optimized average secrecy rate $\overline{R}^{\star}_{s}$ for the different sizes of PD. . 98
4.11 The comparison of secrecy rates under the different proposed schemes, the joint scheme, the ternary scheme, the continuum model, and the artificial noise transmission according to the location of PE. 101
4.12 The beamforming and jamming vectors with the artificial noise. the UE is located at $(0, 0, 0)$. The 15×15 LED transmitters are uniformly distributed on a square lattice in the 30×30 m^2 room. $H = 2.2$ m, $\phi_{1/2} = 60^\circ$ and $\rho = 0.5$ are used. 102
4.13 The secrecy outage probability under the different proposed schemes, such as the joint scheme, the ternary scheme, the continuum model, and the artificial noise transmission. the UE is located at $(0, 0)$ and 15×15 LEDs are uniformly distributed on a square lattice in 30×30 m^2 room. $A_{\mathrm{PD},E} = 10$ cm^2 is used. 104

5.1 The SNR according to the receiver locations when ZF precoding is utilized. The UE and the AED are located at (2, 2) and (1, 1), respectively. 110
5.2 Rectangular room configuration for VLC systems. 113
5.3 A flow chart of the point generation procedure using the Lloyd algorithm. 124
5.4 The points obtained using Lloyd's algorithm with $|\mathcal{X}| = 200$. $\gamma(\mathbf{x}, \mathbf{w})$ for Figure 5.1(a) is adopted. 125
5.5 The SNR according to the receiver locations. The 10×10 LEDs are uniformly distributed on a square lattice. The locations of the UE and the AED are $(2, 2)$ and $(1, 1)$, respectively. $\rho_U = 50$ dB, $\rho_{AE} = 10$ dB, $\overline{\rho}_{PE} = 35$ dB, and $|\mathcal{X}| = 100$ are used. 130

5.6 The SNR according to the receiver locations when a smaller number of LEDs, i.e., $N = 5 \times 5$, are present. The locations of the UE and the AED are $(2, 2)$ and $(3.5, 3.5)$, respectively. $\rho_U = 40$ dB, $\rho_{AE} = 10$ dB, $\overline{\rho}_{PE} = 35$ dB, and $|\mathcal{X}| = 100$ are used. 132
5.7 The SNR according to the receiver locations when two AEDs are present. The 10×10 LEDs are uniformly distributed on a square lattice. The locations of the UE and the two AEDs are $(0, 0)$, $(1, 1.5)$, and, $(-1.5, -0.5)$ respectively. $\rho_U = 50$ dB, $\rho_{AE} = 10$ dB, $\overline{\rho}_{PE} = 35$ dB, and $|\mathcal{X}| = 100$ are used. 133
5.8 The SOP plotted as a function of the number of AEDs N_A. The location of the UE is $(0, 0)$, while N_A AEDs are randomly located in a circle with radius 3 m centered at the UE. For ZF beamforming, $\overline{\rho}_{PE} = 25$ dB is used. For relaxed ZF beamforming, ρ_U is set to be similar to the maximum ρ_U obtained by ZF beamforming for each simulation trial, and $\rho_{AE} = 10$ dB, $\overline{\rho}_{PE} = 25$ dB, and $|\mathcal{X}| = 100$ are used. 134
5.9 The SOP plotted as a function of the radius of the circle in which two AEDs are randomly located. The location of the UE is $(0, 0)$, and the circle is centered at the UE. For ZF beamforming, $\overline{\rho}_{PE} = 25$ dB is used. For relaxed ZF beamforming, ρ_U is set to be similar to the maximum ρ_U obtained by ZF beamforming for each simulation trial, and $\rho_{AE} = 10$ dB, $\overline{\rho}_{PE} = 25$ dB, and $|\mathcal{X}| = 100$ are used. 136

6.1 An example of VLC systems with a jamming strategy, where the ED is equipped with a narrow FoV PD, oriented directly toward the information LED transmitter. 141

List of Tables

3.1 Simulation Parameters 54

4.1 Simulation Parameters 92

5.1 Simulation parameters. 128

List of Mathematical Notations

L	Length of a room
W	Width of a room
H	Height from the ceiling to the work plane
N	Number of transmitters
N_A	Number of active eavesdroppers
α	Modulation index
I_{DC}	Fixed bias current
η	Current-to-light conversion efficiency
$\phi_{1/2}$	Half illuminance angle
$A_{\text{PD},k}$	Physical area of photodiode
$\phi_{i,k}$	Angle of irradiance
$\psi_{i,k}$	Angle of incidence
κ_k	Refractive index of an optical concentrator
$\mathbf{\Psi}_k$	Received field of view of a photodiode
$R_{\text{rsp.},k}$	Photodetector's responsivity
T_k	Transimpedance amplifier gain
$\mathbb{R}$	Set of real numbers
$\mathbb{R}_+$	Set of non-negative real numbers
$\mathbb{1}$	All-ones column vector
$\mathbb{0}$	All-zeros column vector
$\mathbf{I}$	Identity matrix
$\mathbb{E}[\cdot]$	Expectation operator
$[\cdot]^T$	Transpose operator
$\mathbb{P}(\cdot)$	Probability operator
$\mathbb{h}(\cdot)$	Differential entropy operator
$\mathbb{I}(\cdot;\cdot)$	Mutual information operator
$\|\cdot\|_1$	1-norm operator
$\log(\cdot)$	Natural logarithm
$\lfloor\cdot\rceil$	Rounding operator
$\Gamma(x, y)$	Upper incomplete gamma function

Chapter 1

Introduction

1.1 Overview

1.1.1 Visible Light Communication: A Future Wireless Network

Recently commercialized fifth generation (5G) technology will support the emergence of new digital services and technology, such as virtual/augmented reality, autonomous driving, the Internet of Things, and wireless backhaul. Now that 5G has passed fully into development, it is natural to look toward the future at technologies that will improve data rates and lower latencies beyond even what is promised by 5G. To fulfill this goal, we might consider communication solutions at higher frequencies than those used by 5G, perhaps encompassing a combination of the 1-3 GHz band and the millimeter-wave (mmWave) band (30-300 GHz), but also straying into the terahertz band (0.06-10 THz) [1].

One focus area in 'beyond-5G' research is the utilization for communication of the visible light spectrum – a broad patch of mostly untouched, unlicensed bandwidth [2]. Visible Light Communication (VLC) is an enabling technology that uses visible light as its communication medium and exploits the light infrastructure currently in use

for illumination to provide high-speed indoor wireless communication. VLC has been extensively studied among researchers and engineers with a view to its implemention and commercialization in future wireless systems. The standardization of VLC has been carried out by the Visible Light Communication Consortium in Japan and by the Institute of Electrical and Electronics Engineers (IEEE) in the United States, which have published four VLC standards: Japan Electronics and Information Technology Industries Association (JEITA): JEITA CP-1221; JEITA CP-1222; JEITA CP1223; and IEEE 802.15.7 [3].

VLC has several notable advantages that can offer significantly higher capacity, due to broader modulation bandwidth; high area spectral efficiency; reduced cost of wireless communications, due to the unlicensed spectrum; and energy-saving, since the VLC transmitters can be simultaneously used for illumination and communications. Lastly, VLC can be useful for achieving secure data transmission thanks to an intrinsic property of visible light – it cannot penetrate opaque objects [4].

1.1.2 Secure Communications in VLC

Compared to radio frequency (RF) channels, VLC exploits line-of-sight (LoS) propagation and has relatively good signal confinement properties. However, the VLC channel is still of a broadcast nature. Therefore, securing VLC transmissions is an important issue, particularly if the technology is to be deployed in open places, such as public libraries, offices, and shopping malls.

Physical layer security (PLS) is one of many possible security approaches: this is a set of methods that utilize channel randomness to transmit a message with a well-designed coding technique; this allows appropriate redundancy so that only the user equipment (UE) can reliably decode the message. It also introduces enough randomness so that an eavesdropper (ED) experiences significant uncertainty when attempting to decode the message [5].

PLS is a promising secure method of communicating since security in this context is provable in the information-theoretic sense. For example, in a typical wiretap model, PLS theory intimates that secure communication is possible when the capacity of the intended communication channel is higher than that of the eavesdropping channel. Since Wyner's seminal work [6], numerous PLS enhancement techniques for RF systems have been studied, including beamforming, antenna selection, artificial interference, etc. [7–9].

Motivated by the advantages presented by PLS, a recent topic of interest in the research community has been the investigation of PLS applied to VLC systems using various transmission methods, e.g., zero-forcing (ZF) beamforming, robust beamforming, jamming, etc. [10–18]. Based on various secrecy performance measures, the proposed methods have been designed and optimized to secure the VLC systems at the physical layer.

1.2 Motivation

Fundamental investigations of PLS for VLC systems typically assume that a single or multiple EDs are present in the system, and that the locations and channel properties associated with these EDs are known [10–18]. However, in practice, since EDs may try to escape the vigilance of a UE or network manager, identifying the types, locations, and numbers of the EDs is impractical; thus, it may be the case that the locations and number of eavesdropping devices are not known.

On the other hand, for PLS studies in RF communication systems, the mathematical theory of stochastic geometry has been used as a powerful tool for dealing with spatial uncertainty [19, 20]. Since the analysis of secrecy capacity in spatial networks inherently depends upon these geometric properties, the impact of random ED locations on secrecy performance for RF communications has been investigated by the use

of stochastic geometric methods in recent years [8, 21–23]. More specifically, in [21], the locations of multiple legitimate pairs and EDs were represented as independent two-dimensional point processes, and the average secrecy throughput in such a wireless network was studied. Multiple-input multiple-output (MIMO) transmission with beamforming was considered later to enhance secrecy performance in [22, 23]. Transmit antenna selection and full-duplex schemes have also been used to enhance secrecy performance with randomly located EDs [8].

Inspired by the contributions mentioned above that exploit stochastic geometry in RF communications, this thesis investigates PLS techniques in VLC systems that do not require the precise locations or the CSI of unknown passive EDs, instead only requiring statistical information on the locations of the EDs. As in the RF studies, tools from stochastic geometry are utilized to deal with the randomness of ED locations. More specifically, the location distribution of EDs is modeled as a Poisson point process (PPP) or a binomial point process (BPP). In practice, statistical information on the locations of EDs can be effectively acquired by analyzing user behavior characteristics and the layout of the room in which VLC systems are deployed. Even when the locations of EDs are entirely random (and therefore unknown), the locations can be modeled as homogeneous or uniform distributions.

1.3 Thesis Organization and Contribution

In this thesis, we propose and investigate three PLS beamforming and jamming transmission techniques for different VLC system scenarios, varying the distributions and types of ED. To provide a logical roadmap for readers, we set out here the organization of the thesis and the technical contributions of each chapter. Note that most nomenclatures and mathematical notations are independently defined in each chapter for clarity. Meanwhile, most of the analytical results given throughout this

thesis are derived with the assistance of Mathematica or manually; in other cases, special notes and/or references are provided. Numerical and Monte Carlo simulation results are generated via MATLAB. All the work carried out in this thesis was done in collaboration with Prof. Justin P. Coon and Dr. Gaojie Chen.

Chapter 2 starts by providing background to the research, aiming at laying out preliminary knowledge and giving a full picture of this technology to readers. First, we provide the fundamental concepts and characteristics of VLC systems, and explain the intrinsic differences between the channel capacity in optical communications and RF systems. Then, we briefly discuss the PLS theories, such as the wiretap channel, the secrecy capacity, and the wiretap codes. The third part of this background is a literature review regarding PLS for VLC systems. Finally, essential tools from stochastic geometry are briefly explained.

Chapter 3 is the first of three research chapters. This work proposes a new multiple-input single-output (MISO) beamforming solution for the case when only information about the ED intensity measure, i.e., statistical information about the ED locations (not the precise locations), is available at the transmitters. Various tools from stochastic geometry are used to deal with the randomness of the ED locations. The related optimization problems for obtaining the optimal beamforming weights are formulated and solved in two ways: 1) by minimizing the *average* signal-to-noise ratio (SNR) of the EDs subject to a constraint on the minimum required SNR of the UE; and 2) by maximizing the SNR of the UE while constraining the *average* SNR of the EDs. Also, this work demonstrates that the proposed beamforming method is well approximated by a simple light-emitting diode (LED) selection scheme, in the case where only the nearest LED is chosen to transmit an information signal to the UE. Closed-form bounds on the secrecy outage probability (SOP) with LED selection are obtained, indicating that the SOP can be decreased by increasing the number of transmitters to reduce the coverage area, which is defined as the area where a

transmitter is responsible for supporting the UE. This research has been published in *IEEE Transactions on Wireless Communications* [24] and *The Proc. 2017 IEEE ICC Workshops* [25].

Chapter 4 proposes a joint strategy for beamforming and jamming. As in **Chapter 3**, this method can be implemented in the presence of a *randomly* located ED. Firstly, the optimization problem for the beamforming and jamming vectors that maximize the signal-to-interference-plus-noise ratio (SINR) of a UE while suppressing the SINR of an ED is formulated. Since the optimization problem is not convex, we utilize a heuristic method called the convex-concave procedure (CCP) [26] to find the local solution. However, due to its high computational complexity when a large number of transmitters is considered, we propose a simpler version of the joint scheme called the ternary scheme, which is inspired by the behavior that is observed when analyzing the joint beamforming and jamming scheme. An assignment optimization problem is formulated for the ternary scheme, and this is based on the SINR metric in a similar way to the joint scheme. Tabu search (TS) is invoked to obtain the solution to the assignment problem. Additionally, the problem of maximizing the average secrecy rate is investigated by utilizing a continuous LED model, which significantly relaxes the complication that rises from calculating the expectation concerning the location of the ED. The numerical results show that the proposed schemes are useful to combat the augmented ED. The research has been published in *IEEE Transactions on Information Forensics and Security* [27] and *The Proc. 2019 IEEE ICC* [28].

In **Chapter 5**, we propose a novel ZF beamforming scheme that can cope with active and passive EDs simultaneously. Most existing studies, even those on the beamforming methods proposed in **Chapter 3 and 4**, assume that either active *or* passive EDs are present, but not both simultaneously. Thus, we formulate an optimization problem to find a beamforming weight vector that lies in the null space of the active ED channel, while maximizing the SNR of the UE and constraining the average SNR

of the passive EDs. The proposed beamforming scheme directs the transmission along a particular eigenmode related to the null space of the active ED channel and the intensity of the passive ED point process. We adopt an inverse free preconditioned Krylov subspace projection method [29] to estimate the eigenmode iteratively. On the other hand, for unfavorable VLC secrecy environments, the proposed ZF beamformer appears to be incapable of effectively coping with the passive EDs due to the strict condition that the SNRs of the active EDs must be zero. Hence, an alternative beamforming scheme is proposed by relaxing the constraint on the SNRs of the active EDs. The related optimization problem is formulated to reduce the secrecy outages caused by passive EDs, while simultaneously satisfying the target constraints on the SNRs of the UE and the active EDs. In order to simplify the mathematical complexity of the approach, Lloyd's algorithm is employed to sample the SNR field; this in turn discretizes the problem, thus making it tractable for practical implementation. The research has been published in *IEEE Transactions on Information Forensics and Security* [30] and *The Proc. 2020 IEEE Globecom* [31].

Finally, in **Chapter 6**, the thesis is concluded, and several potential directions for future work are provided.

Chapter 2

Background

2.1 Visible Light Communication

2.1.1 What Is VLC?

VLC indicates a type of communication in which data signals are communicated through the modulation of the light waves in the visible spectrum, ranging from 380 nm to 750 nm wavelengths, as shown in Figure 2.1. Compared to RF communications, such as Wi-Fi, mobile networks, millimeter-wave (mmWave) communications, etc., which utilize the spectrum ranging from 3 KHz to 300 GHz, VLC utilizes the visible light spectrum from 430 THz to 790 THz, which is 10,000 times larger than the entire RF spectrum. Here, 'visible' implies that human eyes can recognize the light; however, transmitting data is conducted imperceptibly by maintaining the average optical power constant and by varying the instantaneous signal strength at high rates [4, 32].

The development of VLC has been closely linked to the rapid and increasing adoption of LEDs around the world. Initially, LEDs were adopted in electronic devices, such as television screens, computer monitors, mobile phone displays, digital billboards, etc. However, their clear advantages over competing lighting technologies

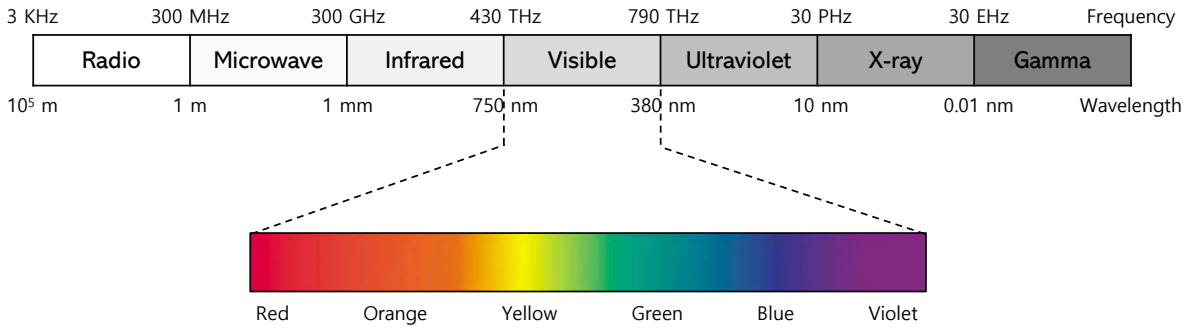


Figure 2.1. The electromagnetic spectrum.

in energy efficiency, longevity, and color rendering capability have encouraged many lightbulb companies to develop and adopt LEDs as new illumination sources [33]. Moreover, compared to traditional light bulbs, mostly incandescent or fluorescent, which did not allow precise and high-speed control of illumination, the output optical power emitted from the LEDs can be accurately driven by the input current signal (which contains information) at a high rate. Thus, the popularization of LED bulbs in the last decade offers a new opportunity to research VLC systems.

Thanks to the intrinsic characteristics of vlight, VLC has many advantages over RF systems [34, 35], such as the following:

- The spectrum of visible light is license-free and 10,000 times greater than radio waves.

- VLC is intrinsically safe and does not interfere with RF systems. This system is suitable for hospital, industrial and aerospace applications that are sensitive to electromagnetic energy.

- Visible light can be controlled sufficiently well for it to be emitted in the intended direction and confined by opaque boundaries. This allows for the coexistence of many non-interfering links and the spatial re-use of modulation bandwidth in VLC systems.

- Since visible light cannot penetrate a wall, VLC systems can offer a high level

of secrecy at the physical layer.

- VLC systems are easy to integrate into existing lighting infrastructure with simple and cheap front-end devices: LEDs and photodiodes (PDs).

- LEDs use approximately one-twentieth the amount of energy that a conventional light source consumes. Moreover, VLC makes additional use of illumination energy for communication purposes at little expense. Therefore, VLC could represent an eco-friendly communications technology.

2.1.2 Recent Achievements

Over recent decades, there has been increased interest in VLC systems in universities and industry, creating a need to standardize various aspects of them. In 2011, the IEEE 802.15.7 VLC Task Group published the first draft of the IEEE 802.15.7 standard, which covers numerous aspects essential to ensure the delivery of data at rates sufficient to provide multimedia services, as well as to satisfy the illumination compatibility with the visible light infrastructure. Specifically, the standard addresses network topologies, transmitter and receiver devices, communication architecture, physical layer characteristics, medium access control with dimming and flickering support, and security specifications [36].

The development of VLC has progressed alongside advancements in LED technologies. There are various categories of LEDs, such as Phosphor Converted LED, Multi-Chip LEDs, Organic LED, Micro LEDs, Resonant Cavity LEDs, etc. These types have distinct features, allowing them to be specifically chosen for applications with differing requirements. To be used in VLC systems as illuminators and transmitters simultaneously, the LEDs should satisfy the various demands of the color rendering index, lifetime, frequency response, etc. For example, since Phosphor Converted LEDs have advantages in terms of low cost and low complexity, they have been

widely adopted as light bulbs for the last decade; however, they offer only a narrow modulation bandwidth, 3–5 MHz [37], which limits the maximum achievable data rate. In contrast, μ-LEDs are known as the best-performing LED technology; they yield more than 10 Gb/s data rates in the laboratory [38], thanks to their broader modulation bandwidth ($\leq$ 300 MHz). However, their high cost and high complexity impose difficulties in adopting them as light bulbs in VLC systems.

On the one hand, various efforts to overcome the challenges restricting the advantages of the visible light spectrum have been conducted. First, the slow response of phosphor, which is needed for the emission of white, and intersymbol interference, due to multipath propagation, limit the modulation bandwidth to a few megahertz, which is much less than the VLC channel bandwidth [39]. To resolve this problem, placing a blue optical filter on a receiver and adopting a receiver equalizer is a possible way of making the frequency response flatter and allowing a broader modulation bandwidth [40, 41]. In addition, orthogonal frequency division multiplexing (OFDM) for VLC systems has been proposed as a solution to combat intersymbol interference and achieve a high spectral efficiency [42, 43]. However, the performance of traditional OFDM used for RF in VLC is limited due to the positive and real signal characteristic of VLC systems, which is imposed by the intensity modulation and by the illumination and dimming requirements [44]. Besides, the non-linearity of the relationship between the current and the emitted light of the LED imposes a significant challenge to improving the performance of OFDM in VLC systems [45]. Despite these challenges, however, OFDM for VLC holds extraordinary potential with achievable link rates on the scale of multiple Gbps [37, 42]. With the continuous developments and improvements in VLC technologies, such as advanced modulation techniques and new LED bulb technologies, VLC is expected to reach a data rate of hundreds of Gb/s, or even Tb/s, in the post-5G era.

In addition to the studies improving communication rates in VLC, there are dis-

cussions about its practical implementation in future wireless technologies. For example, an uplink transmission with visible light might be undesirable, since the light radiating from the user devices would cause a visual disturbance for users. Thus, hybrid systems of Wi-Fi (uplink) and VLC (downlink) have been developed and have received significant attention from the academic community [46–48]. Moreover, power line communication (PLC) was also considered to connect LED transmitters to the Internet without installing additional cables, since power lines are already ubiquitous [49]. In addition, there are efforts being made to allow smartphones to receive visible light waves without any modification in hardware, which would encourage smartphone manufacturers to make their phones compatible with VLC [50]. Since smartphones are already equipped with a camera and external LEDs, these might be used as a receiver and a transmitter, respectively, without additional cost.

2.1.3 Modulation Scheme

In general VLC systems, an electric data signal is piggybacked on a light signal by modulating the output intensity of the LEDs since most light sources emit waves that undergo random phase changes millions of times per second. Such light signal is called incoherent. At the receiver site, the light signal is recovered to an electric signal by using simple PDs. Although the use of laser diodes as transmitters can result in a higher data rate [51], these diodes are not accessible for illumination purposes since they are more expensive and potentially can cause eye and skin injuries. Employing imaging receivers can improve data rates, but this comes with increased complexity and cost. Therefore, throughout the thesis, we consider the VLC transceiver components to consist of LEDs and PDs.

In order to take advantage of VLC systems of high energy efficiency and lower infrastructure cost, LEDs should be used for both illumination and data transmission. Such LEDs are incoherent light sources; thus, the data cannot be encoded in the phase

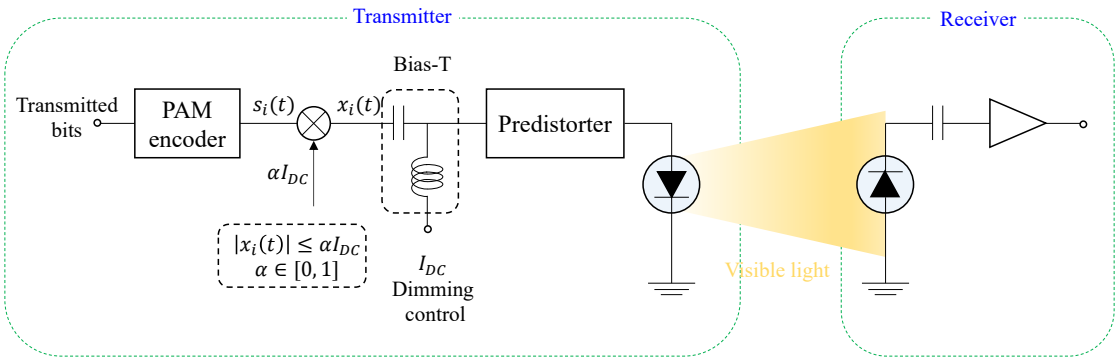


Figure 2.2. Simplified block diagram of a PAM VLC system.

or amplitude of the light signal [52]. Instead, the information has to be encoded in the varying intensity of the emitting light signal, and the receiver should decode the information by measuring the intensity of the received signal. Note that light signal's intensity can be interpreted as the average amplitude of incoherent waves' superposition. The set of these modulation techniques is called the intensity-modulated/direct detection modulation, which will be used throughout this thesis.

A direct-current (DC) biased pulse-amplitude modulation (PAM) VLC scheme [10, 11] is illustrated in Figure 2.2. The LED transmitter is driven by a fixed bias current $I_{DC} \in \mathbb{R}_+$ that sets the average radiated optical power $P_{opt} = \eta I_{DC}$, where η (W/A) is the current-to-light conversion efficiency. The PAM VLC system at the ith transmitter stochastically encodes transmitted bits into the data signal $s_i(t) \in \mathbb{R}$ such that $\mathbb{E}[s_i(t)] = 0$ and $|s_i(t)| \leq 1$. Then, the data signal $s_i(t)$ is superimposed on a fixed bias current $I_{DC} \in \mathbb{R}_+$, where the fixed bias I_{DC} is used for the purpose of illumination. Here, in order to maintain linear current-to-light conversion and avoid clipping distortion, the data signal $s_i(t)$ is modulated to $x_i(t) = \alpha I_{DC} s_i(t)$, where $\alpha \in [0, 1]$ is termed the modulation index. Note that the amplitude of $x_i(t)$ is constrained such that $|x_i(t)| \leq \alpha I_{DC}$. Thus, the dynamic range of the LED is $I_{DC} \pm \alpha I_{DC}$. Also, since $\mathbb{E}[x_i(t)] = 0$, the modulated signal does not affect illumination. The current-power response of a typical LED is depicted in Figure 2.3.

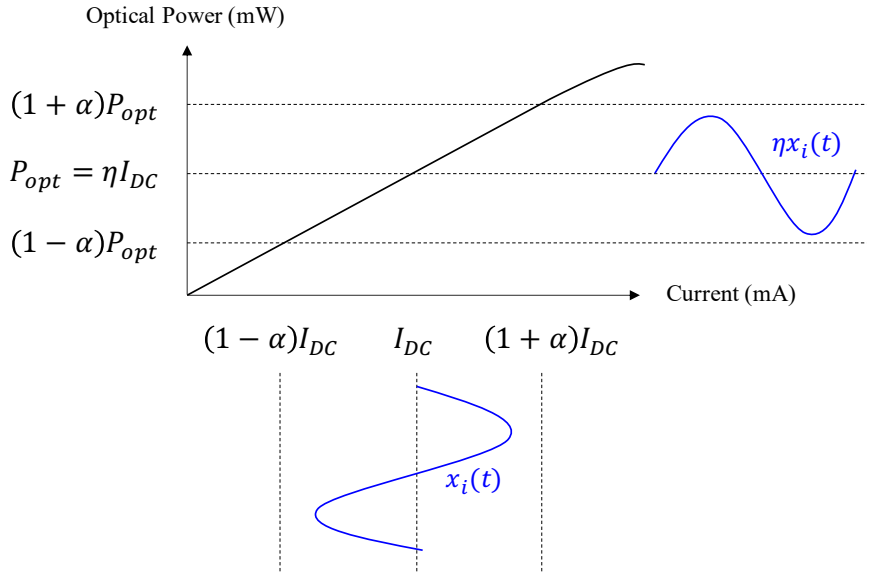


Figure 2.3. Current-power response of a typical LED.

2.1.4 Optical Channel Gain

The geometry of a typical indoor VLC system is illustrated in Figure. 2.4, where W, L, and H denote the width, the length, and the height of the ceiling relative to the work plane, respectively. This room may be an open space, such as a shopping mall or a large office. The receiver node is assumed to be located on the gray work plane. N transmitters (denoted by the blue dots) are attached to the ceiling of the room.

According to [53], the channel gain $h_{i,k} \in \mathbb{R}_+$ from the ith transmitter to receiver k corresponding to an LED with a generalized Lambertian emission pattern in a VLC system is given by

$$h_{i,k} = \eta G_{i,k} R_{\text{rsp.},k} T_k \tag{2.1}$$

where $R_{\text{rsp.},k}$ (mA/mW) is the photodetector's responsivity, and T_k (V/A) is the transimpedance amplifier gain. Further, according to [53], the LoS path gain $G_{i,k}$ is

$$G_{i,k} = \begin{cases} \dfrac{(m+1)A_{\text{PD},k}}{2\pi l_{i,k}^2} \dfrac{\kappa_k^2 \cos^m(\phi_{i,k})}{\sin^2(\Psi_c)} \cos(\psi_{i,k}) & \text{for} \quad |\psi_{i,k}| \le \Psi_c, \\ 0 & \text{for} \quad |\psi_{i,k}| > \Psi_c \end{cases} \tag{2.2}$$

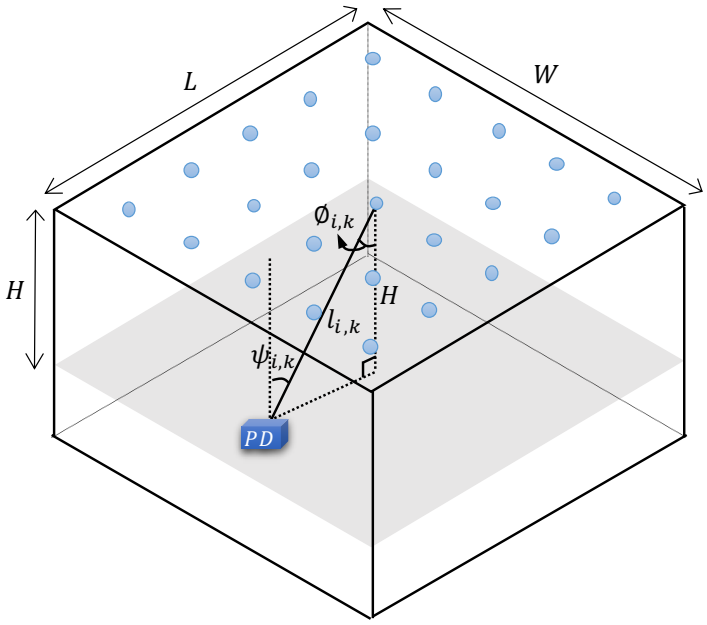


Figure 2.4. Rectangular room configuration for VLC systems.

where $m = -\ln(2)/\ln(\cos(\phi_{1/2}))$ is the order of Lambertian emission with half illuminance at $\phi_{1/2}$, and $A_{\text{PD},k}$ (m^2) is the physical area of the PD at the receiver. In addition, $l_{i,k}$ (m) denotes the distance between the ith transmitter and receiver k. $\phi_{i,k}$ is the angle of irradiance, and $\psi_{i,k}$ is the angle of incidence. Note that when the PD's orientation faces up normal to the work plane, we can have the relation $\phi_{i,k} = \psi_{i,k}$. κ_k is the refractive index of the optical concentrator, and Ψ_c denotes the received field-of-view (FoV) of the PD.

2.1.5 Beamforming for the MISO VLC Channel

Figure 2.5 illustrates a MISO VLC system utilizing transmit beamforming alongside PAM [10]. A MISO beamforming vector can be defined as $\mathbf{w} = [\omega_1, \omega_2, ..., \omega_N]^T$, where $\omega_i \in \mathbb{R}$ for $i \in \{1, 2, ..., N\}$ is a weight for the ith transmitter and $|\omega_i| \leq 1$. The ith LED transmitter multiplies the modulated data signal $x_i(t)$ by ω_i before transmitting. In the MISO VLC system considered here, the data signal $s_i(t)$ for the ith transmitter is assumed to be identically $s(t)$ for all transmitters. Therefore, the

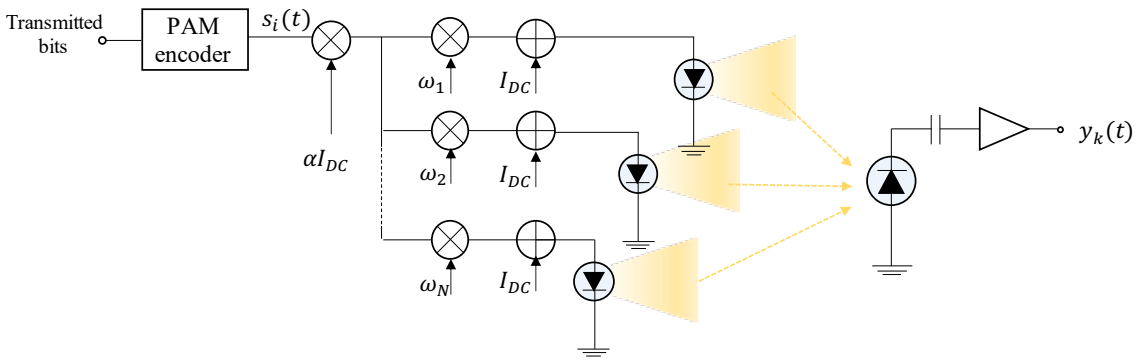


Figure 2.5. Simplified block diagram of a MISO beamforming of VLC.

signal at the receiver k in the MISO VLC system can be described as

$$y_k(t) = \alpha I_{DC} \mathbf{h}_k^T \mathbf{w} s(t) + n_k(t) \tag{2.3}$$

where $\mathbf{h}_k = [h_{1,k}, h_{2,k}, ..., h_{N,k}]^T \in \mathbb{R}^N$ denotes the channel gain vector. Further, n_k signifies a zero mean additive white Gaussian noise (AWGN) random variable with variance σ_k^2 at receiver k.

2.1.6 Channel Capacity Under Amplitude Constraints

VLC systems use the intensity-modulated/direct detection modulation scheme, in which the data is modulated onto the light waves of the LEDs. Typical LEDs have a limited linear operation region in which electro-optical conversion becomes linear, as shown in Figure 2.3. Thus, it is crucial to ensure that the modulating information signal is within the linear operation region to maintain linear current-to-light conversion and avoid clipping distortion. Although such a non-linearity can be partially compensated for via a predistortion of the input current signal, its benefit is limited in the region which the output intensity would entirely saturate [54].

In contrast to the massive body of literature on the Gaussian wiretap channel under the average power constraint in RF systems, obtaining analytic capacity ex-

pressions with amplitude constraints on the channel input is difficult since the amplitude constraint prohibits the usage of the Gaussian input distribution. Shannon has pointed out the challenge of obtaining an analytic expression for the capacity of the peak-limited Gaussian channel; instead, he derived a lower bound and an asymptotic upper bound that is valid at high peak SNR [55]. Later, in [56, 57], Smith reached the somewhat remarkable result that the capacity-achieving input distribution under the amplitude-constrained Gaussian channel is discrete with finite support, i.e., it has a finite number of mass points. In addition, Lapidoth *et al.* derived closed-form lower and upper bounds on the capacity of the amplitude-constrained Gaussian channel [58].

Although the closed-form expressions for the channel capacity bounds do not provide an exact specification of the limit of the wireless systems considered, they are often preferred for engineering systems. Therefore, in this thesis, we utilize the closed-form upper and lower bounds of the capacity under the amplitude constraint in the presence of independent and memoryless additive Gaussian noise in [58, Theorem 5], which are given as

$$C^{\text{upper}} = \frac{1}{2}\log\left(1+\gamma\right), \tag{2.4a}$$

$$C^{\text{lower}} = \frac{1}{2}\log\left(1+\frac{2\gamma}{\pi e}\right) \tag{2.4b}$$

respectively. Here, γ denotes the *peak* SNR at the receiver. Note that, in contrast, the channel capacity expression in RF systems is generally a function of average SNR [55], which is the ratio of the *average* signal power to the noise; the capacity bound expressions in (2.4) are functions of the peak SNR, which is the ratio of the *peak* signal power to the noise.

2.2 Physical Layer Security

2.2.1 The Wiretap Channel and the Secrecy Capacity

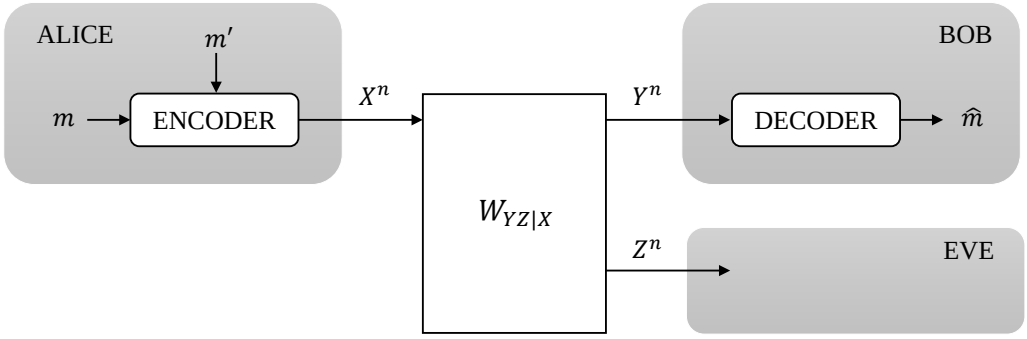


Figure 2.6. Wyner's wiretap channel

PLS is a set of techniques that enable a transmitter and a legitimate receiver to securely communicate by utilizing the randomness of the channel between them [5]. PLS is a promising secure method of communicating since security in this context is provable in the information-theoretic sense.

As illustrated in Figure. 2.6, the first basic model of PLS, called the *wiretap channel*, was proposed by Wyner [59]. The objective of the transmitter (Alice) is to securely communicate with the UE (Bob) in the presence of the ED (Eve). The communication messages are denoted by $m \in \{1, ..., 2^{nR}\}$ and encoded into codewords X^n of length n. The encoding of m is assisted by a random number $m' \in \{1, ..., 2^{nR'}\}$, which is randomly generated at Alice's location. Alice transmits the encoded codewords X^n over a noisy memoryless channel, characterized by a transition probability $W_{YZ|X}$. Bob receives Y^n and should be able to correctly estimate $\hat{m}$ of m with high probability. On the other hand, Eve receives Z^n. To securely and reliably communicate between Alice and Bob, the following conditions should be satisfied

$$\lim_{n\to\infty} \mathbb{P}(m \neq \hat{m}) = 0 \text{ (reliability)} \quad \text{and} \quad \lim_{n\to\infty} \mathbb{I}(m; Z^n) = 0 \text{ (secrecy)} \tag{2.5}$$

where $\mathbb{I}(\cdot;\cdot)$ denotes the mutual information.

In order to satisfy the requirements of both reliability and secrecy, Alice's transmission rate must be adjusted appropriate to the channel conditions of Bob and Eve. The *secrecy capacity* hints at how the transmission rate could be adjusted [60]. More specifically, the secrecy capacity is the supremum of all achievable secrecy rates satisfying (2.5), which can be expressed by

$$C_s = \max_{p_X}(\mathbb{I}(X;Y) - \mathbb{I}(X;Z))) \tag{2.6}$$

where p_X is the input distribution. From (2.6), we can observe that the secrecy capacity is positive when $\mathbb{I}(X;Y) - \mathbb{I}(X;Z)$ is positive. This means that if the capacity of the intended data transmission channel (between Alice and Bob) is higher than that of the eavesdropping channel (between Alice and Eve), the data can be securely and reliably transmitted at a rate close to the difference in their capacities – the so-called secrecy capacity – so that only the intended receiver can successfully decode the data.

On the other hand, when the CSI of an ED is not available at the transmitter, while only its statistical information is possible, a SOP is used as a primary security performance metric instead of the secrecy capacity [61]. The SOP metric is defined as the likelihood that the instantaneous secrecy capacity C_s is less than a threshold value C_{th}

$$P_{\text{SO}} = \mathbb{P}(C_s \leq C_{\text{th}}). \tag{2.7}$$

Note that since the instantaneous CSI of the ED is not available at the transmitter, the transmitter selects a constant secrecy rate; thus, perfect secrecy is not always guaranteed.

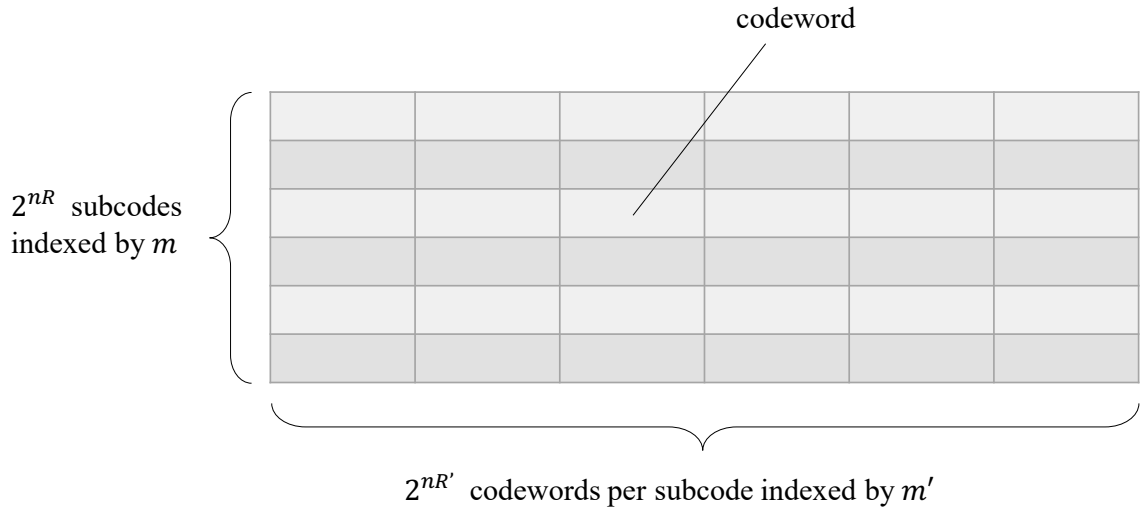


Figure 2.7. Nested structure of a wiretap code.

2.2.2 Wiretap Code

Many PLS transmission techniques have been proposed and investigated to increase the secrecy capacity of wireless systems, i.e., the gap between the capacities of the intended data transmission channel and the eavesdropping channel. Here, it would be worthwhile to mention that the positive secrecy capacity is a necessary but not sufficient condition to secure transmissions. In other words, it is essential to not only achieve a positive secrecy capacity with the PLS techniques but also to construct and employ an appropriate secrecy codebook to encode messages. The secrecy codebook, which is revealed to all receivers, should allow appropriate redundancy so that only Bob can reliably decode messages, while it should also introduce enough randomness for Eve to experience significant uncertainty when attempting to decode them [5].

To understand why standard codes cannot be used as wiretap codes and why randomization in the encoding is required, it is useful to consider a simple nested structure of wiretap codes, as depicted in Figure. 2.7, which stochastically encodes messages. For simplicity, we consider the noiseless main channel for Bob, while Eve observes the codewords through a channel that erases each codeword symbol with probability ϵ, and leaves the symbol unaffected with probability $1 - \epsilon$. According

to (2.6), the secrecy capacity of this channel is $C_s = \epsilon$. In the nested wiretap codebook, for a given message (row), there are $2^{nR'}$ different corresponding codewords (columns). Hence, when Alice transmits a message $m \in \{1, ..., 2^{nR}\}$, she generates a random number $m' \in \{1, ..., 2^{nR'}\}$ and transmits the m'th codeword in the mth row in the nested wiretap codebook. Since the noiseless main channel for Bob is assumed, Bob can estimate the transmitted message without error by decoding the received complete codeword. In contrast, since the codeword observed at Eve retains erased symbols, there are multiple potential estimates concerning the incomplete received codeword. Therefore, Eve cannot correctly estimate the transmitted message without error. In order to ensure both reliability and secrecy requirements in (2.5), the wiretap codebooks must have lengths of codewords appropriate to the channel capacities of Bob and Eve [5].

On the one hand, while PLS can provide perfect secrecy, it relies on a priori knowledge of the communication channel to decide the transmission rate and sacrifices the communication rate. In contrast, while the computation security of the upper layers does not provide information-theoretic secrecy, it does not rely on the communication channel. These two security techniques have their pros and cons. We can therefore conclude that PLS techniques would be complementary to computational security, rather than being used for the transmission of a large data stream by itself. For example, PLS could be a means of refreshing the secret keys used in the upper layers without requiring a key management infrastructure [5].

2.3 PLS for VLC

2.3.1 Differences in the RF and VLC Security Environments

PLS can be split into two main categories. The first is the transmission of a message with a well-designed coding technique allowing appropriate redundancy so that only

the UE can reliably decode the message, while introducing enough randomness so that an ED experiences significant uncertainty when attempting the same. The second is the generation and distribution of a secret key between a transmitter and an intended user by utilizing the distinct physical characteristics of their reciprocal channel [5].

The two assumptions that the latter PLS category requires – i.e., the reciprocity and the uncorrelatedness of the channel – are challenging to achieve in indoor VLC systems. First, reciprocity of the channel between a transmitter and a UE's receiver should be achieved so that they can extract a secret key from the shared CSI. However, unlike in RF systems where a single antenna can act as a transmitter and a receiver, in VLC systems, the transmitter and receiver are distinct components: they consist of an LED and a PD, respectively. Hence, reciprocity can hold only when the LED and PD are located at the same place or are in very close proximity, and when the characteristics of the LED and PD for the uplink and downlink are identical. In reality, these are impractical restrictions on indoor VLC systems. Furthermore, an uplink transmission with visible light might be undesirable, since the light radiating from the user devices would cause a visual disturbance to users; thus, RF or infrared communication is typically considered for uplink transmissions. For these reasons, sharing a secret key between a transmitter and a UE by using channel reciprocity is not a natural assumption in VLC systems.

Second, the fact that fading does not exist in VLC systems, since the PD's detector area is much larger than the wavelength of visible light, precludes the channel for the intended link from being uncorrelated with that of the ED. Therefore, instead of studying the latter category, comprised of secret key agreement techniques, the majority of existing PLS studies for VLC systems have focused on the former key-less techniques, which requires the condition that the UE should retain a superior channel relative to that of the ED to achieve a positive, secure transmission rate.

In VLC systems, it might even be difficult for a UE to achieve a higher SNR than

that experienced by an ED, which imposes challenges on developing PLS techniques for VLC. The SNR is typically determined based on the strength of a received desired signal and of the noise caused at a receiving device. Thus, in RF systems, in order to facilitate a higher SNR at a UE, a transmitter with multiple antennas can enhance the strength of the received signal only at a legitimate site by, for example, utilizing beam-steering transmission, antenna selection, or artificial jamming strategies [22, 62–65]. An ED in RF systems does not have many options to increase its SNR under these PLS transmission schemes, except to reduce the noise generated in its electronic circuitry and antenna(s), and there are to some extent technical limitations to doing this. Although an RF ED with multiple antennas is capable of increasing its SNR and somewhat reducing the secrecy rate, it has been shown that it is very challenging to achieve a SNR higher than that of a UE when suitable multi-antenna techniques are employed [66].

On the other hand, in VLC systems, considering the channel model of visible light in [53], the ED can significantly augment its receiver capability by implementing possible device modifications, such as increasing the area of the PD, adopting a high gain optical lens, and accurately adjusting the receiver's orientation toward the LED transmitter. The UE also can increase its receiver sensitivity using these methods. However, the UE must consider the different constraints on hardware requirements, user convenience, communication efficiency, etc., of various applications, which limit the gain of the UE. On the other hand, EDs can ignore these issues, since their primary goal is eavesdropping. Moreover, the LED transmitters should be spatially distributed over the ceiling to illuminate the entire room evenly. This system design requirement enables the ED to selectively receive a light signal emitted from a particular LED by modifying its receiver's FoV and adjusting its orientation, avoiding beamforming and jamming interference. Thus, in PLS-enabled VLC systems, an ED with an additional improvement and/or modification on its receiver architecture may be able to achieve

a higher SNR than the UE.

Overall, the differences in the security environments between RF and VLC systems impose an additional challenge to secure the VLC transmission. In order for the intended user to trust that the communication is secure, it is necessary to understand clearly the intrinsic characteristic of VLC systems.

2.3.2 Existing PLS Schemes for VLC

Motivated by the advantage of PLS for RF systems, a recent topic of interest in the research community has been the investigation of PLS applied to VLC systems using various transmission methods. An extensive study of this was first made by Mostafa *et al.* [10–14]. In [10], they analyzed the achievable secrecy rates for the cases of both single-input single-output (SISO) and MISO, and proposed an LED beamforming. Also, they developed null-steering, artificial noise, and friendly jamming strategies when an ED's CSI is initially present and then absent at the transmitter [11, 12]. Moreover, in [13], they utilized the excessive spatial degrees of freedom offered by a large number of LEDs to direct the main lobe, allowing the LEDs to transmit important data only to the intended user, located in a non-secure zone. In [14], the beamforming weight vector maximizing the achievable secrecy rate was designed and solved by converting a non-convex optimization problem into a solvable quasi-convex search problem.

Another extensive series of studies has been conducted by Alouini *et al.* [15,16,67]. In [15, 16], they investigated the secrecy rates with various input distributions under the amplitude constraint on the input signal. In particular, in [15], the secrecy rate with the cooperative jamming scheme was analyzed when the truncated Gaussian input distribution was utilized. In [16], the authors investigated the secrecy rate for various input signaling distributions, including the truncated generalized normal and uniform distributions, via transmit beamforming and artificial noise schemes.

Furthermore, recently, the PLS performance based on spatial modulation for VLC systems was investigated in terms of secrecy rate, and improved transmitter selection schemes – called an adaptive channel selection and a greedy selection – were proposed [67].

In addition, Arfaoui *et al.* proposed various precoding schemes for maximizing the max-min fairness, the harmonic mean, the proportional fairness, and the weighted fairness, respectively [68]. Notably, an achievable secrecy rate was provided for the system as a function of the precoding matrix. Also, Pham *et al.* studied the PLS for multiuser MISO VLC systems utilizing ZF and artificial noise-aided precoding, respectively [17, 18]. More specifically, [17] employed a ZF precoder to maximize the secrecy sum-rate. When the CSI of the ED is not available, the proposed scheme increases the achievable sum-rate without taking the ED's reception into account. In [18], an optimal artificial noise-aided precoding scheme to improve the SINR of the UE and EDs was designed, ensuring the fairness of the UE's SINRs while impairing the quality of ED's channel as much as possible.

2.3.3 The Secrecy Capacity Bounds for VLC

The secrecy capacity of the VLC channel is given in [5] by

$$C_s = \max_{p_X} \left(\mathbb{I}(X; Y_U) - \mathbb{I}(X; Y_E) \right), \tag{2.8a}$$

$$\text{s.t.} \quad |X| \leq 1 \tag{2.8b}$$

where X denotes the transmitted optical signal and p_X is the input distribution of X. Also, Y_k for $k \in \{U, E\}$ denotes the signal observed by the UE and the ED, respectively. The relationship between X and Y_k can be written as $Y_k = H_k X + N_k$, where H_k is the channel gain between the transmitter and R_k. N_k is noise at R_k. Note that (2.8) is identical to the secrecy capacity expression in (2.6), except for the amplitude

constrain $|X| \leq 1$. As discussed in **Section 2.1.6**, the amplitude constraint on the channel input makes deducing a closed-form solution for (2.8) infeasible. Instead, it was shown in [69,70] that the optimal probability distribution p_X of the optimization problem (2.8) is unique and discrete with a finite support set, and that thus it can be efficiently solved using numerical methods. Nevertheless, closed-form expressions are often of great interest for system design purposes. Thus, in the following discussion, we explain some closed-form expressions on the upper and lower bounds of the secrecy capacity investigated in the recent literature.

In [10], Mostafa *et al.* derived the closed-form expressions of the secrecy capacity bounds subject to amplitude constraints for the cases of both SISO and MISO. First, the secrecy capacity for the SISO case is lower-bounded and upper-bounded by

$$C_s^{\text{SISO}} \geq \max\left\{\frac{1}{2}\log\left(\frac{6\gamma_U + 3\pi e}{\pi e \gamma_E + 3\pi e}\right), 0\right\}, \tag{2.9a}$$

$$C_s^{\text{SISO}} \leq \max\left\{\frac{1}{2}\log\left(\frac{\gamma_U + 1}{\gamma_E + 1}\right), 0\right\} \tag{2.9b}$$

respectively, where γ_U and γ_E denotes the received peak SNRs at the UE and ED, respectively. e in (2.9a) is the base of the natural logarithm. Note that the lower bound in (2.9a) was obtained by exploiting the lower and upper bounds on the channel capacity under the amplitude constraint in (2.4) and by assuming a uniform distribution on p_X over the interval $[-1, 1]$. Also, the upper bound (2.9b) was obtained by relaxing the amplitude constraint $|X| \leq 1$ into the average power constraint $\mathbb{E}\left[X^2\right] \leq 1$. See the detailed proof in Appendices A and B in [10]. In addition, for the MISO case (utilizing the MISO beamforming technique described in **Section 2.1.5**), the lower bound of the achievable secrecy rate is expressed as

$$R_s^{\text{MISO}} \geq \max\left\{\frac{1}{2}\log\left(\frac{6\alpha^2 I_{DC}^2 \mathbf{w}^T \mathbf{h}_U \mathbf{h}_U^T \mathbf{w} + 3\pi e\sigma^2}{\pi e \alpha^2 I_{DC}^2 \mathbf{w}^T \mathbf{h}_E \mathbf{h}_E^T \mathbf{w} + 3\pi e\sigma^2}\right), 0\right\}. \tag{2.10}$$

In addition, in [15], Zaid *et al.* provided an achievable secrecy rate under the artificial noise scheme using truncated Gaussian input distributions, instead of the uniform ones of [10]. The probability density function (PDF) of a truncated Gaussian distribution defined over $[-A, A]$, denoted by $\mathcal{N}_A(0, \sigma_1^2)$, is given by

$$f(x) = \frac{\phi\left(\frac{x}{\sigma_1}\right)}{\Phi\left(\frac{A}{\sigma_1}\right) - \Phi\left(\frac{-A}{\sigma_1}\right)} \tag{2.11}$$

where $\phi(x) = (1/\sqrt{2\pi})e^{-x^2/2}$, $\Phi(\cdot)$ is the cumulative distribution function (CDF) of $\phi(\cdot)$, and $\sigma_1 \in \mathbb{R}_+$. In this work, the received signals for the UE and the ED are modeled as

$$y_U = h_{D,U}x + \mathbf{h}_{J,U}\mathbf{s} + n_U \overset{(a)}{=} h_{D,U}x + n_U, \tag{2.12a}$$

$$y_E = h_{D,E}x + \mathbf{h}_{J,E}\mathbf{s} + n_E \overset{(a)}{=} h_{D,E}x + \mathbf{h}_{J,E}\mathbf{w}j + n_E \tag{2.12b}$$

respectively, where $h_{D,k}$ for $k \in \{U, E\}$ is the channel gain from the information transmitter to the UE and the ED, respectively, and $\mathbf{h}_{J,k}$ for $k \in \{U, E\}$ are the channel gain vectors from the jammers to the UE and the ED, respectively. Also, x and $\mathbf{s} \in \mathbb{R}_+^{N_J}$ signify the data and jamming signals, respectively, where N_J denotes the number of jammers. In addition, for (a), a beamforming strategy for jammers is adopted such that it lies in the orthogonal subspace of $\mathbf{h}_{J,U}$ and $\mathbf{s} = \mathbf{w}j$, where $j \in \mathbb{R}_+$ is a zero mean random jamming symbol, and $\mathbf{w} \in \mathbb{R}^{N_J}$ is a beamforming vector ($|\mathbf{w}| \preceq \mathbb{1}$). With the channel models in (2.12), the authors obtained the lower bound of the secrecy rate as

$$R_s = \frac{1}{2}\log_2\left(1 + \frac{\sigma_1^2 h_{D,U}^2 e^{2\zeta}}{\sigma^2}\right) - \mathbb{h}(V_0) + \frac{1}{2}\log_2\left(2\pi e\sigma_1^2\right) + \log_2\left(|\mathbf{h}_{J,E}^T\mathbf{w}|\right) \tag{2.13}$$

where $V_0 = h_{D,E}X_t + \left(\mathbf{h}_{J,E}^T\mathbf{w}\right)J_t$, X_t and J_t follow the truncated Gaussian distribution

$\mathcal{N}_A(0, \sigma_1^2)$, $\zeta = \log(Z) + (\alpha\phi(\alpha) - \beta\phi(\beta))/2Z$, and $Z = \Phi(\beta) - \Phi(\alpha)$ with $\beta = A/\sigma_1$ and $\alpha = -A/\sigma_1$. In [15], it has been numerically shown that the secrecy rate expression (2.13) utilizing a truncated Gaussian distribution outperforms the one induced in [12] that adopted a uniform input distribution under the considered jamming strategy.

2.4 Stochastic Geometry

The mathematical theory of stochastic geometry is a powerful tool for dealing with spatial uncertainty [19, 20]. In communications engineering, stochastic geometry has been widely adopted to model, analyze, and design a wireless network with random topologies [71,72]. In RF systems, large-scale, ad hoc wireless networks, random channel access, carrier sensing multiple access, single- and multi-tier cellular networks, and networks with cognitive elements have been usefully studied with stochastic geometry [73].

Even in PLS studies using stochastic geometric methods, the impact of random ED locations on secrecy performance for RF communications has been investigated in recent years [8, 21–23]. The location distribution of EDs can be modeled as a PPP or a BPP. Furthermore, even in VLC systems, since the analysis of secrecy performance on the physical layer inherently depends upon these geometric properties, i.e., the locations of transmitter and receiver, stochastic geometry can be a useful tool to characterize the locations of randomly distributed EDs. Thus, in the following subsections, we introduce representative point processes: BPP and PPP.

2.4.1 BPP

The description relates specifically for a homogeneous BPP. A spatial BPP characterizes the distribution of the random points with two parameters: the number of points

and the bounded area. With these parameters, the probability that a certain number of points exist in the certain area can be modeled with a BPP [74]. More specifically, let us place a fixed number n of points at random locations inside a bounded region $A \subset \mathbb{R}^2$. Let $X_1, ..., X_n$ be independent and identically distributed random points which are randomly distributed in A. Thus, the PDF of each X_i is $f(x) = 1/|A|$, where $|A|$ denotes the area of A. Therefore, we can have for any bounded set $B \subset A$

$$\mathbb{P}(X_i \in B) = \int_B f(x)\,\mathrm{d}x = \frac{|B|}{|A|} \tag{2.14}$$

$$\mathbb{P}(\Phi(B) = k) = \binom{N}{k}\left(\frac{|B|}{|A|}\right)^k\left(1 - \frac{|B|}{|A|}\right)^{N-k} \tag{2.15}$$

where $\Phi(A)$ denotes the number of points in A.

2.4.2 PPP

A spatial PPP is the most widely used model for the spatial locations of wireless nodes. In a PPP, the location of each node is independent, and the point process is defined on the entire plane. In a two-dimensional continuous space $A \subset \mathbb{R}^2$, if the number of the points generated in the space is Poisson distributed, it has the probability

$$\mathbb{P}(\Phi(B) = k) = \frac{(\Lambda)^k}{k!}\exp(-\Lambda) \tag{2.16}$$

where $\Lambda = \int_B \lambda(\mathbf{x})\,\mathrm{d}\mathbf{x}$ and $\lambda(\mathbf{x})$ is the intensity function for any bounded set $B \subset A$. If $\lambda(\mathbf{x})$ is a non-negative constant, the PPP is homogeneous; otherwise, it is inhomogeneous.

In addition, the expectation of random sums over a PPP can be calculated by Campbell's Theorem [75] as:

$$\mathbb{E}\left[\sum_{\mathbf{x}\in\Phi} u(\mathbf{x})\right] = \int_B \lambda(\mathbf{x})u(\mathbf{x})\,\mathrm{d}\mathbf{x}. \tag{2.17}$$

where $u(\mathbf{x})$ denotes a real-valued function of the event location $\mathbf{x}$. Also, the expectation of random products over a PPP is defined by the probability generating functional lemma (PGFL) [75] as

$$\mathbb{E}\left[\prod_{\mathbf{x}\in\Phi} v(\mathbf{x})\right] = \exp\left\{-\int_B \lambda(\mathbf{x})\left[1 - v(\mathbf{x})\right] \mathrm{d}\mathbf{x}\right\}. \tag{2.18}$$

where $v(\mathbf{x})$ denotes a real-valued function of the event location $\mathbf{x}$ and $0 < v(\mathbf{x}) \leq 1$ for all $\mathbf{x} \in B$.

2.5 Summary

In this chapter, we provided background to the research. First, the preliminary knowledge for understanding the technical contents in this thesis and the fundamentals of VLC systems were explained. Following these fundamentals, we briefly discussed the PLS theories, which are based on Wyner's seminal work. Then, a brief review of PLS for VLC systems was provided, alongside some recent achievements in this research area. In addition, representative tools from stochastic geometry were briefly explained. Based on this overview and current research achievements related to the PLS for VLC systems, in the following chapters, we propose and develop three novel beamforming and jamming strategies, which are possible in the presence of randomly located EDs.

Chapter 3

Beamforming and LED Selection

Due to the rapid proliferation of mobile communication devices and the associated difficulties in adequately allocating spectra to support new services, VLC has become an increasingly attractive topic of research in academia and industry. The VLC medium does not interfere with RF systems, and the VLC spectrum can be easily reused (spatially) since light can be confined to a specific indoor area. Moreover, VLC uses an unregulated spectrum with a wide bandwidth (430 to 790 THz) and is capable of exploiting existing LED light infrastructure for communication [4, 76].

Compared to RF channels, VLC exploits LoS propagation and has relatively good signal confinement properties. However, the VLC channel is still of a broadcast nature. Therefore, securing VLC transmissions is an important issue, particularly for deployments in open places such as public libraries, offices, and shopping malls. To cope with the security issue in RF systems, the focus on PLS, which is based on the information-theoretic notion of employing coding to achieve secure communication, has accelerated since Wyner's seminal work [59]. Due to the broadcast nature of RF communications, both the UE and EDs may receive data from the source. However, the principle of PLS states that if the capacity of the intended data transmission channel is higher than that of the eavesdropping channel, the data can be transmitted

at a rate close to the difference in their capacities, the so-called *secrecy capacity*, so that only the intended receiver can successfully decode the data [5].

It is difficult to obtain knowledge of passive ED locations unlike active ED cases. Note that the difference between active and passive EDs in VLC systems lies with the availability of the CSI of the EDs at the transmitter sites. Nevertheless, the analysis of secrecy capacity in spatial networks inherently depends upon these geometric properties. The mathematical theory of stochastic geometry is a powerful tool for dealing with spatial uncertainty [19, 20]. By using stochastic geometric methods, the impact of random ED locations on secrecy performance for RF communications has been investigated in recent years [8, 21–23]. The location distribution of EDs can be modeled as a PPP or a BPP.

Inspired by the contributions mentioned above exploiting stochastic geometry in RF communications, in this chapter, we model ED locations in VLC systems as a point process and propose new MISO beamforming solutions. The contributions of this chapter can be summarized comprehensively as follows:

- we propose a MISO beamforming solution that optimizes secrecy performance measures (e.g., the SNR and secrecy rate bounds) subject to a signal amplitude constraint for VLC systems when only information about the ED intensity measure is available at the transmitter;

- we demonstrate that the proposed beamforming method is well approximated by a simple LED selection scheme when the distance between the UE and one of the transmitting LEDs is small;

- we obtain closed-form bounds on the SOP when LED selection is adopted.

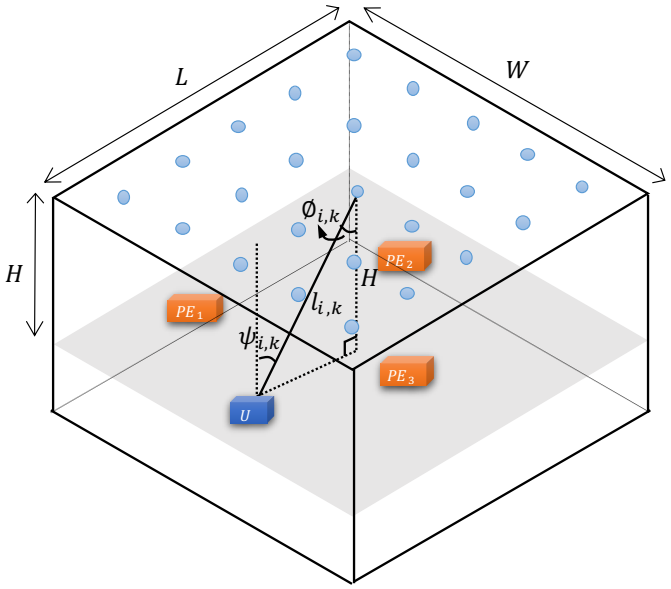


Figure 3.1. Rectangular room configuration for VLC systems. W and L are the room's width and length, and H denotes the height from the ceiling to the work plane. Dots denote LED transmitters.

3.1 System Framework

3.1.1 Data Transmission

We consider the downlink of a VLC system in a rectangular room, as shown in Figure 3.1, where W, L, and H denote the width, the length, and the height of the ceiling relative to the work plane, respectively. We assume that multiple UEs use optical time-division multiple access (TDMA) [4] as the channel access scheme; thus, only one fixed active UE can exist at a time. Also, multiple passive EDs are assumed to be randomly distributed according to a PPP Φ_E with intensity λ_E in the room. Note that there is no assumption that the PPP is homogeneous. The UE and passive EDs are denoted by U and PE_q for $q \in \Phi_E$, respectively.

We assume all the receiver nodes are located on the same work plane, and N transmitters are attached to the ceiling of the room. Each transmitter — i.e., an LED fixture consisting of multiple individual LEDs — is assumed to be capable of communicating independently of other transmitters [10]. We assume that EDs act

independently of one another (i.e., there is no collusion).

Therefore, assuming that the PAM described in Figure 2.2 is employed and the data signal $s_i(t)$ for the ith transmitter is identically $s(t)$ for all transmitters, the signal at the receiver $k \in \{U, PE_q\}$ in the MISO VLC system can be described as

$$y_k(t) = \mathbf{h}_k^T \mathbf{x}(t) + n_k(t) \tag{3.1}$$

where $\mathbf{h}_k \in [h_{1,k}, h_{2,k}, ..., h_{N,k}]^T$ is the channel gain vector, $\mathbf{x}(t) = [x_1(t), x_2(t), ..., x_N(t)]^T$ is the transmitted signal vector, and $n_k(t)$ is the zero-mean AWGN at the receiver k. Accordingly, the transmitted signal $\mathbf{x}_k(t)$ is subject to the amplitude constraint $|\mathbf{x}_k(t)| \preceq \alpha I_{DC} \mathbb{1}$, where $\preceq$ denotes the componentwise inequality. The channel gain $h_{i,k} \in \mathbb{R}_+$ in a VLC system corresponding to an LED with a generalized Lambertian emission pattern is given in (2.1). Note that this channel model considers only an LoS component and small scale fading does not exist in VLC systems since the detector area is much larger than the wavelength of visible light [77]. Furthermore, by assuming that a receiver's PD faces up normal to the work plane, i.e., $\phi_{i,k} = \psi_{i,k}$, we can rewrite (2.1) in terms of the distance between the ith transmitter and receiver k, i.e., $l_{i,k}$, as

$$h_{i,k} = \eta \frac{(m+1)A_{PD,k}}{2\pi l_{i,k}^2} \frac{\kappa_k^2}{\sin^2(\Psi_c)} \left(\frac{H}{l_{i,k}}\right)^m \left(\frac{H}{l_{i,k}}\right) R_{\text{rsp.},k} T_k = K l_{i,k}^{-(m+3)} \tag{3.2}$$

where $K = \left(\eta(m+1)A_{PD,k} H^{m+1} \kappa_k^2 R_{\text{rsp.},k} T_k\right) / \left(2\pi \sin^2(\Psi_c)\right)$.

As described in Figure. 2.5, a MISO beamforming vector can be defined as $\mathbf{w} = [w_1, w_2, ..., w_N]^T$, where w_i for $i \in \{1, 2, ..., N\}$ is a weight for the ith transmitter and $|w_i| \leq 1$. Thus, the transmitted signal vector $\mathbf{x}(t)$ can be written as $\mathbf{x}(t) = \mathbf{w}\alpha I_{DC} s(t)$. Therefore, the received signal at U and PE_q for $q \in \Phi_E$ with MISO beamforming can

be described as

$$y_U(t) = \alpha I_{DC} \mathbf{h}_U^T \mathbf{w} s(t) + n_U(t), \tag{3.3a}$$

$$y_{PE_q}(t) = \alpha I_{DC} \mathbf{h}_{PE_q}^T \mathbf{w} s(t) + n_{PE_q}(t) \tag{3.3b}$$

respectively, where $\mathbf{h}_U$ and $\mathbf{h}_{PE_q} \in \mathbb{R}^N$ are the channel gain vectors from the transmitters to U and PE_q, respectively, and n_U and n_{PE_q} are zero-mean AWGN random variables at U and PE_q, respectively, each with variance σ^2. For notational convenience, the time index t is ignored for the remainder of the chapter.

3.1.2 Performance Measures

For Gaussian VLC MISO channels with amplitude constraints, the peak SNR at the UE and the passive ED with beamforming can be written as

$$\gamma_U = \frac{\alpha^2 I_{DC}^2 \mathbf{w}^T \mathbf{h}_U \mathbf{h}_U^T \mathbf{w}}{\sigma^2}, \tag{3.4a}$$

$$\gamma_{PE_q} = \frac{\alpha^2 I_{DC}^2 \mathbf{w}^T \mathbf{h}_{PE_q} \mathbf{h}_{PE_q}^T \mathbf{w}}{\sigma^2} \tag{3.4b}$$

respectively. We use SNR to denote the peak, rather than average, SNR for the remainder of the chapter. Note that this SNR is given only under the assumption of the proposed beamforming scheme. This is because the beamforming is not proven to be optimal for the Gaussian VLC MISO wiretap channel subject to amplitude constraints, unlike the Gaussian RF MISO wiretap channel considered in [78]. However, beamforming in VLC systems may be preferred as it permits a simple implementation [11]. Of course, other VLC MISO transmission schemes may also be considered, and it is hoped that this work will stimulate further investigations on this topic.

The capacity of the VLC channel is given by [58]

$$C = \max_{p_X} \mathbb{I}(X;Y) \tag{3.5}$$

where p_X is the input distribution and $\mathbb{I}(\cdot;\cdot)$ denotes the mutual information. The relationship between X and Y can be written as $Y = HX + N$, where H is the channel gain between the transmitter and receiver. Note that the random variable X has an amplitude constraint, i.e., $|X| \leq \alpha I_{DC}$. It is infeasible to calculate the closed-form solution for (3.5) due to this amplitude constraint [69]. Thus, the upper and lower bounds on the transmission rate under the beamfoming scheme proposed in (3.3) are used for our analysis, which are given in (2.4). Note that these bounds on the rate are based on the SISO channel [58], but we translate these bounds into the MISO channel by setting the input of the SISO channel as $\alpha I_{DC} \mathbf{h}_k^T \mathbf{w} s(t)$ using the proposed beamforming scheme in a similar manner to [79].

We define the SOP as the probability that the secrecy capacity C_s is lower than a threshold secrecy rate C_{th}, i.e.,

$$P_{\text{SO}} = \mathbb{P}(C_s \leq C_{\text{th}}). \tag{3.6}$$

However, since the closed-form of the secrecy capacity with the input amplitude constraint is also not readily available, we employ the lower and upper bounds on the secrecy rate as defined in [10, Theorem 1], which are given by

$$C_s^{\text{lower}} = \max\left\{\frac{1}{2}\log\left(\frac{6\gamma_U + 3\pi e}{\pi e \gamma_{PE}^* + 3\pi e}\right), 0\right\}, \tag{3.7a}$$

$$C_s^{\text{upper}} = \max\left\{\frac{1}{2}\log\left(\frac{\gamma_U + 1}{\gamma_{PE}^* + 1}\right), 0\right\} \tag{3.7b}$$

where $\gamma_{PE}^* = \max_{q \in \Phi_{PE}} \gamma_{PE_q}$ (i.e., the *worst case* ED with the highest SNR) and e in (3.7a) is the base of the natural logarithm. Note that the upper bound also can be

possible only under the proposed beamforming scheme. Applying these bounds yields the following upper and lower bounds on the SOP:

$$P_{\mathrm{SO}}^{\mathrm{upper}} = \mathbb{P}(C_s^{\mathrm{lower}} \leq C_{\mathrm{th}}), \tag{3.8a}$$

$$P_{\mathrm{SO}}^{\mathrm{lower}} = \mathbb{P}(C_s^{\mathrm{upper}} \leq C_{\mathrm{th}}). \tag{3.8b}$$

3.2 Beamforming

In this section, we propose beamformer designs based on the formulation of several optimization problems that aim to improve secrecy performance when only information about the intensity of the ED PPP is known. Crucially, we demonstrate that the proposed beamforming solutions apply to both homogenous and inhomogeneous ED processes.

3.2.1 Beamforming Based on SNR

Without knowledge of ED locations, a natural objective is to minimize the *average* SNR of EDs $\overline{\gamma}_{PE}$ subject to a constraint on the minimum required UE SNR γ_U. The same approach is taken in RF communications [64, 80, 81]. A related, alternative objective may be to maximize γ_U subject to a constraint on $\overline{\gamma}_{PE}$. In this subsection, both of these cases will be investigated.

3.2.1.1 Minimizing Average Eavesdropper SNR

The SNR of the UE (3.4a) can be written as

$$\gamma_U = \varphi \mathbf{w}^T \mathbf{H}_U \mathbf{w} \tag{3.9}$$

where $\varphi = \alpha^2 I_{DC}^2/\sigma^2$ and $\mathbf{H}_U = \mathbf{h}_U \mathbf{h}_U^T$. Note that the rank of $\mathbf{H}_U$ is one. Also, from (3.4b), the average SNR of an ED can be written as

$$\overline{\gamma}_{PE} = \mathbb{E}[\varphi \mathbf{w}^T \mathbf{h}_{PE_q} \mathbf{h}_{PE_q}^T \mathbf{w}] = \varphi \mathbf{w}^T \mathbb{E}[\mathbf{h}_{PE_q} \mathbf{h}_{PE_q}^T] \mathbf{w} = \varphi \mathbf{w}^T \overline{\mathbf{H}}_{PE} \mathbf{w} \tag{3.10}$$

where $\overline{\mathbf{H}}_{PE} = \mathbb{E}[\mathbf{h}_{PE_q} \mathbf{h}_{PE_q}^T]$. The element in the ith row and jth column of $\overline{\mathbf{H}}_{PE}$ is given by

$$\overline{H}_{PE_{i,j}} = \frac{1}{N_E} \int_{\frac{-L}{2}}^{\frac{L}{2}} \int_{\frac{-W}{2}}^{\frac{W}{2}} \frac{\lambda_E(x,y) K^2}{l_i^{m+3}(x,y) l_j^{m+3}(x,y)} \, \mathrm{d}x \, \mathrm{d}y \tag{3.11}$$

where $\lambda_E(x,y)$ is the intensity of EDs at the point (x,y) in the work plane, and $l_i(x,y)$ for $i \in \{1, 2, \cdots, N\}$ is the distance between the ith transmitter and the point (x,y). Note that $\lambda_E(x,y)$ is a constant when the ED point process is homogeneous. Also, N_E denotes the average number of EDs, which is given by

$$N_E = \int_{\frac{-L}{2}}^{\frac{L}{2}} \int_{\frac{-W}{2}}^{\frac{W}{2}} \lambda_E(x,y) \, \mathrm{d}x \, \mathrm{d}y. \tag{3.12}$$

From the formulation given above, it is clear that the beamforming vector $\mathbf{w}^*$ is given by

$$\mathbf{w}^* = \arg\min_{\mathbf{w}} \ \varphi \mathbf{w}^T \overline{\mathbf{H}}_{PE} \mathbf{w} \tag{3.13a}$$

$$\text{s. t.} \begin{cases} \varphi \mathbf{w}^T \mathbf{H}_U \mathbf{w} \geq \rho_U \\ |\mathbf{w}| \preceq \mathbb{1} \end{cases} \tag{3.13b}$$

where ρ_U denotes the required SNR of the UE. Note that the beamformer $\mathbf{w}^*$ is $\mathbf{0} \in \mathbb{R}^N$ without the first constraint. Then, we form the Lagrangian [82] as follows

$$\mathcal{L} = \varphi \mathbf{w}^T \overline{\mathbf{H}}_{PE} \mathbf{w} - \lambda \left(\varphi \mathbf{w}^T \mathbf{H}_U \mathbf{w} - \rho_U \right) - \mu_-^{\mathbf{T}} (\mathbf{w} + \mathbb{1}) + \mu_+^{\mathbf{T}} (\mathbf{w} - \mathbb{1}) \tag{3.14}$$

where $\lambda \in \mathbb{R}$ and μ_-, $\mu_+ \in \mathbb{R}^N$ are the Lagrange multipliers. To let $\mathcal{L}$ have the non-

trivial minimum value with respect to $\mathbf{w}$ and analytically calculate the solution of (3.13), we must have

$$\mu_- = \mu_+ = \mathbf{0}. \tag{3.15}$$

According to the local sensitivity analysis in [82], zero Lagrange multipliers μ_- and μ_+ imply that the second inequality constraint is slack, i.e., $|w_i| < 1$ for $i \in \{1, 2, ..., N\}$. The condition (3.15) can be satisfied or not, depending on the given VLC environments, such as a particular distribution of LED transmitters, the location of the UE, the LED transmit power, the value of ρ_U, etc. For example, if ρ_U is set low and there is an LED transmitter close to the UE, transmitting the information signal only from the nearest transmitter can achieve ρ_U. In this case, the beamformers of other transmitters must not be ± 1. Moreover, without loss of generality, we can assume that the beamforming element of the nearest LED can be very close to ± 1, but not equal to ± 1.

Thus, with assuming that (3.15) is satisfied, computing the partial derivative of $\mathcal{L}$ with respect to $\mathbf{w}$ and setting the result equal to zero leads to

$$(\overline{\mathbf{H}}_{PE} - \lambda \mathbf{H}_U)\mathbf{w} = \mathbf{0}. \tag{3.16}$$

The beamforming vector must satisfy (3.16). If $\lambda = 0$ (i.e., the UE SNR constraint is inactive), $\mathbf{w}$ should belong to the null space of $\overline{\mathbf{H}}_{PE}$. Referring to (3.11), it should be clear that the rank of $\overline{\mathbf{H}}_{PE}$ depends on the intensity of the ED process. Indeed, it is possible that the intensity is such that $\overline{\mathbf{H}}_{PE}$ is reduced rank. In this case, letting $\mathbf{w}$ be in the null space of $\overline{\mathbf{H}}_{PE}$ yields $\overline{\mathbf{H}}_{PE}\mathbf{w} = \mathbf{0}$, thus all the vectors in the null space of $\overline{\mathbf{H}}_{PE}$ satisfying (3.13b) can be the solution of (3.13). On the other hand, if $\overline{\mathbf{H}}_{PE}$ is full rank[1], we have

$$\overline{\mathbf{H}}_{PE}^{-1}\mathbf{H}_U\mathbf{w} = \eta\mathbf{w} \tag{3.17}$$

[1]This condition can be confirmed when the ED PPP is homogeneous, for example.

Algorithm 1 CCP algorithms for solving (3.13)

given an initial feasible point $\mathbf{w}_0$
$k := 0$
repeat
1. *Convexify.* Form $g(\mathbf{w}; \mathbf{w}_k) \triangleq \varphi \mathbf{w}_k^T \mathbf{A} \mathbf{w}_k + 2\varphi(\mathbf{A}\mathbf{w}_k)^T(\mathbf{w} - \mathbf{w}_k)$
2. *Solve.* Set the value of $\mathbf{w_{k+1}}$ to a solution of the convex problem

$$\mathbf{w}^* = \arg\min_{\mathbf{w}} \varphi \mathbf{w}^T \overline{\mathbf{H}}_{PE} \mathbf{w}$$
$$\text{s. t.} \begin{cases} g(\mathbf{w}; \mathbf{w}_k) \geq \rho_U \\ |\mathbf{w}| \preceq \mathbb{1} \end{cases}$$

3. *Update iteration.* $k := k + 1$.

until stopping criterion (e.g., 10^{-4} used in Section 3.4) is satisfied.

where $\eta = 1/\lambda$. This implies that η is an eigenvalue of $\overline{\mathbf{H}}_{PE}^{-1}\mathbf{H}_U$ and $\mathbf{w}$ is the corresponding eigenvector. Hence, the solution satisfies

$$\overline{\gamma}_{PE} = \varphi \mathbf{w}^T \overline{\mathbf{H}}_{PE} \mathbf{w} = \varphi \frac{1}{\eta} \mathbf{w}^T \mathbf{H}_U \mathbf{w} \geq \frac{1}{\eta_{\max}} \rho_U. \tag{3.18}$$

From this, we deduce that the minimum $\overline{\gamma}_{PE}$ is inversely proportional to the maximum eigenvalue $\eta_{\max}$. Here, since $\mathbf{H}_U$ is rank one, we have that $\overline{\mathbf{H}}_{PE}^{-1}\mathbf{H}_U$ is rank one since

$$0 < \operatorname{rank}\left(\overline{\mathbf{H}}_{PE}^{-1}\mathbf{H}_U\right) \leq \min\left\{\operatorname{rank}\left(\overline{\mathbf{H}}_{PE}\right), \operatorname{rank}(\mathbf{H}_U)\right\} = 1. \tag{3.19}$$

Hence, there exists a single non-zero eigenvalue $\eta_{\max}$, and the beamformer $\mathbf{w}^*$ is obtained by scaling the corresponding eigenvector such that $\varphi \mathbf{w}^{*T} \mathbf{H}_U \mathbf{w}^* = \rho_U$ and $|\mathbf{w}^*| \prec \mathbb{1}$. When feasible, the fact that only one non-zero eigenvalue exists implies the solution is unique. Hence, it is clear that this approach gives a simple method of calculating the beamforming vector. Lastly, the assumption that (3.15) is satisfied must be verified to confirm the feasibility of $\mathbf{w}^*$. If any element of $\mathbf{w}^*$ is strictly in between -1 and 1, (3.15) is satisfied; thus, the acquired solution $\mathbf{w}^*$ is confirmed to be the optimal solution.

On the other hand, if ρ_U is high so that (3.15) cannot be satisfied, the solution $\mathbf{w}^*$

can be found numerically with the CCP algorithm [26], which is a powerful heuristic method to find local solutions. Given an initial feasible point $\mathbf{w}_0$, we transform the first constraint in (3.13b) into an affine function (i.e., convex) by applying the first-order Taylor approximation and solve the convex optimization problem. Then, we set the solution to $\mathbf{w}_1$ and repeat the same procedure until the improvement in the objective value is less than some threshold ϵ. The detailed iterative algorithm is given in Algorithm 1.

3.2.1.2 Maximizing User SNR

We now investigate the problem of maximizing the SNR of the UE γ_U while constraining the average SNR of the EDs $\overline{\gamma}_{PE}$. Similar to the previous subsection, we can formulate the optimization problem as

$$\mathbf{w}^* = \arg\max_{\mathbf{w}} \ \varphi \mathbf{w}^T \mathbf{H}_U \mathbf{w} \tag{3.20a}$$

$$\text{s. t.} \begin{cases} \varphi \mathbf{w}^T \overline{\mathbf{H}}_{PE} \mathbf{w} \leq \overline{\rho}_{PE} \\ |\mathbf{w}| \preceq \mathbb{1} \end{cases} \tag{3.20b}$$

where $\overline{\rho}_{PE}$ is the target constraint on the average SNR of EDs.

Following the same approach as above leads to an analogous result:

$$(\mathbf{H}_U - \lambda \overline{\mathbf{H}}_{PE})\mathbf{w} = \mathbf{0}. \tag{3.21}$$

When $\overline{\mathbf{H}}_{PE}$ is singular, unlike the previous approach, we cannot guarantee that the vectors in the null space of $\overline{\mathbf{H}}_{PE}$ satisfying the constraint (3.20b) maximize the objective function (3.20a). Thus, in this case, this problem should be solved by a numerical method as proposed in Algorithm 1. If $\overline{\mathbf{H}}_{PE}$ is nonsingular, we have

$$\overline{\mathbf{H}}_{PE}^{-1} \mathbf{H}_U \mathbf{w} = \lambda \mathbf{w}. \tag{3.22}$$

Hence, λ and $\mathbf{w}$ are an eigenvalue-eigenvector pair for $\overline{\mathbf{H}}_{PE}^{-1}\mathbf{H}_U$. The solution satisfies

$$\gamma_U = \varphi \mathbf{w}^T \mathbf{H}_U \mathbf{w} = \varphi \lambda \mathbf{w}^T \overline{\mathbf{H}}_{PE} \mathbf{w} \leq \lambda_{\max} \overline{\rho}_{PE} \tag{3.23}$$

where $\lambda_{\max}$ is the maximum (indeed, the only nonzero) eigenvalue, and the beamformer $\mathbf{w}^*$ is the associated eigenvector after being scaled such that $\varphi \mathbf{w}^{*T} \overline{\mathbf{H}}_{PE} \mathbf{w}^* = \overline{\rho}_{PE}$ and $|\mathbf{w}| \prec \mathbb{1}$ (if feasible).

3.2.2 Beamforming Based on Rate

In this subsection, we will investigate beamforming based on the achievable transmission rate of the UE and EDs under the proposed beamforming scheme.

3.2.2.1 Minimizing Eavesdropper Average Rate

Since the closed-form expression for the capacity of a VLC channel is not available, we will use the upper and lower bounds given in (2.4). Thus, the beamformer $\mathbf{w}^*$ minimizing the average ED rate upper bound under the proposed beamforming is given by

$$\mathbf{w}^* = \arg\min_{\mathbf{w}} \mathbb{E}\left[\frac{1}{2}\log\left(1+\gamma_{PE_q}\right)\right] \tag{3.24a}$$

$$\text{s.t.} \begin{cases} \dfrac{1}{2}\log\left(1+\dfrac{2\gamma_U}{\pi e}\right) \geq \xi_U \\ |\mathbf{w}| \preceq \mathbb{1} \end{cases} \tag{3.24b}$$

where ξ_U is the required rate lower bound for the UE. However, since the objective function (3.24a) does not lend itself to tractable analysis and a practically implementable solution, we revise the objective function using Jensen's inequality, i.e., it becomes $(1/2)\log(1+\overline{\gamma}_{PE})$, which allows us to obtain the alternative beamformer $\mathbf{w}^*$. In addition, since $\log(\cdot)$ is a monotonic increasing function, (3.24) can be reformulated

to

$$\mathbf{w}^* = \arg\min_{\mathbf{w}} \ \varphi \mathbf{w}^T \overline{\mathbf{H}}_{PE} \mathbf{w} \tag{3.25a}$$

$$\text{s. t.} \begin{cases} \varphi \mathbf{w}^T \mathbf{H}_U \mathbf{w} \geq M_1 \\ |\mathbf{w}| \preceq \mathbb{1} \end{cases} \tag{3.25b}$$

where $M_1 = \left(2^{2\xi_U} - 1\right) \pi e / 2$. Note that (3.25) has an identical form to (3.13). When $\overline{\mathbf{H}}_{PE}$ is invertible, it follows that the altenative beamformer $\mathbf{w}^*$ is the eigenvector corresponding to the maximum eigenvalue of $\overline{\mathbf{H}}_{PE}^{-1} \mathbf{H}_U$ after being scaled such that $\varphi \mathbf{w}^{*T} \mathbf{H}_U \mathbf{w}^* = M_1$ and $|\mathbf{w}| \prec \mathbb{1}$. If $\overline{\mathbf{H}}_{PE}$ is reduced rank, the vectors of the null space of $\overline{\mathbf{H}}_{PE}$ satisfying (3.25b) can be the solution of (3.25).

3.2.2.2 Maximizing User Rate

The optimization problem for maximizing the lower bound of the UE's rate subject to an ED rate constraint can be formulated as

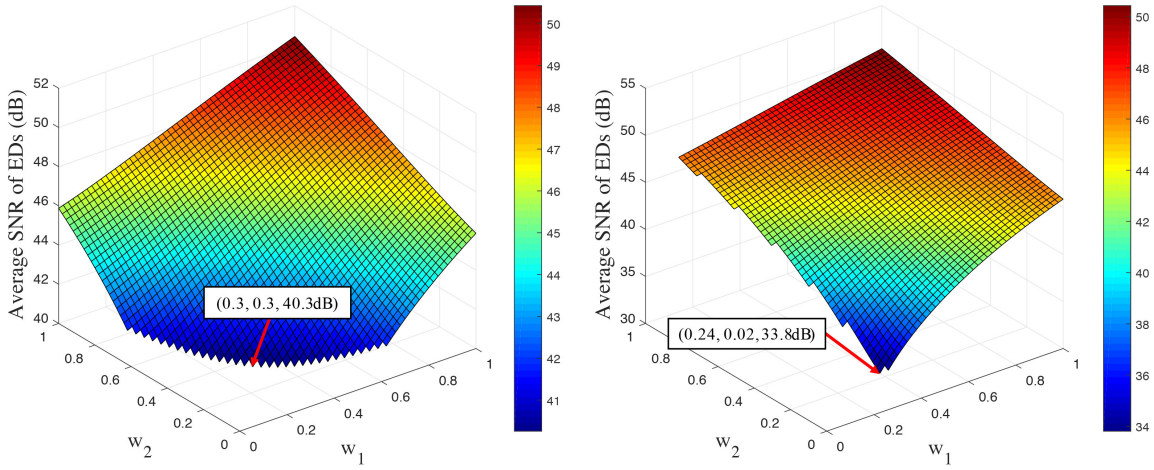
$$\mathbf{w}^* = \arg\max_{\mathbf{w}} \frac{1}{2} \log\left(1 + \frac{2\gamma_U}{\pi e}\right) \tag{3.26a}$$

$$\text{s. t.} \begin{cases} \frac{1}{2}\mathbb{E}\left[\log(1 + \gamma_{PE_q})\right] \leq \overline{\xi}_E \\ |\mathbf{w}| \preceq \mathbb{1} \end{cases} \tag{3.26b}$$

where $\overline{\xi}_E$ is the target constraint for the average rate upper bound of EDs. Again, by applying Jensen's inequality to the constraint, we arrive at the alternative formulation

$$\mathbf{w}^* = \arg\max_{\mathbf{w}} \ \mathbf{w}^T \mathbf{H}_U \mathbf{w} \tag{3.27a}$$

$$\text{s. t.} \begin{cases} \varphi \mathbf{w}^T \overline{\mathbf{H}}_{PE} \mathbf{w} \leq M_2 \\ |\mathbf{w}| \preceq \mathbb{1} \end{cases} \tag{3.27b}$$



(a) The average SNR of EDs for a UE at $(0, 1)$ (b) The average SNR of EDs for a UE at $(2, 1)$

Figure 3.2. The average SNR of EDs for different UE locations plotted against beamforming weights. Two transmitters T_1 and T_2 are located at $(2.5, 0)$ and $(-2.5, 0)$, respectively. The room size is $L = 8$ m, $W = 8$ m, and $H = 3$ m. $\rho_U = 40$ dB is applied.

where $M_2 = 2^{2\bar{\xi}_E} - 1$. Hence, if $\overline{\mathbf{H}}_{PE}$ is invertible, we deduce that the alternative beamforming vector is the eigenvector corresponding to the maximum eigenvalue of $\overline{\mathbf{H}}_{PE}^{-1}\mathbf{H}_U$ scaled appropriately, which is similar to the problem (3.20). If $\overline{\mathbf{H}}_{PE}$ is not invertible, the solution should be numerically found via the CCP algorithm proposed in Algorithm 1.

3.2.3 Comparing MISO Beamforming to LED Selection

In the previous subsection, we showed that the beamformer for SNR and rate objectives is universally related to the maximum eigenmode of $\overline{\mathbf{H}}_{PE}^{-1}\mathbf{H}_U$. The proposed beamforming vector cannot be a null-steering solution as was the case in [11] unless a condition occurs that makes $\overline{\mathbf{H}}_{PE}$ singular.

Since $\mathbf{H}_U$ depends on the UE's location and $\overline{\mathbf{H}}_{PE}$ depends on the transmitter locations and the intensity function of the EDs, we can note that when the UE is located near to a transmitter, the beamformer looks like a transmitter selection process, i.e., the nearest transmitter's weight is dominant to the others. This is because

the eigenvector corresponding to the maximum eigenvalue is significantly affected by the maximum diagonal element of $\mathbf{H}_U$ when the UE is near to the transmitter.

To illustrate this point, let us take an example of a simple VLC network where two transmitters are located at $T_1 = (2.5, 0)$ and $T_2 = (-2.5, 0)$ in an 8×8 m^2 square room. The center of the room is located at the origin of our coordinate system. Figures. 3.2(a) and (b) show the average SNR of EDs according to a different set of beamformer weights when the UE is located at $(0, 1)$ and $(2, 1)$, respectively. The required SNR of the UE is $\rho_U = 40$ dB, which is set appropriate to allow the assumption (3.15) to be satisfied. In Figure 3.2(a), since the UE is located at the exact middle point of the two transmitters, the weight values for the two transmitters that minimize the average SNR of the EDs are equivalent, i.e., $\mathbf{w}^* \approx (0.3, 0.3)$. However, when the UE is nearer to T_1 as in Figure 3.2(b), we can see that the beamformer resembles LED selection. More specifically, $\mathbf{w}^* \approx (0.24, 0.02)$ in this example. We can thus surmise that secrecy performance will be similar for beamforming and transmitter selection when the UE is located close to a transmitter[2].

With regard to practicalities of implementation, the complexity of the beamforming scheme can be reasonably high due to the use of multiple transmitters. Even though we can efficiently find an eigenvector related to the maximum eigenvalue by using the power method or the Rayleigh quotient method, the computational complexity still can be significant since complexity grows with N^2. Additionally, it might not be practical to accurately estimate the intensity function that describes ED locations. These arguments motivate further investigation of the performance of LED selection in the context of VLC systems with randomly distributed EDs.

[2]We will further explore the secrecy performance for both schemes later in Section 3.4.

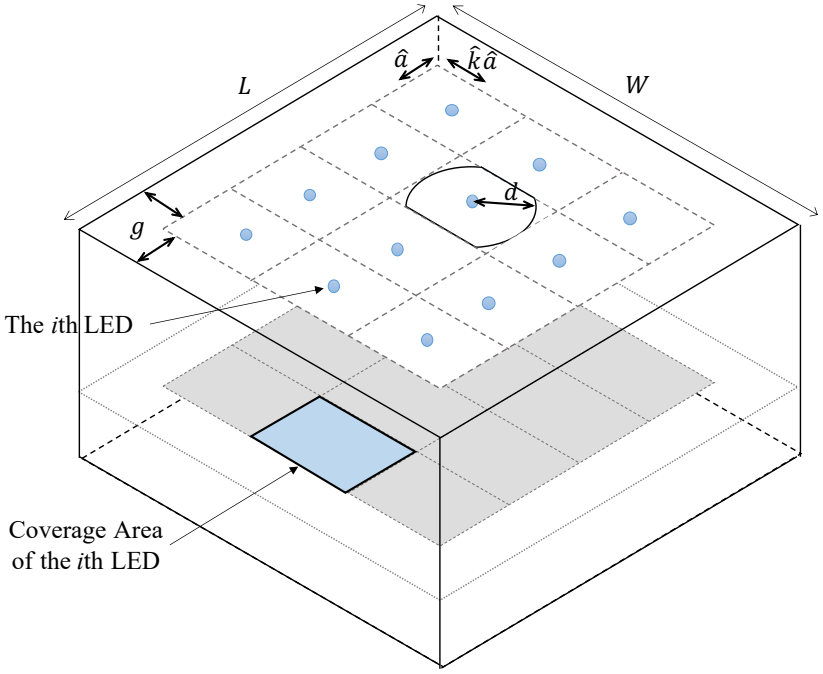


Figure 3.3. The room configuration for LED selection.

3.3 LED Selection

We turn our attention to the simple method of LED selection. In the LED selection scheme, the nearest transmitter to the UE is selected to transmit the information bearing signal. In this section, we first investigate the SNR and transmission rate performance metrics with LED selection. We then analyze the SOP. Closed-form expressions for the upper and lower bounds of the SOP with the LED selection are derived.

The room configuration in Figure 3.3 is used for our analysis, where multiple transmitters are attached to the ceiling such that the coverage area is identical (but translated in the work plane) for each of them. The coverage area is defined as the area where a transmitter is responsible for supporting the UE as shown in Figure 3.3. According to the LED selection scheme, the coverage area is determined by the distance between the transmitter and the UE; the nearest transmitter is responsible for supporting the UE. Note that the shape of the coverage area depends on the

arrangement of LED transmitters, and we assume the rectangular coverage area in this chapter. We assume that the UE can be located in the coverage area[3], i.e., the shaded area, while multiple EDs can (randomly) position themselves anywhere in the entire area of the room. The parameters $\hat{a}$ and $\hat{k}$ in the figure denote the half length of the rectangular coverage area's width and the ratio of length to width of the coverage area. By defining the number of rows and columns of the LED arrangement as N_r and N_c, respectively, the relations $\hat{a} = (L/2 - g)/N_r$ and $\hat{k} = (W/2 - g)/(N_c\hat{a})$ can be deduced, where g denotes the thickness of the edge zone. The UE and the EDs are assumed to be uniformly distributed according to a homogeneous BPP (with one point) and a homogeneous PPP $\mathbf{\Phi}_E$ with intensity λ_E, respectively.

3.3.1 SNR and Transmission Rate Analysis

Since only the nearest transmitter is selected to transmit a signal to the UE, the vector representing LED selection $\mathbf{w}_s$ can be described by

$$\mathbf{w}_s = \omega\, \mathbf{e}_i \tag{3.28}$$

where ω is the weight of the selected transmitter and $\mathbf{e}_i$ is the ith column of the identity matrix corresponding to the maximum diagonal element of $\mathbf{H}_U$, i.e., the ith transmitter is the nearest. Therefore, the average SNR of the EDs when LED selection is employed is given by

$$\overline{\gamma}_{PE} = \varphi \mathbf{w}_s^T \overline{\mathbf{H}}_{PE} \mathbf{w}_s. \tag{3.29}$$

If there exists a constraint on the average SNR of the EDs ($\overline{\rho}_{PE}$, as in (3.20)), ω should satisfy $\omega^2 \overline{H}_{PE_{i,i}}^2 \leq \overline{\rho}_{PE}$, where $\overline{H}_{PE_{i,i}}$ is the ith diagonal element of $\overline{\mathbf{H}}_{PE}$. Similarly,

[3]One may think of this restriction as a policy instigated to guarantee the security of UE, through the restriction of the UE to a "safety zone". On the other hand, it is fairly easy to see that this model reflects many realistic scenarios.

the SNR of the UE can be described by

$$\gamma_U = \varphi \mathbf{w}_s^T \mathbf{H}_U \mathbf{w}_s. \tag{3.30}$$

Also, if there exists a required SNR for the UE (ρ_U, as in (3.13)), ω should satisfy $\varphi\omega^2 H_{U_{i,i}}^2 \geq \rho_U$, where $H_{U_{i,i}}$ denotes the maximum diagonal element of $\mathbf{H}_U$.

Moreover, the average upper bound on the transmission rate of the ED channel with LED selection can be written as

$$\overline{C}_E^{\text{upper}} = \mathbb{E}\left[\frac{1}{2}\log\left(1 + \varphi\omega^2 h_{i,PE_q}^2\right)\right] \tag{3.31}$$

where h_{i,PE_q} is the channel gain from the ith transmitter to PE_q. Also, the lower bound on the transmission rate of the UE is given by

$$C_U^{\text{lower}} = \frac{1}{2}\log\left(1 + \frac{2\varphi \mathbf{w}_s^T \mathbf{H}_U \mathbf{w}_s}{\pi e}\right). \tag{3.32}$$

3.3.2 Secrecy Outage Probability

Here, we calculate upper and lower bounds on the SOP for the LED selection scheme. To this end, we necessarily must know something about the SNR statistics for the UE and the *nearest* ED, hence, the *worst case* ED. Thus, we begin by providing results for the PDF and the CDF for these random variables. To simplify the calculation of the SOP, we assume the weight of the selected transmitter's beamforming vector is always one. This assumption is justified since the nearest LED to the UE can increase the SNR of the UE the most, rather than other passive EDs, considering the fact the channel gain in VLC systems largely depends on the distance between the transmitter and receiver. This assumption would result in the lowest SOP given the LED selection.

Lemma 1. *The CDF and PDF of the received UE SNR γ_U are given by*

$$F_{\gamma_U}(y) = \tag{3.33}$$

$$\begin{cases} 1 - \left(K_4 \left((y/\zeta)^{\frac{-1}{m+3}} - H^2 \right) + K_3 \left((y/\zeta)^{\frac{-1}{m+3}} - H^2 \right)^{3/2} \right) / (4\hat{k}\hat{a}^2) & for \quad y_1 < y \leq y_2 \\ 1 - \left(K_2 \left((y/\zeta)^{\frac{-1}{m+3}} - H^2 \right) + K_1 \left((y/\zeta)^{\frac{-1}{m+3}} - H^2 \right)^{3/2} \right) / (4\hat{k}\hat{a}^2) & for \quad y_2 < y \leq y_3 \\ 1 - \pi \left((y/\zeta)^{\frac{-1}{m+3}} - H^2 \right) / (4\hat{k}\hat{a}^2) & for \quad y_3 < y \leq y_4 \end{cases} \tag{3.34}$$

and

$$f_{\gamma_U}(y) = \tag{3.35}$$

$$\begin{cases} (y/\zeta)^{-\frac{1}{m+3}} \left(3K_3 \sqrt{(y/\zeta)^{-\frac{1}{m+3}} - H^2} + 2K_4 \right) / (8\hat{a}^2\hat{k}(m+3)y) & for \quad y_1 < y \leq y_2 \\ (y/\zeta)^{-\frac{1}{m+3}} \left(3K_1 \sqrt{(y/\zeta)^{-\frac{1}{m+3}} - H^2} + 2K_2 \right) / (8\hat{a}^2\hat{k}(m+3)y) & for \quad y_2 < y \leq y_3 \\ \pi (y/\zeta)^{-\frac{1}{m+3}} / (4\hat{a}^2\hat{k}(m+3)y) & for \quad y_3 < y \leq y_4 \end{cases} \tag{3.36}$$

respectively, where $\zeta = (\alpha^2 I_{DC}^2 K^2)/\sigma^2$, and y_i and K_i for $i \in \{1,2,3,4\}$ are given by

$$\begin{aligned} y_1 &= \zeta(\hat{a}^2(1+\hat{k}^2) + H^2)^{-3-m}, \\ y_2 &= \zeta(\hat{a}^2\hat{k}^2 + H^2)^{-3-m}, \\ y_3 &= \zeta(\hat{a}^2 + H^2)^{-3-m}, \\ y_4 &= \zeta H^{-2(3+m)} \end{aligned} \tag{3.37}$$

and

$$
\begin{aligned}
K_1 &= \frac{\left(2\sqrt{\hat{k}^2-1}/\hat{k}^2 - 2\arccos\left(\frac{1}{\hat{k}}\right)\right)}{a(\hat{k}-1)},\\
K_2 &= \pi - \hat{a}K_1,\\
K_3 &= 2\left(\arccos\left(\frac{1}{\hat{k}}\right) - \arccos\left(\frac{1}{\sqrt{\hat{k}^2+1}}\right) - \arccos\left(\frac{\hat{k}}{\sqrt{\hat{k}^2+1}}\right)\right.\\
&\quad \left. + \frac{2\hat{k}}{\hat{k}^2+1} - \frac{\sqrt{\hat{k}^2-1}}{\hat{k}^2}\right) / \left(\hat{a}(\sqrt{\hat{k}^2+1}-\hat{k})\right),\\
K_4 &= \pi - 2\left(\arccos\left(\frac{1}{\hat{k}}\right) - \frac{\sqrt{\hat{k}^2-1}}{\hat{k}^2}\right) - \hat{k}\hat{a}K_3.
\end{aligned}
\tag{3.38}
$$

Proof. See Appendix 3.A.1. □

Lemma 2. *The CDF and PDF of the received SNR for the nearest ED relative to the selected transmitter γ_E^* are given by*

$$
F_{\gamma_E^*}(x) = e^{\lambda_E \pi\left(H^2 - \left(\frac{x}{\zeta}\right)^{-\frac{1}{m+3}}\right)}, \tag{3.39a}
$$

$$
f_{\gamma_E^*}(x) = \frac{\lambda_E \pi \left(\frac{x}{\zeta}\right)^{-\frac{1}{m+3}}}{x(m+3)} e^{\lambda_E \pi\left(\left(\frac{x}{\zeta}\right)^{-\frac{1}{m+3}} - H^2\right)} \tag{3.39b}
$$

for $0 \le x \le \zeta H^{-2(m+3)} = y_4$.

Proof. See Appendix 3.A.2. □

According to (3.8), the upper and lower bounds of the SOP can be written as

$$
\begin{aligned}
P_{\mathrm{SO}}^{\mathrm{upper}} &= \mathbb{P}(C_s^{\mathrm{lower}} \le C_{\mathrm{th}})\\
&= \mathbb{P}\left(\frac{6\gamma_U + 3\pi e}{\pi e \gamma_E^* + 3\pi e} \le 2^{2C_{\mathrm{th}}}\right)\\
&= \mathbb{P}(\gamma_U \le a\gamma_E^* + 3a - \pi e/2)
\end{aligned}
\tag{3.40}
$$

and

$$\begin{aligned} P_{\mathrm{SO}}^{\mathrm{lower}} &= \mathbb{P}(C_s^{\mathrm{upper}} \leq C_{\mathrm{th}}) \\ &= \mathbb{P}\left(\frac{\gamma_U + 1}{\gamma_E^* + 1} \leq 2^{2C_{\mathrm{th}}}\right) \\ &= \mathbb{P}(\gamma_U \leq b\gamma_E^* + b - 1) \end{aligned} \tag{3.41}$$

respectively, where $a = \pi e 2^{2C_{\mathrm{th}}}/6$ and $b = 2^{2C_{\mathrm{th}}}$. Thus, the upper and lower bounds on the SOP can be calculated by appropriately integrating over the PDFs of γ_U and γ_E^*.

Firstly, the upper bound on the SOP can be calculated to yield

$$\begin{aligned} P_{\mathrm{SO}}^{\mathrm{upper}} = &\underbrace{\int_{y_1}^{y_4} \int_{\frac{y-3a+\pi e/2}{a}}^{\frac{y_4-3a+\pi e/2}{a}} f_{\gamma_E^*}(x) f_{\gamma_U}(y)\,\mathrm{d}x\,\mathrm{d}y}_{U_1} \\ &+ \underbrace{\int_{y_1}^{y_4} \int_{\frac{y_4-3a+\pi e/2}{a}}^{y_4} f_{\gamma_E^*}(x) f_{\gamma_U}(y)\,\mathrm{d}x\,\mathrm{d}y}_{U_2}. \end{aligned} \tag{3.42}$$

Here, we ignore the $(-3a + \pi e/2)/a$ term in the integration limits, because it is small enough[4] not to meaningfully affect our calculation. Thus, we calculate the first term U_1 to yield

$$\begin{aligned} U_1 &\approx \int_{y_1}^{y_4} \left(F_{\gamma_E^*}\left(\frac{y_4}{a}\right) - F_{\gamma_E^*}\left(\frac{y}{a}\right)\right) f_{\gamma_U}(y)\,\mathrm{d}y \\ &= F_{\gamma_E^*}\left(\frac{y_4}{a}\right) \int_{y_1}^{y_4} f_{\gamma_U}(y)\,\mathrm{d}y - \int_{y_1}^{y_4} F_{\gamma_E^*}\left(\frac{y}{a}\right) f_{\gamma_U}(y)\,\mathrm{d}y \end{aligned}$$

[4]The absolute value of this term is less than 3 for $C_{\mathrm{th}} = 1$ bit/Hz/s, while y_1/a is larger than 5×10^3 with the parameters used in Section 3.4. The high SNR is obtainable in VLC system, which is an indirect consequence of the illumination requirements [83].

$$= F_{\gamma_E^*}\left(\frac{y_4}{a}\right) - \underbrace{\int_{y_1}^{y_2} e^{\lambda_E \pi\left(H^2-\left(\frac{y}{a\zeta}\right)^{-\frac{1}{m+3}}\right)} \frac{\left(\frac{y}{\zeta}\right)^{-\frac{1}{m+3}}\left(3K_3\sqrt{\left(\frac{y}{\zeta}\right)^{-\frac{1}{m+3}}-H^2}+2K_4\right)}{8\hat{a}^2\hat{k}(m+3)y}\,\mathrm{d}y}_{J_1}$$
$$- \underbrace{\int_{y_2}^{y_3} e^{\lambda_E \pi\left(H^2-\left(\frac{y}{a\zeta}\right)^{-\frac{1}{m+3}}\right)} \frac{\left(\frac{y}{\zeta}\right)^{-\frac{1}{m+3}}\left(3K_1\sqrt{\left(\frac{y}{\zeta}\right)^{-\frac{1}{m+3}}-H^2}+2K_2\right)}{8\hat{a}^2\hat{k}(m+3)y}\,\mathrm{d}y}_{J_2}$$
$$- \underbrace{\int_{y_3}^{y_4} e^{\lambda_E \pi\left(H^2-\left(\frac{y}{a\zeta}\right)^{-\frac{1}{m+3}}\right)} \frac{\pi\left(\frac{y}{\zeta}\right)^{-\frac{1}{m+3}}}{4\hat{a}^2\hat{k}(m+3)y}\,\mathrm{d}y}_{J_3}. \tag{3.43}$$

Then, the closed-form expressions for J_1, J_2, and J_3 in (3.43) can be calculated by (2.325.6) in [84] as

$$J_1 = \frac{1}{8\hat{a}^2\hat{k}}\left(\frac{2a^{\frac{-1}{m+3}}e^{\lambda_E\pi H^2}}{\lambda_E\pi}\left(e^{-\lambda_E\pi\left(\frac{y_2}{a\zeta}\right)^{\frac{-1}{m+3}}}-e^{-\lambda_E\pi\left(\frac{y_1}{a\zeta}\right)^{\frac{-1}{m+3}}}\right)K_4+\frac{3e^{-\lambda_E\pi H^2\left(-1+a^{\frac{1}{m+3}}\right)}K_3}{2\pi^{3/2}}\right.$$
$$\left.\cdot\sum_{i\in\{1,2\}}(-1)^{i+1}\left(\frac{\left(\left(\frac{y_i}{\zeta}\right)^{\frac{-1}{m+3}}-H^2\right)^{3/2}\left(\sqrt{\pi}-2\Gamma\left(\frac{3}{2},a^{\frac{1}{m+3}}\lambda_E\pi\left(\left(\frac{y_i}{\zeta}\right)^{\frac{-1}{m+3}}-H^2\right)\right)\right)}{\left(a^{\frac{1}{m+3}}\lambda_E\left(\left(\frac{y_i}{\zeta}\right)^{\frac{-1}{m+3}}-H^2\right)\right)^{3/2}}\right)\right) \tag{3.44a}$$

$$J_2 = \frac{1}{8\hat{a}^2\hat{k}}\left(\frac{2a^{\frac{-1}{m+3}}e^{\lambda_E\pi H^2}}{\lambda_E\pi}\left(e^{-\lambda_E\pi\left(\frac{y_3}{a\zeta}\right)^{\frac{-1}{m+3}}}-e^{-\lambda_E\pi\left(\frac{y_2}{a\zeta}\right)^{\frac{-1}{m+3}}}\right)K_2+\frac{3e^{-\lambda_E\pi H^2\left(-1+a^{\frac{1}{m+3}}\right)}K_1}{2\pi^{3/2}}\right.$$
$$\left.\cdot\sum_{i\in\{2,3\}}(-1)^{i}\left(\frac{\left(\left(\frac{y_i}{\zeta}\right)^{\frac{-1}{m+3}}-H^2\right)^{3/2}\left(\sqrt{\pi}-2\Gamma\left(\frac{3}{2},a^{\frac{1}{m+3}}\lambda_E\pi\left(\left(\frac{y_i}{\zeta}\right)^{\frac{-1}{m+3}}-H^2\right)\right)\right)}{\left(a^{\frac{1}{m+3}}\lambda_E\left(\left(\frac{y_i}{\zeta}\right)^{\frac{-1}{m+3}}-H^2\right)\right)^{3/2}}\right)\right) \tag{3.44b}$$

$$J_3 = \frac{1}{4\hat{a}^2\hat{k}\lambda_E}\left(a^{\frac{-1}{m+3}}e^{\lambda_E\pi H^2}\left(e^{-\lambda_E\pi\left(\frac{y_4}{a\zeta}\right)^{\frac{-1}{m+3}}} - e^{-\lambda_E\pi\left(\frac{y_3}{a\zeta}\right)^{\frac{-1}{m+3}}}\right)\right). \tag{3.44c}$$

Finally, the second term U_2 in (3.42) can be written as

$$U_2 \approx F_{\gamma_E^*}(y_4) - F_{\gamma_E^*}\left(\frac{y_4}{a}\right). \tag{3.45}$$

The lower bound on the SOP can be calculated to yield

$$\begin{aligned} P_{\text{SO}}^{\text{lower}} = &\int_{y_1}^{y_4}\int_{\frac{y-b+1}{b}}^{\frac{y_4-b+1}{b}} f_{\gamma_E^*}(x) f_{\gamma_U}(y)\,\mathrm{d}x\,\mathrm{d}y \\ &+ \int_{y_1}^{y_4}\int_{\frac{y_4-b+1}{b}}^{y_4} f_{\gamma_E^*}(x) f_{\gamma_U}(y)\,\mathrm{d}x\,\mathrm{d}y. \end{aligned} \tag{3.46}$$

Here, we ignore the $(-b+1)/b$ term in a similar manner as in (3.42). Therefore, since (3.46) has an identical expression to (3.42), we have the closed-form of the lower bound on SOP by simply changing the variable a to b in the closed-form expression of the upper bound.

From the closed-form expressions for the upper and lower bounds on the SOP, we note that the SOP is proportional to $4\hat{a}^2\hat{k}$ (see (3.44)), which is the coverage area of each transmitter. In other words, if the room size is fixed, then the SOP can be decreased by increasing the number of transmitters to reduce the coverage area.

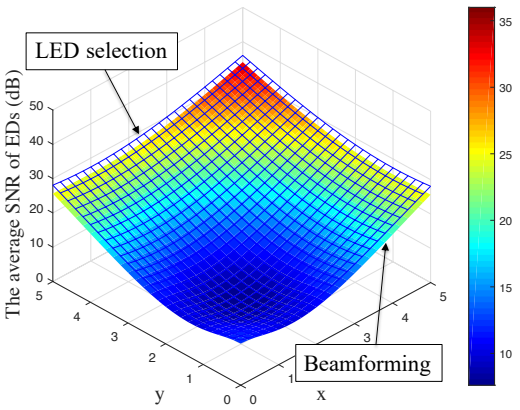
3.4 Numerical Results

In this section, we provide numerical results to verify our analysis. All of the theoretical and simulation results are obtained via MATLAB. Especially, the simulations, which are related to Figure 3.8 and 3.9, are conducted via the Monte Carlo approach in which we generate random positions of EDs for 10^4 times and evaluate

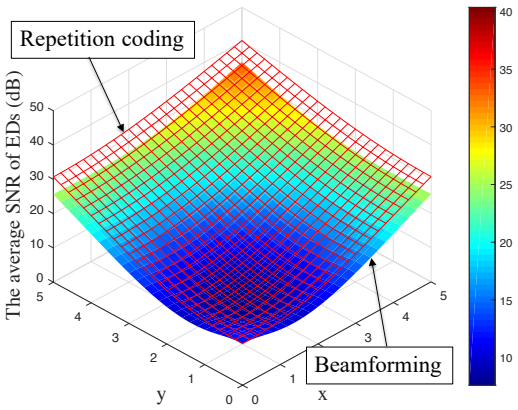
Table 3.1. Simulation Parameters

Room configuration	
Length (L) × Width (W)	10×10 m^2
Height from the work plane (H)	3 m
Number of light fixtures	4
Number of LEDs per fixture	72
LED electrical and optical characteristics	
Average optical power per LED	1 W
Current-to-light conversion efficiency η	1 W/A
Nominal half-intensity angle $\Phi_{1/2}$	60°
Modulation index α	0.5
Optical receiver characteristics	
Photodetector's responsivity $R_{\text{rsp.}}$	0.54 mA/mW
Photodetector's physical area A_{PD}	1 cm^2
Lens refractive index κ	1.5
Noise power σ^2	−98.35 dBm
Field of View Ψ_c	60°
Transimpedance amplifier gain T	50 V/A

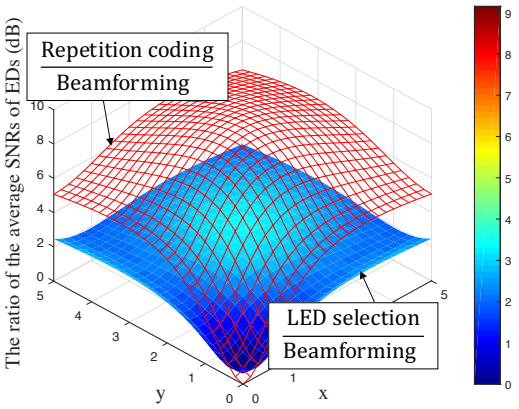
the average secrecy performance. In addition, the room configuration and simulation parameters are provided in Table 3.1. Here, we utilize the characteristics of the LED transmitters and receivers employed in [10], which considered a typical office room and common lightening devices. In addition, emitted light is assumed to be "warm-white," i.e., color temperature is between 2700 and 3000 K, with luminous efficiency 284 lm/W [85, Table 3.2]. Based on this assumption, we adjust the number of light fixtures and the number of LEDs per fixture such that the considered LED arrangement satisfies the lighting standards, e.g., from 400 to l000 lx for a typical office [86]. According to the Lumen method [87], the considered configuration yields the light level of 589 lx in the room. Also, we use the Cartesian coordinate system to identify positions of transmitters and receivers, where the center of the room is located at the origin. We consider a VLC network where four transmitters are symmetrically located, i.e., their locations can be described by $(\pm d_0, \pm d_0)$. A homogeneous PPP describes the ED locations.



(a) The average SNR of EDs with beamforming and LED selection



(b) The average SNR of EDs with beamforming and repetition coding

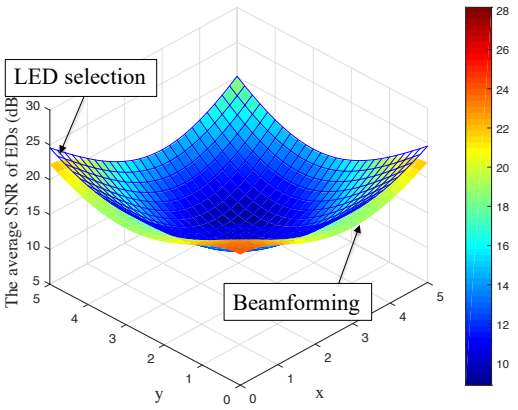


(c) The ratio of the average SNRs of EDs generalized by beamforming

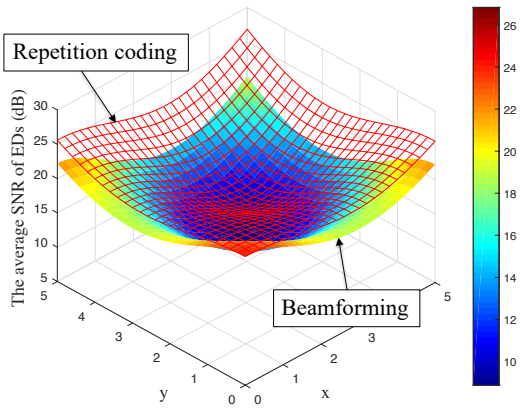
Figure 3.4. The average SNR of EDs as a function of the UE location. The full-color surfaces in (a) and (b) denote the results for the beamforming (identical). The monochromatic mesh surfaces denote LED selection and repetition coding, respectively. In (c), the ratio of the average SNRs of EDs are given in which the monochromatic mesh surface denotes the ratio of repetition coding and beamforming, and the full-color surface denotes the ratio of LED selection and beamforming, respectively. $\lambda_E = 0.05$ and $\rho_U = 20$ dB are used. Four LED transmitters are symmetrically located at $(\pm 1, \pm 1)$.

3.4.1 Signal-to-Noise Ratio

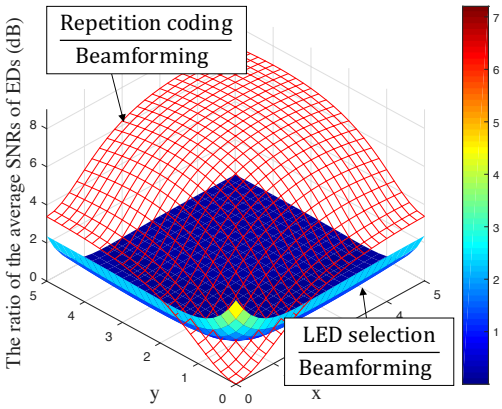
Figures. 3.4 and 3.5 show the comparison of the average SNR of EDs as a function of the UE location by using beamforming, LED selection and repetition coding schemes for the different locations of transmitters at $(\pm 1, \pm 1)$ and $(\pm 3, \pm 3)$, respectively, where



(a) The average SNR of EDs with beamforming and LED selection



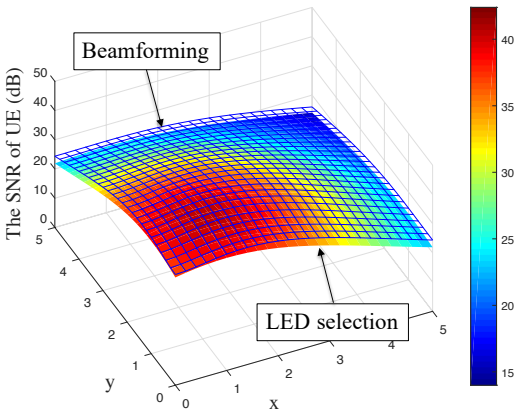
(b) The average SNR of EDs with beamforming and repetition coding



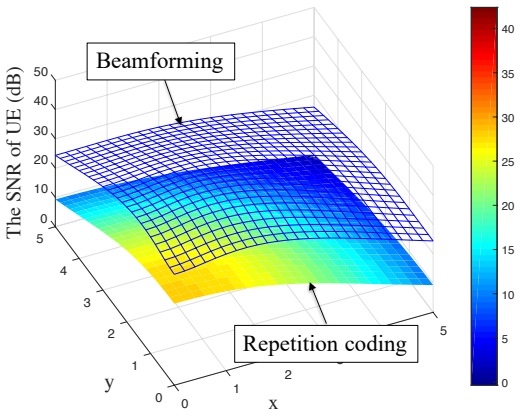
(c) The ratio of the average SNRs of EDs generalized by beamforming

Figure 3.5. The average SNR of EDs as a function of the UE location. The full-color surfaces in (a) and (b) denote the results for the beamforming (identical). The monochromatic mesh surfaces denote LED selection and repetition coding, respectively. In (c), the ratio of the average SNRs of EDs are given in which the monochromatic mesh surface denotes the ratio of repetition coding and beamforming, and the full-color surface denotes the ratio of LED selection and beamforming, respectively. $\lambda_E = 0.05$ and $\rho_U = 20$ dB are used. Four LED transmitters are symmetrically located at $(\pm 3, \pm 3)$.

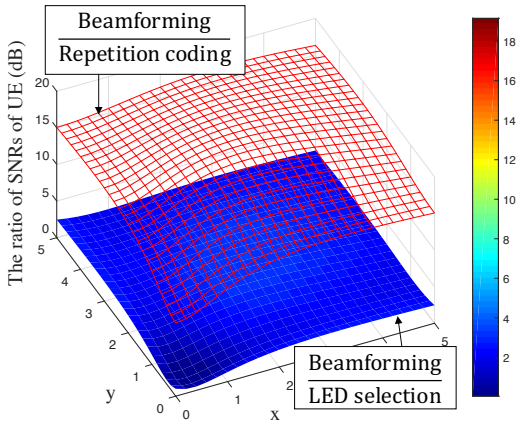
$\lambda_E = 0.05$ and $\rho_U = 20$ dB. Note that $\lambda_E = 0.05$ yields five EDs on average in the considered 10×10 m^2 room and ρ_U is set appropriate to allow the assumption (3.15) to be satisfied for a given LED arrangement. Since four transmitters are symmetrically located, we only show the results for the UE locations within the first quadrant. The repetition coding scheme [88] is given as a benchmark in which all of the precoding



(a) The SNR of UE with beamforming and LED selection



(b) The SNR of UE with beamforming and repetition coding

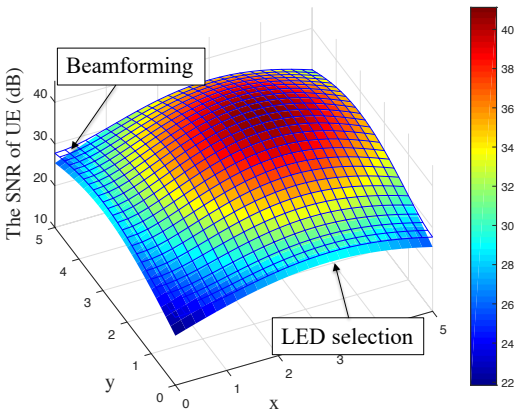


(c) The ratio of the SNRs of UE generalized by beamforming

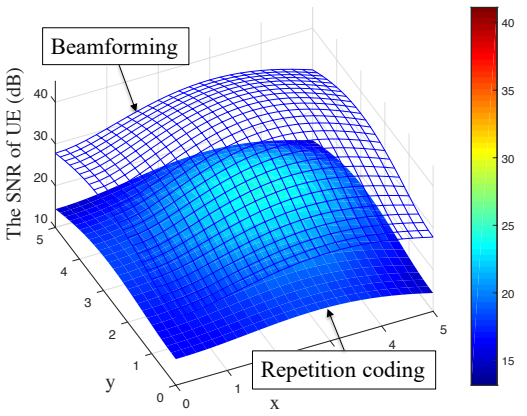
Figure 3.6. The SNR of the UE as a function of the UE locations. The monochromatic mesh surfaces in (a) and (b) denote the result for the beamforming (identical). The full-color surfaces denote LED selection and repetition coding, respectively. In (c), the ratio of the SNRs of UE are given in which the monochromatic mesh surface denotes the ratio of beamforming and repetition coding, and the full-color surface denotes the ratio of beamforming and LED selection, respectively. $\lambda_E = 0.05$ and $\overline{\rho}_{PE} = 30$ dB are used. Four LED transmitters are symmetrically located at $(\pm 1, \pm 1)$.

weights are set to one, i.e., $\mathbf{w} = \mathbb{1}$, since there is only one active UE at a time in the considered configuration. In addition, for a fair comparison, we scale down the modulation index α such that the SNR of the UE when using the repetition coding meets ρ_U.

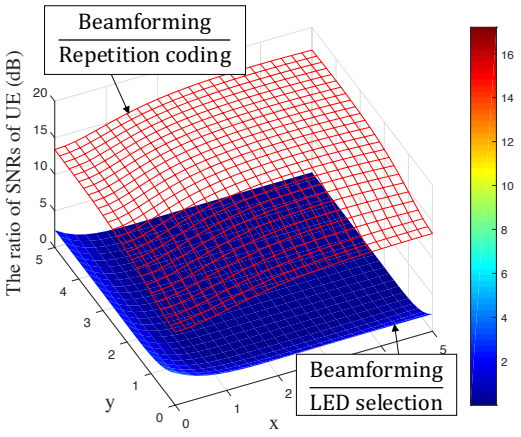
All of the full-color surfaces in (a) and (b) of Figures. 3.4 and 3.5 denote the



(a) The SNR of UE with beamforming and LED selection



(b) The SNR of UE with beamforming and repetition coding



(c) The ratio of the SNRs of UE generalized by beamforming

Figure 3.7. The average SNR of the UE as a function of the UE locations. The monochromatic mesh surfaces in (a) and (b) denote the result for the beamforming (identical). The full-color surfaces denote LED selection and repetition coding, respectively. In (c), the ratio of the SNRs of UE are given in which the monochromatic mesh surface denotes the ratio of beamforming and repetition coding, and the full-color surface denotes the ratio of beamforming and LED selection, respectively. $\lambda_E = 0.05$ and $\overline{\rho}_{PE} = 30$ dB are used. Four LED transmitters are symmetrically located at $(\pm 3, \pm 3)$.

average SNR of EDs as a function of the UE location when using the beamforming, and the monochromatic mesh surfaces in (a) and (b) of Figures. 3.4 and 3.5 denote the results for the LED selection and the repetition coding, respectively. Firstly, when four transmitters are located close to each other in the center area of the room, as in Figure 3.4, the transmitters emit a signal with high power to the UE that is located

in the outer area to satisfy ρ_U. Due to the broadcasting characteristic of light, the EDs can eavesdrop the signal easily; thus their average SNR also increases as shown in Figures. 3.4(a) and 3.4(b). In this case, the EDs can achieve a higher average SNR than ρ_U if the UE is away from the transmitter. On the contrary, when the distance between the transmitter and the UE decreases, one can see that the average SNR of the EDs also decreases because of the decrease in transmitted power. On the other hand, we see that when the four transmitters are adequately separated from each other as in Figure 3.5, both beamforming and LED selection exploit the spatial advantage to decrease the average SNR of EDs. The average SNR of EDs is less than ρ_U for most of the area except for around the center point of the transmitters, i.e., near (0,0).

Furthermore, in Figures 3.4(c) and 3.5(c), the ratio of the average SNRs of EDs when using the LED selection and the beamforming is given as the full-color surface, and the ratio of the average SNRs of EDs when using the repetition coding and the beamforming is given as the monochromatic mesh surface. We can easily note that the average SNR of EDs with repetition coding is much higher than the beamforming in both configurations. On the contrary, the ratio of the average SNRs of EDs of LED selection and beamforming is small when the UE is located near to the transmitter, while beamforming can slightly outperform LED selection when the UE is away from the transmitter.

Figures. 3.6 and 3.7 show a comparison of the SNR of the UE as a function of the UE location using beamforming, LED selection, repetition coding schemes for different locations of transmitters at $(\pm 1, \pm 1)$ and $(\pm 3, \pm 3)$, respectively, where $\lambda_E = 0.05$ and $\overline{\rho}_{PE} = 30$ dB. Note that $\overline{\rho}_{PE}$ is set appropriate to allow the assumption (3.15) to be satisfied for a given LED arrangement. Similarly, since four transmitters are symmetrically located, we only show the results for the UE locations within the first quadrant. All of the monochromatic mesh surfaces in (a) and (b) of Figures. 3.6

and 3.7 denote the SNR of the UE as a function of the UE location when using beamforming, and the full-color surfaces in (a) and (b) denote the results for the LED selection and the repetition coding, respectively. Firstly, when the transmitters are located closely together as in Figure 3.6, the SNR of the UE can be high when the UE is located near to the transmitter. However, when the UE moves away from the transmitter, it is difficult for the UE to achieve an SNR higher than $\overline{\rho}_{PE}$. This is because the transmitter should convey the signal with high enough power to reach the UE, which enables the EDs to overhear the signal easily. In contrast, when the transmitters are sufficiently separated as in Figure 3.7, we note that the UE can achieve a higher SNR than $\overline{\rho}_{PE}$ over almost the entire area of the room except for at the center point of the room, i.e., near (0,0), as shown in Figure 3.7(a). This can be possible by selectively transmitting a signal to the UE without excessively increasing the signal power of other transmitters, thus exploiting the spatial benefit.

In addition, in Figures. 3.6(c) and 3.7(c), the ratio of the SNRs of the UE when using beamforming and LED selection is given as the full-color surface, and the ratio of the SNRs of the UE when using beamforming and repetition coding is given as the monochromatic mesh surface. First, we can note that beamforming significantly outperforms the repetition coding in both configurations. These results show that the beamforming effectively transmits a signal to the UE trying not to expose the signal to EDs by taking the density of ED locations into account for the beamforming weights. In addition, we see from Figure 3.6(c) that the ratio of the SNRs of the UE for beamforming and LED selection is not significant for the UE located near the transmitter, but it slightly increases as the distance between the transmitter and the UE grows. Similarly, from Figure 3.7(c), we note that the ratio of the SNRs of the UE for beamforming and LED selection is not significant when the UE is close to the transmitter. Therefore, when the transmitters are adequately separated, and the UE is near to the transmitters, it is shown that the difference in secrecy

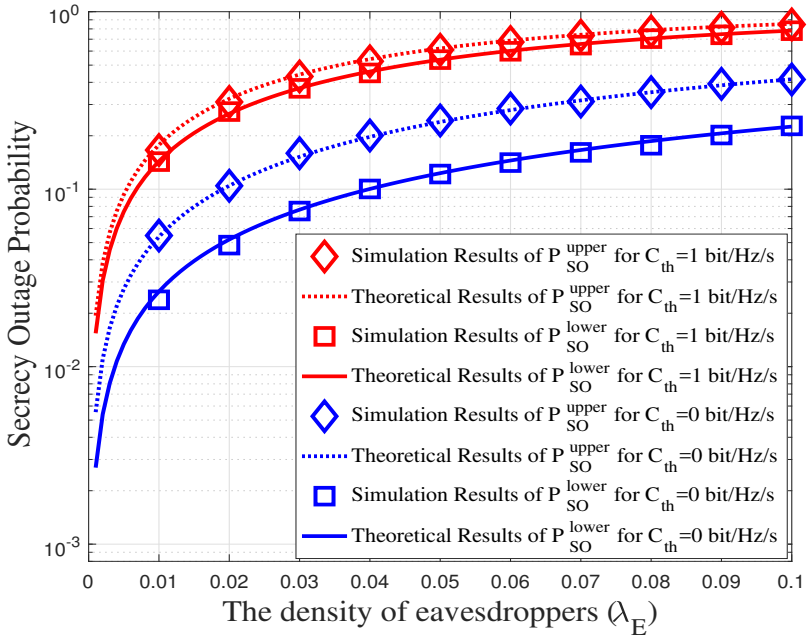


Figure 3.8. The upper and lower bounds on the SOP with LED selection for different C_{th} according to different intensities of EDs λ_E, where $N = 4 \times 4$, $g = 1$ m, $\hat{a} = 1$ m, $\hat{k} = 1.25$, $L = 10$ m, $W = 12$ m, and $H = 3$ m.

performance between beamforming and LED selection is small. Therefore, considering the computational complexity and feasibility of beamforming, we conclude that LED selection may be an attractive option in some scenarios.

3.4.2 Secrecy Outage Probability

Figure 3.8 shows the upper and lower bounds on the SOP with LED selection for different intensities of EDs and different values of C_{th}, where $N = 4 \times 4$, $g = 1$ m, $\hat{a} = 1$ m, $\hat{k} = 1.25$, $L = 10$ m, and $W = 12$ m. Note that the considered 10×12 m^2 rectangular room and the LED arrangement parameters $\hat{a} = 1$ m and $\hat{k} = 1.25$ yield the rectangular coverage area as depicted in Figure 3.3, which is used in our analysis in Section 3.3.2. Theoretical results for the upper and lower bounds on the SOP are calculated from (3.42) and (3.46), respectively, while simulation results are obtained via the Monte Carlo approach with 10^4 trials. Both simulated results and theoretical

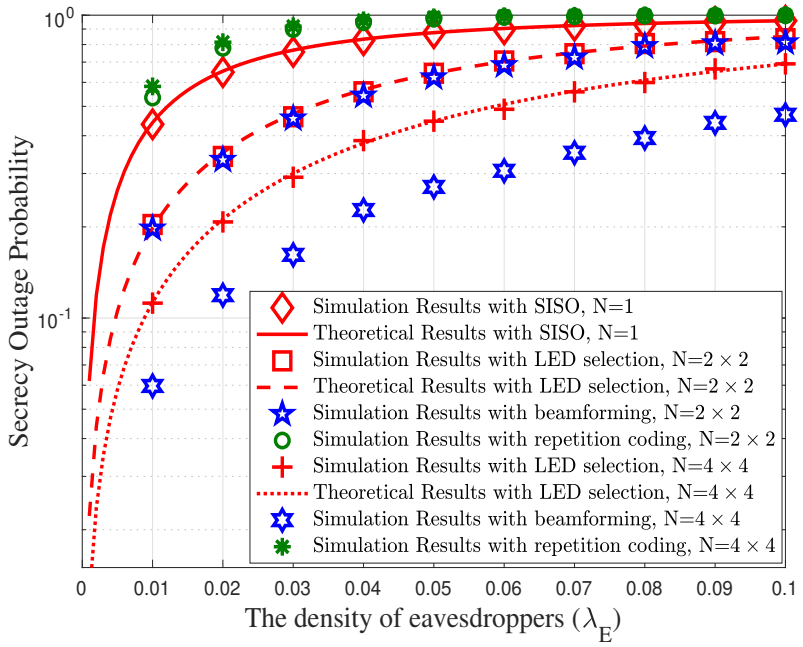


Figure 3.9. A comparison of the upper bound on the SOP between LED selection and beamforming for different numbers of transmitters according to different intensities of EDs λ_E, where $C_{\text{th}} = 0.5$ bit/Hz/s, $g = 1$ m, $L = 10$ m, $W = 12$ m, and $H = 3$ m.

results are shown to perfectly match. As can be seen from the figure, both the SOP upper and lower bounds increase as λ_E and C_{th} increase, as expected.

Figure 3.9 shows a comparison of the upper bound on SOP among beamforming, LED selection and repetition coding for different numbers of transmitters and different values of λ_E, where $C_{\text{th}} = 0.5$ bit/Hz/s, $g = 1$ m, $L = 10$ m, and $W = 12$ m. Theoretical results for the upper bounds on the SOP with the LED selection are calculated from (3.42), while all the simulation results are obtained via the Monte Carlo approach with 10^4 trials. Note that this work does not provide the theoretical analysis on the SOP with the beamforming and repetition coding schemes; thus, only the simulation results are provided for these two schemes. Moreover, the results for the beamforming scheme are obtained by utilizing the optimization design based on the SNR in (3.13) with $\overline{\rho}_{PE} = 30$ dB. It can be seen that as the number of transmitters increases, the upper bound on SOP decreases with beamforming and LED

selection, while it increases with repetition coding. In the proposed beamforming and LED selection, the multiple spatially distributed transmitters efficiently decrease the possibility of eavesdropping by transmitting the legitimate data favorably to the UE. In contrast, in the repetition coding, all of the transmitters emit the legitimate data with an equal power regardless of the location of the UE although the transmitters far away from the UE cannot largely increase the SNR of the UE. Thus, the advantage of repetition coding for EDs is much larger than that of the UE, then the SOP increases. Furthermore, when the number of transmitters is small, i.e., $N = 2 \times 2$, the difference in the SOP for beamforming and LED selection is small. However, when N is large, we can see that the upper bound on the SOP with beamforming is less than for LED selection. Since a large number of transmitters with beamforming can exploit the excessive spatial degrees of freedom to steer the signal toward the UE, the transmitters can significantly increase the SNR of the UE while suppressing the signal everywhere else inside the room. However, we need to consider that finding the maximum eigenvalue and its associated eigenvector with a large number of transmitters requires high computation complexity, which increases proportionally to N^2. It is worth mentioning that the proposed beamforming scheme is still less complicated than the beamforming scheme proposed in [10], which has been shown to be NP-hard [89]. In our proposed beamforming approach, we have a deterministic way, i.e., the eigenvector of $\overline{\mathbf{H}}_{PE}^{-1}\mathbf{H}_U$, to find the beamformer when (17) is satisfied.

3.5 Summary

In this chapter, we studied beamforming schemes and a simpler LED selection scheme to enhance the secrecy performance in VLC systems when multiple EDs are randomly distributed throughout the communication region. By using the beamforming scheme, we can minimize the average SNR of EDs (or indeed the worst case SNR of EDs) and

maximize the SNR of the UE with only statistical information about ED locations. The LED selection scheme is not superior to the beamformer in the respect of secrecy performance; however, when the UE is located near to one of the transmitters, LED selection provides a good practical solution to enhancing secrecy performance without high computational complexity. Based on LED selection, closed-form approximations for the upper and lower bounds on the SOP were derived.

3.A Appendices

3.A.1 Proof of the Lemma 1

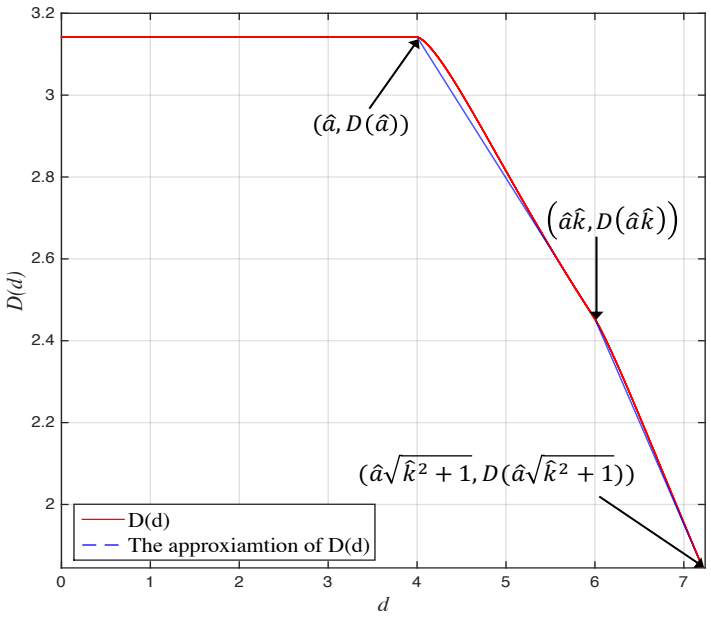


Figure 3.10. An example of $\hat{D}(d)$ for $\hat{a} = 4$ m, $\hat{k} = 1.5$. Note $\hat{a}\hat{k} = 6$ m and $\hat{a}\sqrt{\hat{k}^2+1} = 7.21$ m. $\hat{a}\hat{k} = 6$ m and $\hat{a}\sqrt{\hat{k}^2+1} = 7.21$ m

The UE is randomly located according to a homogeneous BPP in the shaded area in Figure 3.3. Therefore, the distance in the work plane between the transmitter and

the UE d_U cannot exceed $\hat{a}\sqrt{\hat{k}^2+1}$. Thus, the CDF of d_U is given by

$$F_{d_U}(d) = \frac{A(d)}{4\hat{k}\hat{a}^2} \quad \text{for} \quad 0 < d \leq \hat{a}\sqrt{\hat{k}^2+1} \tag{3.47}$$

where $A(d)$ denotes the area of the circle bounded by the rectangle as shown in Figure 3.3. When the radius of the circular area where the UE locates, i.e., d, equals to $\hat{a}$, its circumference hits the small rectangle. Also, if d increases further, the circular area starts to be bounded by the rectangle since the UE cannot exist out of the bounded circular area. If the UE locates out of the bounded circular area, the UE would select another nearest transmitter. $A(d)$ is described as

$$A(d) = \begin{cases} \pi d^2 & \text{for} \quad 0 < d \leq \hat{a} \\ \pi d^2 - 2\left(d^2 \arccos\left(\frac{\hat{a}}{d}\right) - \hat{a}\sqrt{d^2-\hat{a}^2}\right) & \text{for} \quad \hat{a} < d \leq \hat{k}\hat{a} \\ \pi d^2 - 2\left(d^2 \arccos\left(\frac{\hat{a}}{d}\right) - \hat{a}\sqrt{d^2-\hat{a}^2}\right) - 2\left(d^2 \arccos\left(\frac{\hat{a}\hat{k}}{d}\right) - \hat{a}\hat{k}\sqrt{d^2-(\hat{a}\hat{k})^2}\right) & \text{for} \quad \hat{k}\hat{a} < d \leq \hat{a}\sqrt{\hat{k}^2+1}. \end{cases} \tag{3.48}$$

Here, $A(d)$ can be described as $A(d) = D(d) \cdot d^2$, where $D(d)$ can be approximated by applying a piecewise approximation with a linear function of d, i.e.,

$$\hat{D}(d) = \begin{cases} \pi & \text{for} \quad 0 < d \leq \hat{a} \\ K_1 d + K_2 & \text{for} \quad \hat{a} < d \leq \hat{k}\hat{a} \\ K_3 d + K_4 & \text{for} \quad \hat{k}\hat{a} < d \leq \hat{a}\sqrt{\hat{k}^2+1}. \end{cases} \tag{3.49}$$

To find the optimal K_i for $i \in \{1,2,3,4\}$, we evaluate three coordinates $D(\hat{a})$, $D(\hat{a}\hat{k})$, and $D(\hat{a}\sqrt{\hat{k}^2+1})$ as shown in Figure 3.10. Using these values, we can easily calculate

the approximation constants as shown in (3.38).

Finally, from (3.2) and (3.4a), the SNR of the UE can be described as a function of d according to

$$\gamma_U(d) = \frac{\alpha^2 I_{DC}^2 K^2 (d^2 + H^2)^{-(m+3)}}{\sigma^2} = \zeta (d^2 + H^2)^{-(m+3)} \tag{3.50}$$

where $\zeta = (\alpha^2 I_{DC}^2 K^2)/\sigma^2$. Thus, the CDF and PDF of γ_U can be written as (3.33) and (3.35), respectively.

3.A.2 Proof of the Lemma 2

Since the EDs are randomly distributed according to a homogeneous PPP Φ_E with intensity λ_E on the work plane, the CDF of the minimum distance in the work plane between the selected transmitter and the nearest ED, i.e., $d_E^* = \min_{q \in \Phi_E} d_{PE_q}$, where d_{PE_q} is the distance in the work plane between the selected transmitter and PE_q, is given by

$$F_{d_E^*}(d) = 1 - \exp(-\lambda_E \pi d^2) \tag{3.51}$$

for $0 \leq d \leq \infty$. This follows from the contact distance distribution to the nearest point of the PPP [90]. Here, the unbounded upper limit implies that the number of EDs can be zero. The PDF of d_E^* can be calculated as $f_{d_E^*}(d) = 2\lambda_E \pi d \exp(-\lambda_E \pi d^2)$ for $0 \leq d \leq \infty$. Therefore, since γ_E^* also has the same relation with d_E^* as (3.50), the PDF and CDF of γ_E^* can be calculated as below.

$$\begin{aligned} f_{\gamma_E^*}(x) &= \frac{\lambda_E \pi \left(\frac{x}{\zeta}\right)^{-\frac{1}{m+3}}}{x(m+3)} e^{-\lambda_E \pi \left(-H^2 + \left(\frac{x}{\zeta}\right)^{-\frac{1}{m+3}}\right)}, \\ F_{\gamma_E^*}(x) &= \int_0^x f_{\gamma_E^*}(u)\, \mathrm{d}u \\ &= \int_0^x \frac{\lambda_E \pi \left(\frac{u}{\zeta}\right)^{-\frac{1}{m+3}}}{u(m+3)} e^{-\lambda_E \pi \left(-H^2 + \left(\frac{u}{\zeta}\right)^{-\frac{1}{m+3}}\right)} \mathrm{d}u \end{aligned} \tag{3.52}$$

$$
\begin{aligned}
&= \int_{\left(\frac{x}{\zeta}\right)^{-\frac{1}{m+3}}}^{\infty} \lambda_E \pi e^{-\lambda_E \pi (v - H^2)} \, \mathrm{d}v \\
&= e^{\lambda_E \pi \left(H^2 - \left(\frac{x}{\zeta}\right)^{-\frac{1}{m+3}} \right)}
\end{aligned} \tag{3.53}
$$

for $0 \leq x \leq \zeta H^{-2(m+3)}$, respectively, where $v = \left(\frac{u}{\zeta}\right)^{-\frac{1}{m+3}}$.

Chapter 4

Simultaneous Beamforming and Jamming

In **Chapter 3**, the beamforming and LED selection schemes that do not require the knowledge on the ED locations were newly proposed and analytically investigated, assuming that the ED retains the identical receiver architectures as the UE. However, a practical and feasible VLC eavesdropping scenario is that the ED augments its receive capability by, e.g., increasing the area of a PD, adopting a high gain optical lens, and accurately adjusting the receiver's orientation toward the LED transmitter. For example, in [91], a telescope was used to increase the gain of the receiver in an experimental test, which showed that VLC channels could be eavesdropped with a high-quality receiver even at a far distance. In the presence of an ED equipped with a better receiver than the intended user, a secrecy outage can occur with a high probability. To cope with this scenario, multiple jamming or artificial noise schemes for VLC systems were proposed in [11, 12, 15, 16, 92]. These are powerful and practical approaches to securing VLC systems since even EDs with powerful receiver architectures cannot distinguish between the random information jamming signals.

To date, almost all works on jamming in VLC systems have assumed that the

locations and/or the CSI of EDs are available at the transmitter, which may not be practical. This chapter deviates from this assumption by proposing a joint strategy of beamforming and jamming, which can be implemented in the presence of a *randomly* located ED, i.e., it does not require knowledge of the exact location or the CSI of an ED, instead only requiring the statistical information of the location of the ED.

On the other hand, [11, 12] also proposed user-friendly jamming strategies assuming that LED transmitters do not retain the knowledge of the precise location of an ED. However, those strategies make unrealistic assumptions and exhibit performance limitations. More specifically, in the artificial noise scheme [11], the LEDs transmit randomly-generated noise symbols in the nullspace of the intended user with the hope that interference is caused at the ED site. However, this scheme left the resulting secrecy performance to luck depending on the nullspace of the intended user; thus, it does not always perform in a way that optimizes the secrecy performance[1]. When engineering secure VLC systems, the secrecy performance changes with the nullspace of the intended user, which may cause difficulties in determining properties of a wiretap code [5]. Also, the friendly jamming scheme in [12] assumed that an ED is expected or permitted to exist within a certain *bounded* area known to the jammers. Then, a max-min optimization problem maximizing the worst-case secrecy rate over all the channel realizations of the bounded ED was formulated. However, in large open spaces, it would be impractical to anticipate or restrict the region of an ED's possible location, since the ED can be located anywhere, even at a far distance, being equipped with a high-quality receiver trying to escape the vigilance of the UE. In contrast, our proposed scheme is the approach that *optimizes* the secrecy performance (without leaving anything to luck) by simultaneously utilizing beamforming and jamming and does not set any constraint on the possible location of the ED, while requiring only statistical information of the ED's location. In practice, the statistical information

[1]We will provide an example for this situation in Section 4.5.

of the location of an ED can be effectively acquired by analyzing the user behavior characteristics and the layout of the room. Moreover, note that the uniform distribution of the ED's location, as we will assume in later sections, means that the ED's location is completely random (unknown), which is the worst case from the secrecy viewpoint [22, 93].

Firstly, we formulate the optimization problem for jointly determining the beamforming and jamming vectors that maximize the SINR of a UE while suppressing the SINR of an ED. Since the optimization problem is not convex, we utilize a heuristic method called the concave-convex procedure (CCP) [26] to find the local solution. However, due to its high computational complexity when a large number of transmitters is considered, we propose a simpler version of the joint scheme called the *ternary scheme*, which is inspired by the behavior that is observed when analyzing the joint beamforming and jamming scheme. An assignment optimization problem is formulated for the ternary scheme, and this is based on the SINR metric in a similar way to the joint scheme. *Tabu search* (TS) is invoked to obtain the solution to the assignment problem.

The most important objective of PLS enhancement work is to increase the secrecy capacity [5]. However, in VLC systems, deriving a closed-form analytic expression for the secrecy capacity has proved elusive due to the amplitude constraint. Hence, upper and lower bounds for various channel models have been studied instead [10, 15, 94, 95]. Similarly, in this chapter, by utilizing the truncated Gaussian distribution on the input and jamming signals as in [15], we derive a closed-form secrecy rate expression for the joint scheme, given the location of the ED. On the other hand, without knowledge of the location or the CSI of the ED, with only statistical information available, it is more appropriate to define and utilize the *average* secrecy rate as a metric to increase the secrecy performance [96, 97]. However, the expectation of the proposed secrecy rate cannot be written in closed-form, and the optimization problem

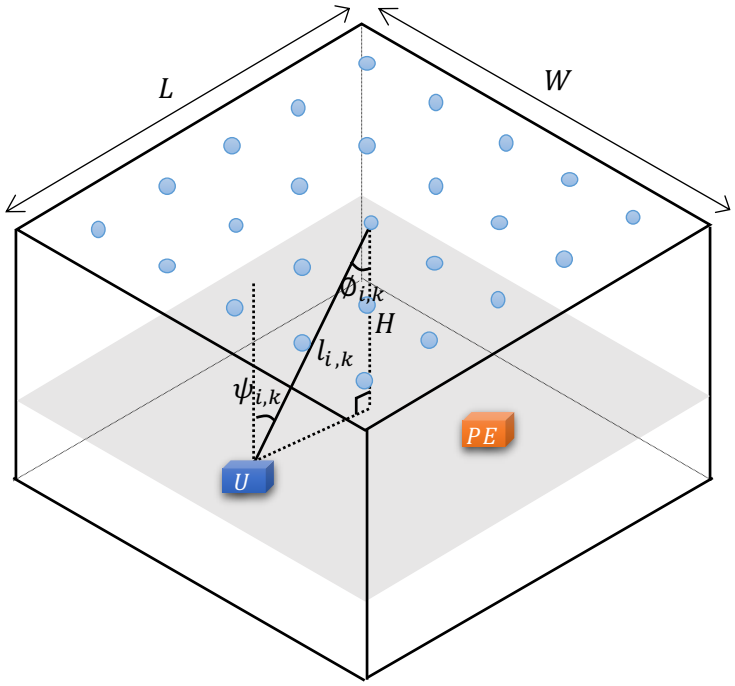


Figure 4.1. Rectangular room configuration for VLC systems. W and L are the room's width and length, and H denotes the height from the ceiling to the work plane. Dots denote LED transmitters.

maximizing the average secrecy rate is shown to be non-convex; thus, it is impractical to solve the problem directly, either by analytic or numerical means. Consequently, we propose a continuous LED model to mitigate the aforementioned complications and to solve the optimization problem numerically. We show that the continuum model can significantly simplify the optimization problem based on the average secrecy rate metric by transforming the problem with $2N$ optimization variables, where N is the number of LED transmitters, into a problem with only three optimization variables.

4.1 System Framework

4.1.1 Data Transmission and Jamming

We consider the downlink of a VLC system in a rectangular room as shown in Figure 4.1, where W, L, and H denote the width, the length, and the height of the

ceiling relative to the work plane, respectively. Also, one UE and one passive ED are present in the room, where the passive ED is assumed to be randomly located on the work plane in the room. The UE and passive ED are denoted by U and PE, respectively. N LED transmitters are assumed to be attached to the ceiling of the room and each transmitter, i.e., an LED fixture consisting of multiple individual LEDs, is assumed to be capable of communicating independently of other transmitters. Moreover, throughout this chapter, it is assumed that the transmitters know the location or the CSI of U, while not knowing that of PE.

To enhance PLS in VLC systems, we employ a joint technique of beamforming and jamming. The data signal $s(t) \in [-1, 1]$ in time slot t is generated from the DC biased PAM VLC scheme depicted in Figure 2.2 and multiplied by a beamforming weight ω_i ($|\omega_i| \leq 1$) at the ith transmitter for $i \in \{1, 2, ..., N\}$, similarly to the previous chapter. Also, the ith transmitter is assumed to be capable of independently transmitting a jamming signal $j_i(t) \in [-1, 1]$. Note that $j_i(t)$ must be a random value to prevent PE from canceling the jamming component from the received signal. Therefore, the input signal $x_i(t)$ for the ith transmitter can be expressed as

$$x_i(t) = \alpha I_{DC} \left(\omega_i s(t) + \nu_i j_i(t)\right) \tag{4.1}$$

where $\alpha \in [0, 1]$ is termed the modulation index and $I_{DC} \in \mathbb{R}_+$ is a fixed bias current. The parameter ν_i ($\nu_i \geq 0$) is the jamming intensity for the ith transmitter, where $0 \leq \nu_i + |\omega_i| \leq 1$. The input signal $x_i(t)$ is superimposed on a fixed bias current I_{DC}, which is used for illumination. To maintain linear current-to-light conversion, the amplitude of $x_i(t)$ is constrained such that $|x_i(t)| \leq \alpha I_{DC}$. Therefore, the dynamic range of the LED is $I_{DC} \pm \alpha I_{DC}$. Also, $\mathbb{E}[x_i(t)] = 0$ is assumed; thus the data and jamming signals do not affect illumination.

The channel gain $h_{i,k} \in \mathbb{R}_+$ from the ith transmitter to the receiver $k \in \{U, PE\}$

in a VLC system corresponding to an LED with a generalized Lambertian emission pattern is given in (2.1). Moreover, by assuming that a receiver's PD faces up normal to the work plane, i.e., $\phi_{i,k} = \psi_{i,k}$, we can rewrite (2.1) in terms of $l_{i,k}$ as

$$h_{i,k} = \eta \frac{(m+1)A_{\mathrm{PD},k}}{2\pi l_{i,k}^2} \frac{\kappa_k^2}{\sin^2(\Psi_k)} \left(\frac{H}{l_{i,k}}\right)^{(m+1)} R_k T_k = K l_{i,k}^{-(m+3)} \tag{4.2}$$

where $K = \eta(m+1)A_{\mathrm{PD},k}\kappa_k^2 H^{m+1} R_{\mathrm{rsp.},k} T_k / 2\pi \sin^2(\Psi_k)$. Note that (4.2) is valid only when $|\psi_{i,k}| \leq \Psi_k$ is satisfied. Thus, for the sake of simplicity, we assume that all of the receivers are located such that $l_{i,k} \leq H/\cos(\Psi_k)$ is satisfied for all i.

Therefore, the received signal at the receiver k for $k \in \{U, PE\}$ with the joint scheme of beamforming and jamming can be described as

$$y_k(t) = \alpha I_{DC} \mathbf{h}_k^T (\mathbf{w}s(t) + \mathbf{J}\mathbf{v}) + n_k(t) \tag{4.3}$$

where $\mathbf{h}_k = [h_{1,k}, h_{2,k}, ..., h_{N,k}]^T \in \mathbb{R}^N$ denotes the channel gain vector, and $\mathbf{w} = [\omega_1, \omega_2, ..., \omega_N]^T$ and $\mathbf{v} = [\nu_1, \nu_2, ..., \nu_N]^T$ denote the beamforming and jamming intensity vectors, respectively. Also, $\mathbf{J} = \mathrm{diag}(j_1(t), j_2(t), ..., j_N(t))$ is a diagonal jamming signal matrix, and $n_k(t)$ signifies zero-mean AWGN at receiver k with variance σ^2. For notational convenience, the time index t is ignored for the remainder of the chapter.

4.1.2 Performance Measures

For Gaussian VLC MISO channels with amplitude constraints, we define the peak SINR, rather than the average, by assuming $s = 1$ and $\mathbf{J} = \mathbf{I}$ since the channel capacity bounds of VLC systems are expressed as a function of the peak SINR [10,11]. Therefore, the peak SINRs at U and PE with the proposed joint technique can be

written as

$$\gamma_U = \frac{\alpha^2 I_{DC}^2 \mathbf{w}^T \mathbf{H}_U \mathbf{w}}{\alpha^2 I_{DC}^2 \mathbf{v}^T \mathbf{H}_U \mathbf{v} + \sigma^2}, \tag{4.4a}$$

$$\gamma_{PE} = \frac{\alpha^2 I_{DC}^2 \mathbf{w}^\mathbf{T} \mathbf{H}_{PE} \mathbf{w}}{\alpha^2 I_{DC}^2 \mathbf{v}^\mathbf{T} \mathbf{H}_{PE} \mathbf{v} + \sigma^2} \tag{4.4b}$$

respectively, where $\mathbf{H}_U = \mathbf{h}_U \mathbf{h}_U^T$ and $\mathbf{H}_{PE} = \mathbf{h}_{PE} \mathbf{h}_{PE}^T$. We use SINR to denote the peak SINR for the remainder of the chapter.

According to [98], the secrecy capacity of the wiretap channel in (4.3) can be written as

$$C_s = \max_{p_S, p_{J_i} \forall i} (\mathbb{I}(S; Y_U) - \mathbb{I}(S; Y_{PE})), \tag{4.6a}$$

$$\text{s. t.} \begin{cases} |S| \leq 1 \\ |J_i| \leq 1, \quad \forall i \in \{1, 2, ..., N\} \end{cases} \tag{4.6b}$$

where the maximization is performed over all the input distributions $p_S(s)$ and $p_{J_i}(J_i)$ that satisfy the amplitude constraint. However, it is not feasible to deduce a closed-form solution for (4.6) due to the amplitude constraint [69]. It was shown in [69, 70] that the optimal probability distribution p_X, i.e., the solution of the optimization problem (4.6), is unique and discrete with a finite support set, thus it can be efficiently solved using numerical methods. Nevertheless, closed-form expressions are often preferred for engineering systems. In the following, we provide a closed-form expression for an achievable secrecy rate with the joint scheme of beamforming and jamming.

Firstly, to simplify the wiretap channel model in (4.3), we assume that the jammers emit an identical jamming signal, i.e., $\mathbf{J} = j \cdot \mathbf{I}$, where j is a (random) jamming signal. This simplification might weaken the security, but it may be preferred since it permits a simple implementation. In addition, to simplify deriving a closed-form achievable

secrecy rate expression, we assume that both the data signal s and the jamming signal j follow the truncated Gaussian distribution $\mathcal{N}_T(0, \sigma_T^2)$ defined over $[-1, 1]$ as in [15]. Its PDF is given by

$$f(s) = \frac{\phi\left(\frac{s}{\sigma_T}\right)}{\Phi\left(\frac{1}{\sigma_T}\right) - \Phi\left(\frac{-1}{\sigma_T}\right)} \tag{4.7}$$

where $\phi(\upsilon) = e^{-\upsilon^2/2}/\sqrt{2\pi}$, $\Phi(\tau) = (1 + \text{erf}(\tau/\sqrt{2}))/2$ and $\sigma_T \in \mathbb{R}_+$. Note that the optimal input distribution under the amplitude constraint in VLC systems is not readily available, and the truncated Gaussian distribution was shown to outperform the uniform distribution in the terms of secrecy rates in VLC systems [15]. Therefore, from (4.3), the received signals for U and PE with these simplifications can be rewritten as

$$y_U = \alpha I_{DC} \mathbf{h}_U^T \mathbf{w} s + \alpha I_{DC} \mathbf{h}_U^T \mathbf{v} j + n_U, \tag{4.8a}$$

$$y_{PE} = \alpha I_{DC} \mathbf{h}_{PE}^T \mathbf{w} s + \alpha I_{DC} \mathbf{h}_{PE}^T \mathbf{v} j + n_{PE} \tag{4.8b}$$

respectively. We now present the following lemma, which captures an analytic achievable secrecy rate expression for the system in question.

Lemma 3. *An achievable secrecy rate for the Gaussian wiretap channel in (4.8) with the joint technique of beamforming and jamming can be obtained by lower-bounding the secrecy capacity in (4.6) to give*

$$R_s = \max\left\{\frac{1}{2}\log\left(\frac{e^{2\eta}\left(\mathbf{w}^T\mathbf{H}_U\mathbf{w} + \mathbf{v}^T\mathbf{H}_U\mathbf{v}\right) + C}{\varphi\mathbf{v}^T\mathbf{H}_U\mathbf{v} + C}\right) - \frac{1}{2}\log\left(\frac{\varphi\left(\mathbf{w}^\mathbf{T}\mathbf{H}_{PE}\mathbf{w} + \mathbf{v}^\mathbf{T}\mathbf{H}_{PE}\mathbf{v}\right)}{e^{2\eta}\mathbf{v}^\mathbf{T}\mathbf{H}_{PE}\mathbf{v}}\right), 0\right\} \tag{4.9}$$

where

$$\eta = \log(Z) + \frac{-\frac{1}{\sigma_T}\phi\left(\frac{-1}{\sigma_T}\right) - \frac{1}{\sigma_T}\phi\left(\frac{1}{\sigma_T}\right)}{2Z},$$

$$\varphi = 1 + \frac{\frac{-1}{\sigma_T}\phi\left(\frac{-1}{\sigma_T}\right) - \frac{1}{\sigma_T}\phi\left(\frac{1}{\sigma_T}\right)}{Z} - \left(\frac{\phi\left(\frac{-1}{\sigma_T}\right) - \phi\left(\frac{1}{\sigma_T}\right)}{Z}\right)^2,$$

$$Z = \Phi\left(\frac{1}{\sigma_T}\right) - \Phi\left(\frac{-1}{\sigma_T}\right),$$

$$C = \frac{\sigma^2}{\alpha^2 I_{DC}^2 \sigma_T^2}.$$

Proof. See Appendix 4.A.1. □

4.2 The Joint Strategy of Beamforming and Jamming

4.2.1 Optimization of the Joint Strategy Based on SINR

Without knowledge of the location or the CSI of PE, a natural objective is to maximize the SINR of U subject to a constraint on the *average* SINR of PE, the same as in RF communications [80, 81]. Therefore, in this subsection, we investigate the selection of $\mathbf{w}$ and $\mathbf{v}$ that maximize γ_U subject to a constraint on $\mathbb{E}_{\mathbf{h}_{PE}}[\gamma_{PE}]$.

From the SINR definitions of (4.4), we can formulate the problem of interest as

$$\arg\max_{\mathbf{w},\mathbf{v}} \frac{\alpha^2 I_{DC}^2 \mathbf{w}^T \mathbf{H}_U \mathbf{w}}{\alpha^2 I_{DC}^2 \mathbf{v}^T \mathbf{H}_U \mathbf{v} + \sigma^2} \tag{4.10a}$$

$$\text{s. t.} \begin{cases} \mathbb{E}_{\mathbf{h}_{PE}}\left[\dfrac{\alpha^2 I_{DC}^2 \mathbf{w}^{\mathbf{T}} \mathbf{H}_{PE} \mathbf{w}}{\alpha^2 I_{DC}^2 \mathbf{v}^{\mathbf{T}} \mathbf{H}_{PE} \mathbf{v} + \sigma^2}\right] \leq \rho_{PE} \\ |\mathbf{w}| + \mathbf{v} \preceq \mathbb{1} \\ \mathbf{v} \succeq \mathbb{0}. \end{cases} \tag{4.10b}$$

where ρ_{PE} is the target constraint on $\mathbb{E}_{\mathbf{h}_{PE}}[\gamma_{PE}]$. However, due to the fact that the first constraint does not lead to a tractable analysis, we propose a suboptimal approach by replacing the left term of the first constraint with the ratio of the average received data power to the average interference plus noise power[2], i.e.,

$$\overline{\gamma}_{PE} \coloneqq \frac{\mathbb{E}_{\mathbf{h}_{PE}}\left[\alpha^2 I_{DC}^2 \mathbf{w}^{\mathbf{T}} \mathbf{H}_{PE} \mathbf{w}\right]}{\mathbb{E}_{\mathbf{h}_{PE}}\left[\alpha^2 I_{DC}^2 \mathbf{v}^{\mathbf{T}} \mathbf{H}_{PE} \mathbf{v} + \sigma^2\right]} = \frac{\alpha^2 I_{DC}^2 \mathbf{w}^{\mathbf{T}} \overline{\mathbf{H}}_{PE} \mathbf{w}}{\alpha^2 I_{DC}^2 \mathbf{v}^{\mathbf{T}} \overline{\mathbf{H}}_{PE} \mathbf{v} + \sigma^2} \tag{4.11}$$

where $\overline{\mathbf{H}}_{PE} = \mathbb{E}_{\mathbf{h}_{PE}}[\mathbf{h}_{PE}\mathbf{h}_{PE}^T]$. The element in the ith row and jth column of $\overline{\mathbf{H}}_{PE}$ is given by

$$\overline{H}_{PE_{i,j}} = \frac{1}{L \cdot W} \int_{\frac{-L}{2}}^{\frac{L}{2}} \int_{\frac{-W}{2}}^{\frac{W}{2}} \frac{K^2}{l_i^{m+3}(x,y) l_j^{m+3}(x,y)} \, \mathrm{d}x \, \mathrm{d}y \tag{4.12}$$

where $l_i(x,y)$ for $i \in \{1, 2, \cdots, N\}$ is the distance between the ith transmitter and the point (x,y) in the work plane.

It is worth noting that $\overline{\rho}_{PE}$ is a system parameter to be appropriately chosen according to given VLC environments, such as a particular distribution of LED transmitters, the location of the UE, the LED transmit power, etc. A lower value of $\overline{\rho}_{PE}$ imposes a stricter constraint on the average SINR of PE. With a higher value of $\overline{\rho}_{PE}$, the situation is reversed. For example, suppose $\overline{\rho}_{PE}$ is set too low. In that case, the LED transmitters should reduce the information transmit power or increase the jamming transmit power to satisfy the $\overline{\rho}_{PE}$ constraint. Still, the received signal power at the UE site would also be reduced in a commensurate manner. On the other hand, if the UE is located very close to one of the LED transmitters, the closest LED transmitter to the UE can increase its information transmit power to increase the SNR of the UE while simultaneously satisfying the $\overline{\rho}_{PE}$ constraint. PLS theories suggest choosing the value of $\overline{\rho}_{PE}$ in a way that makes the SNR difference between

[2]Note that $\overline{\gamma}_{PE}$ does not approximate to the expectation of γ_{PE}, i.e., $\mathbb{E}_{\mathbf{h}_{PE}}[\gamma_{PE}]$. For example, when 6×6 LEDs and a room of 30×30 m^2 are assumed, $\overline{\gamma}_{PE} = 0.07$ and $\mathbb{E}_{\mathbf{h}_{PE}}[\gamma_{PE}] = 3.17$ are numerically evaluated. However, as we will see in the following, $\overline{\gamma}_{PE}$ is a very effective metric for suppressing the information reception and increasing the interference at PE, while significantly simplifying the optimization problem.

the UE and the PEDs as large as possible [5].

Now, we consider the optimization problem given by

$$\arg\max_{\mathbf{w},\mathbf{v}} \frac{\alpha^2 I_{DC}^2 \mathbf{w}^T \mathbf{H}_U \mathbf{w}}{\alpha^2 I_{DC}^2 \mathbf{v}^T \mathbf{H}_U \mathbf{v} + \sigma^2} \tag{4.13a}$$

$$\text{s. t.} \begin{cases} \dfrac{\alpha^2 I_{DC}^2 \mathbf{w}^{\mathbf{T}} \overline{\mathbf{H}}_{PE} \mathbf{w}}{\alpha^2 I_{DC}^2 \mathbf{v}^{\mathbf{T}} \overline{\mathbf{H}}_{PE} \mathbf{v} + \sigma^2} \leq \overline{\rho}_{PE} \\ |\mathbf{w}| + \mathbf{v} \preceq \mathbb{1} \\ \mathbf{v} \succeq \mathbb{0}. \end{cases} \tag{4.13b}$$

where $\overline{\rho}_{PE}$ is the target constraint on $\overline{\gamma}_{PE}$. Utilizing the Charnes-Cooper transformation [99], we can simplify the objective function (4.13a). First, we define

$$\mathbf{w} = \frac{\tilde{\mathbf{w}}}{\xi}, \ \mathbf{v} = \frac{\tilde{\mathbf{v}}}{\xi} \tag{4.14}$$

where $\xi > 0$. Then, by plugging (4.14) into (4.13) and setting $\xi = \sqrt{1 - \alpha^2 I_{DC}^2 \tilde{\mathbf{v}}^{\mathbf{T}} \mathbf{H}_U \tilde{\mathbf{v}}}/\sigma$, the quadratic fractional optimization problem (4.13) can be simplified to the non-fractional problem

$$\arg\max_{\tilde{\mathbf{w}},\tilde{\mathbf{v}}} \alpha^2 I_{DC}^2 \tilde{\mathbf{w}}^T \mathbf{H}_U \tilde{\mathbf{w}} \tag{4.15a}$$

$$\text{s. t.} \begin{cases} \alpha^2 I_{DC}^2 \tilde{\mathbf{w}}^T \overline{\mathbf{H}}_{PE} \tilde{\mathbf{w}} - \overline{\rho}_{PE} + \rho_{PE} \alpha^2 I_{DC}^2 \tilde{\mathbf{v}}^T \mathbf{H}_U \tilde{\mathbf{v}} \leq \overline{\rho}_{PE} \alpha^2 I_{DC}^2 \tilde{\mathbf{v}}^T \overline{\mathbf{H}}_{PE} \tilde{\mathbf{v}} \\ |\tilde{\mathbf{w}}| + \tilde{\mathbf{v}} \preceq \mathbb{1} \cdot \sqrt{1 - \alpha^2 I_{DC}^2 \tilde{\mathbf{v}}^T \mathbf{H}_U \tilde{\mathbf{v}}}/\sigma \\ \tilde{\mathbf{v}} \succeq \mathbb{0}. \end{cases} \tag{4.15b}$$

Here, the difficulty of solving (4.15) arises from the fact that it requires the maximization of a convex quadratic objective function and the right side of the first constraint yields a non-convex set. Thus, we apply the CCP approach [26], which is a powerful heuristic method to find a local solution. Given initial feasible points $\tilde{\mathbf{w}}_0$ and $\tilde{\mathbf{v}}_0$, we transform the objective function and the non-convex function in the first constraint

Algorithm 2 CCP algorithms for solving (4.15)

given initial feasible points $\tilde{\mathbf{w}}_0$ and $\tilde{\mathbf{v}}_0$, $k := 0$

repeat

1. *Convexify.* Form

$$g_0(\tilde{\mathbf{w}}; \tilde{\mathbf{w}}_k) \triangleq \alpha^2 I_{DC}^2 \tilde{\mathbf{w}}_k^{\mathrm{T}} \mathbf{H}_U \tilde{\mathbf{w}}_k + 2(\alpha^2 I_{DC}^2 \mathbf{H}_U \tilde{\mathbf{w}}_k)^T (\tilde{\mathbf{w}} - \tilde{\mathbf{w}}_k),$$
$$g_1(\tilde{\mathbf{v}}; \tilde{\mathbf{v}}_k) \triangleq \overline{\rho}_{PE} \alpha^2 I_{DC}^2 \tilde{\mathbf{v}}_k^{\mathrm{T}} \overline{\mathbf{H}}_{PE} \tilde{\mathbf{v}}_k + 2\overline{\rho}_{PE} (\alpha^2 I_{DC}^2 \overline{\mathbf{H}}_{PE} \tilde{v}_k)^T (\tilde{\mathbf{v}} - \tilde{\mathbf{v}}_k)$$

2. *Solve.* Set the value of $\tilde{\mathbf{w}}_{k+1}$ and $\tilde{\mathbf{v}}_{k+1}$ to solutions of the convex problem

$$\arg\max_{\tilde{\mathbf{w}}, \tilde{\mathbf{v}}} \; g_0(\tilde{\mathbf{w}}; \tilde{\mathbf{w}}_k)$$
$$\text{s.t.} \begin{cases} \alpha^2 I_{DC}^2 \tilde{\mathbf{w}}^T \overline{\mathbf{H}}_{PE} \tilde{\mathbf{w}} - \overline{\rho}_{PE} + \rho_{PE} \alpha^2 I_{DC}^2 \tilde{\mathbf{v}}^T \mathbf{H}_U \tilde{\mathbf{v}} \le g_1(\tilde{\mathbf{v}}; \tilde{\mathbf{v}}_k) \\ |\tilde{\mathbf{w}}| + \tilde{\mathbf{v}} \le \mathbb{1} \cdot \dfrac{\sqrt{1 - \alpha^2 I_{DC}^2 \tilde{\mathbf{v}}^T \mathbf{H}_U \tilde{\mathbf{v}}}}{\sigma} \\ \tilde{\mathbf{v}} \ge \mathbb{0} \end{cases}$$

3. *Update iteration.* $k := k + 1$.

until stopping criterion is satisfied.

into affine functions (i.e., convex) by calculating the first-order Taylor approximation. We then solve the convex optimization problem by using a standard optimization programming like the sequential quadratic program (SQP) algorithm [100]. Next, we set the solution to $\tilde{\mathbf{w}}_1$ and $\tilde{\mathbf{v}}_1$ and repeat the same procedure until the improvement in the objective value is less than a predefined threshold ϵ. The details of this iterative algorithm are given in Algorithm 2. Since the CCP is a local heuristic, the final solution depends on the initial points $\tilde{\mathbf{w}}_0$ and $\tilde{\mathbf{v}}_0$. Therefore, it is wise to start the algorithm with several initial points and take as the final choice denoted by $\tilde{\mathbf{w}}^*$ and $\tilde{\mathbf{v}}^*$ which maximizes the objective function. On the other hand, it is worth noting that the initial points can be somewhat anticipated according to the location of the UE, since it is expected that the beamforming weights are relatively high for the transmitters that are near to the UE, while the jamming intensities are relatively high for the transmitters that are far away from the UE.

Finally, from (4.14), we can obtain the optimal solution to the original problem

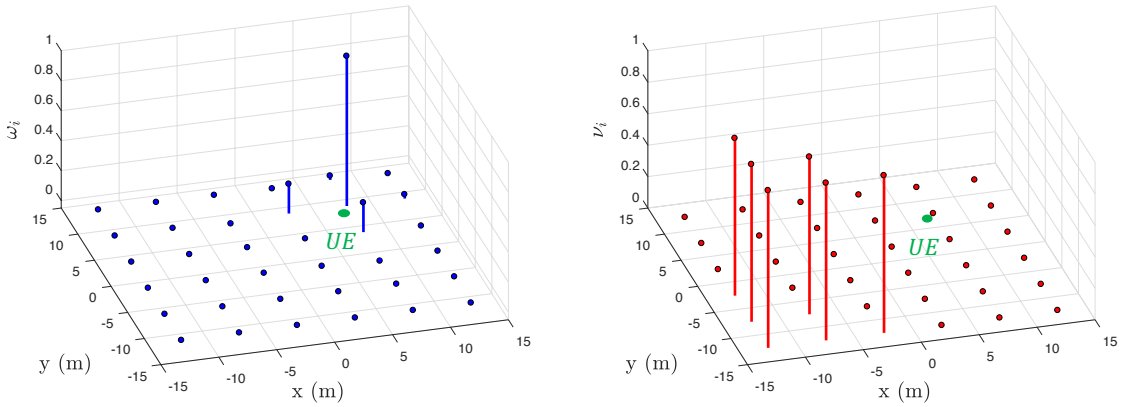
in (4.13) by computing

$$\mathbf{w}^* = \frac{\sigma\tilde{\mathbf{w}}^*}{\sqrt{1-\alpha^2 I_{DC}^2 \tilde{\mathbf{v}}^{*T}\mathbf{H}_U\tilde{\mathbf{v}}^*}},\ \mathbf{v}^* = \frac{\sigma\tilde{\mathbf{v}}^*}{\sqrt{1-\alpha^2 I_{DC}^2 \tilde{\mathbf{v}}^{*T}\mathbf{H}_U\tilde{\mathbf{v}}^*}}. \tag{4.16}$$

4.2.2 Beamforming and Jamming Characteristics

In the previous section, we showed that the beamforming weight and jamming intensity vectors of the optimization problem (4.13), which is based on the SINR, can be effectively found by utilizing the Charnes-Cooper transformation and the CCP. However, this approach suffers from considerable computational overhead as well as a large number of iterations when the number of LED transmitters is large. Because, as we will see later, the joint scheme will be more useful in a huge room consisting of a large number of transmitters, the complexity of finding the beamforming and jamming vectors must be reduced. Therefore, in this subsection, we investigate the characteristics of the beamforming weights and jamming intensities according to the relative locations among the transmitters and the UE. This investigation will enable us to propose a simple ternary scheme in the next section.

Figures 4.2(a) and (b) show an example of the beamforming weights and the jamming intensities of the transmitters according to the locations of the transmitters, which are obtained by solving (4.13). We assume that 6×6 transmitters are located at (x_T, y_T, H) for $x_T, y_T \in \{\pm 2.5, \pm 7.5, \pm 12.5\}$. Also, we assume that one fixed U is located at $(7, 7, 0)$ and one PE is randomly located in the work plane of the room. Other system parameters are given in Table 4.1 in Section 4.5. It is shown that the beamforming weights of the transmitters being located near to the UE are high, while those of the other transmitters are almost zero. In contrast, the jamming intensities of the transmitters being located near to the UE are zero, while those of other transmitters are close to one. Thus, this result verifies that when the transmitters do not retain the information on the location or the CSI of an ED, transmitting data only



(a) The beamforming weight ω_i. (b) The jamming intensity v_i.

Figure 4.2. The values of beamforming weights and jamming intensities according to the locations of different LED transmitters. They are obtained from the optimization problem (4.13). The UE is located at $(7, 7, 0)$. The 6×6 LED transmitters are located at (x_T, y_T, H) for $x_T, y_T \in \{\pm 2.5, \pm 7.5, \pm 12.5\}$. $L = 30$ m, $W = 30$ m, $H = 2.2$ m, $\phi_{1/2} = 60°$ and $\overline{\rho}_{PE} = 0.15$ are used.

by the transmitters being located near to the UE and emitting jamming signals by the faraway transmitters would effectively increase the secrecy performance. In other words, simultaneously transmitting information and jamming signals from the same transmitter would be unusual.

4.3 The Ternary Strategy Based on SINR

As a result of the observations noted in Section 4.2.2, we propose a simple ternary strategy in which the transmitter selects its role among an information transmitter, a jammer or just being silent. In other words, when the transmitter acts as the information transmitter, their beamforming weights are always one, while their jamming intensities are always zero. For jammers, the situation is reversed. Also, a transmitter can remain silent if need be.

In the proposed scheme, the beamforming weights ω_i and the jamming intensities v_i for all $i \in \{1, 2, ..., N\}$ have to be an element of $\{0, 1\}$, subject to $w_i + v_i \leq 1$.

Changing the continuous optimization variables $\mathbf{w}$ and $\mathbf{v}$ in the joint scheme to the binary ones in the ternary scheme can significantly reduce the optimization problem's complexity, which would provide much practical implementation approaches. Thus, we will investigate the assignment optimization problem for the ternary strategy based on the SINR metric, which can be effectively solved by TS [101], which is a meta-heuristic method utilizing local search procedures to find the local optimal solutions. Here, a *meta-heuristic* denotes a higher-level procedure or heuristic algorithm devised to find, generate, or select a partial search algorithm that may provide a sufficiently good solution to an optimization problem, especially with incomplete or imperfect information or limited computation capacity [102].

The optimization problem for the joint scheme based on the SINR (4.13) can be modified under the ternary strategy as

$$\arg\max_{\mathbf{w},\mathbf{v}} \frac{\alpha^2 I_{DC}^2 \mathbf{w}^T \mathbf{H}_U \mathbf{w}}{\alpha^2 I_{DC}^2 \mathbf{v}^T \mathbf{H}_U \mathbf{v} + \sigma^2} \tag{4.17a}$$

$$\text{s.t.} \begin{cases} \dfrac{\alpha^2 I_{DC}^2 \mathbf{w}^{\mathbf{T}} \overline{\mathbf{H}}_{PE} \mathbf{w}}{\alpha^2 I_{DC}^2 \mathbf{v}^{\mathbf{T}} \overline{\mathbf{H}}_{PE} \mathbf{v} + \sigma^2} \leq \overline{\rho}_{PE} \\ |\mathbf{w}| + \mathbf{v} \preceq \mathbb{1} \\ \omega_i,\ v_i \in \{0,1\} \quad \text{for all } i \in \{1,2,...,N\}. \end{cases} \tag{4.17b}$$

A fractional quadratic assignment optimization problem like (4.17) was shown to be NP-hard [103]; thus, it would not be feasible to find an optimal point of (4.17) via a deterministic method. Therefore, we employ TS to find the local optimal solutions $\mathbf{w}^*$ and $\mathbf{v}^*$ of (4.17), where this method uses a local or neighborhood search procedure to iteratively move from one potential solution, e.g., x, to an improved solution x' in the neighborhood of x, until some stopping criterion has been satisfied. TS is designed to prevent a search procedure from becoming trapped at locally optimal solutions by utilizing short-term memory. We implement the TS procedure via MATLAB according to the following specific procedure.

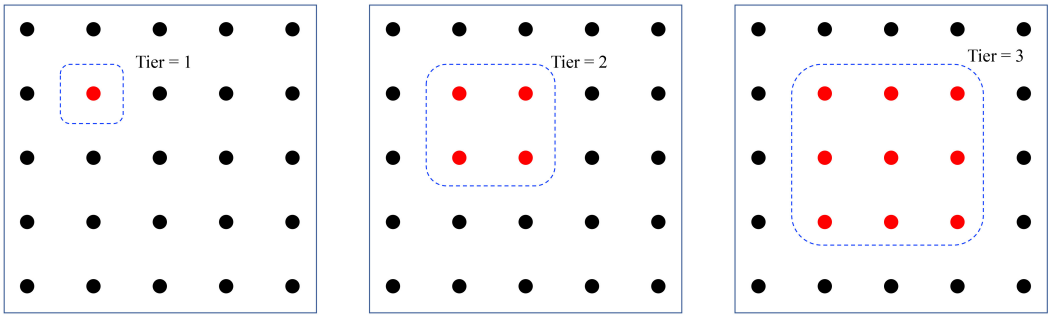
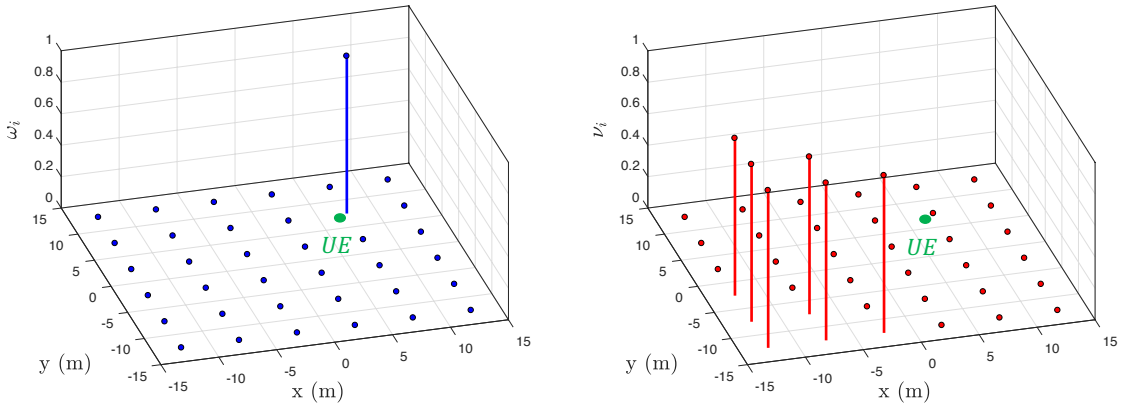


Figure 4.3. Examples of tier groups. The move of the TS changes the roles of transmitters in a tier group.

The TS procedure begins with the initial point $\{\mathbf{w}^*_{(0)}, \mathbf{v}^*_{(0)}\}$ in which the transmitters near to the UE are set as information transmitters, i.e., $\omega_i = 1$, while the others are set as jammers, i.e., $\nu_i = 1$. Setting the initial point in this way comes from the observation in Section 4.2.2 that the transmitters near to the UE are likely to act as information transmitters, while the distant transmitters are likely to act as jammers.

Then, a set of neighboring solutions $N(\{\mathbf{w}^*_{(0)}, \mathbf{v}^*_{(0)}\})$ are generated by applying a set of possible *moves* to $\{\mathbf{w}^*_{(0)}, \mathbf{v}^*_{(0)}\}$. The set of possible moves includes "set information transmitters", "set jammers", "set silent transmitters" and "swap roles". Since the roles of the transmitters largely depend on their locations with respect to the UE, it can be anticipated that the roles of the transmitters being located near to each other would be identical. Thus, we enable the moves to change the roles of the transmitters in a tier group as shown in Figure 4.3. With these grouping moves, we can reduce the possibility that the search procedure is trapped at a local solution. Note that the efficiency and performance of a TS procedure strongly depend on the way that the moves are defined and how well the moves exploit the actual structure of the problem [101].

Next, among the neighborhood solutions $N(\{\mathbf{w}^*_{(0)}, \mathbf{v}^*_{(0)}\})$, the best solution in the terms of maximizing the objective function is selected as the iterate $\{\mathbf{w}^*_{(1)}, \mathbf{v}^*_{(1)}\}$ even if the value of the objective function with $\{\mathbf{w}^*_{(1)}, \mathbf{v}^*_{(1)}\}$ is less than the value with $\{\mathbf{w}^*_{(0)}, \mathbf{v}^*_{(0)}\}$. Also, in order to prevent cycling and to try to escape from local optima,



(a) The beamforming weight ω_i. (b) The jamming intensity ν_i.

Figure 4.4. The beamforming and jamming vectors with the ternary scheme obtained from the assignment optimization problem (4.17). the UE is located at $(7, 7, 0)$. The 6×6 LED transmitters are located at (x_T, y_T, H) for $x_T, y_T \in \{\pm 2.5, \pm 7.5, \pm 12.5\}$. $L = 30$ m, $W = 30$ m, $H = 2.2$ m, $\phi_{1/2} = 60°$ and $\overline{\rho}_{PE} = 0.15$ are used.

the list of tabu moves is maintained. This list forbids the opposite move that has been made at a given step for a certain number of iterations L, which is the length of the tabu list. In addition, if the move added to the tabu list yields an improved solution larger than "aspiration criteria", the move can be made, and its solution can be selected as the best solution for the next iteration.

This procedure repeats for a maximum number of iterations. At each iteration, the best solution $\{\mathbf{w}^*_{(i)}, \mathbf{v}^*_{(i)}\}$ in terms of maximizing the objective of (4.17) and its value of the objective function are stored, and the best solution among them is returned as the final optimal solution.

Figure 4.4 shows the beamforming weights and jamming intensities found via TS under the ternary scheme. It is shown that they are similar to the result in Figure 4.2, except that the values of beamforming weights and jamming intensities are either 1 or 0. Note that on a standard PC (Intel i7, 3.4 GHz) using MATLAB, finding a solution via TS can be executed in a few seconds, while the CCP for solving (4.13) requires hundreds of seconds, including the time for iterations with multiple different initial points, when $N = 36$. Besides, it would be worth mentioning that from

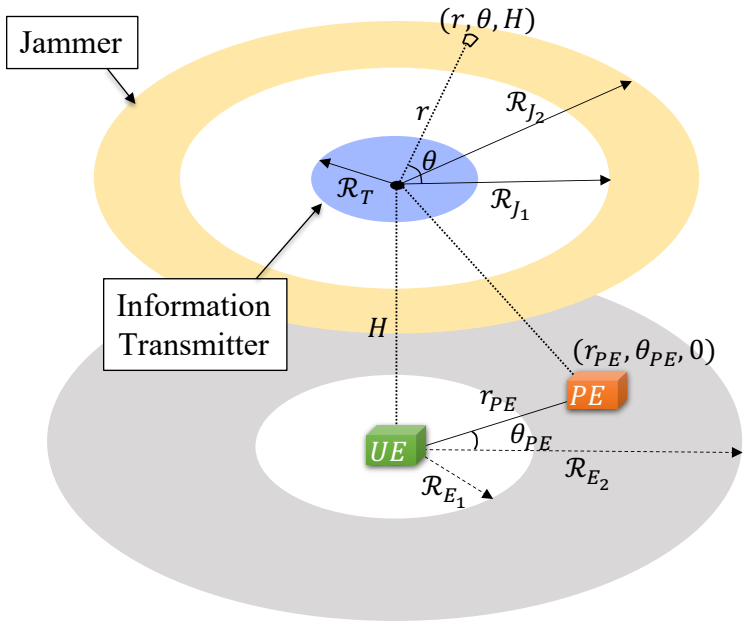


Figure 4.5. Geometry of the ternary scheme with the continuous LED model. The blue shaded circular plane centered at the UE denotes the LEDs that act as the information transmitters, while the yellow annulus denotes the jammers.

the computational complexity point of view, continuous optimization problems, in general, can be considered relatively easy to solve, although they may still be very challenging. However, combinatorial (assignment) problems can be really hard, often NP-hard [104]. In this section, in a reverse manner, we transformed the continuous optimization problem (4.10) to the combinatorial problem (4.17) to reduce the computational complexity. This advantage of the lower complexity was possible since we effectively exploited the VLC channel characteristics and the environmental factors to help the TS algorithm reach the near-optimal solution quickly.

4.4 Optimization Based on Secrecy Rate with the Continuum Model

In this section, we consider a continuum model of the system in an effort to investigate the average secrecy rate with the ternary scheme. Note that, to the best of our knowl-

edge, with the discrete transmitter model described in Figure 4.1, it is only possible to solve the maximum-SINR problem; a solution to the maximum-average-secrecy-rate problem remains elusive. This is due to the fact that the optimization problem is not convex in the $2N$ variables (where N can be large) to be optimized. Furthermore, $\mathbb{E}_{\mathbf{h}_{PE}}[R_s]$ is difficult to evaluate owing to the terms $\mathbf{w}^T\mathbf{H}_{PE}\mathbf{w}$ and $\mathbf{v}^T\mathbf{H}_{PE}\mathbf{v}$, where each element of $\mathbf{H}_{PE}$ is a function of $h_{i,PE}$ as (4.12). However, by utilizing the continuum model, we can make the optimization problem simple enough to be numerically analyzed as we will see below.

Figure 4.5 illustrates the geometry of the continuum model, where an infinite number of LEDs are assumed to be attached to the ceiling in an infinitely large room, and their distances among LEDs are infinitesimal. In practice, a lot of multiple LEDs are uniformly and widely distributed to evenly illuminate an entire room within the lighting standards, e.g., from 400 to 1000 lux for a typical office [86]. Thus, the continuum model can describe practical VLC systems and is able to provide analytic insight into the secrecy performance of the ternary strategy. Without loss of generality, we assume that U is located at the origin and PE is located in a gray annulus with inner radius $\mathcal{R}_{E_1}$ and outer radius $\mathcal{R}_{E_2}$. This assumption can be justified since PE would like to be located not too near to U to escape the vigilance of a UE and not too far from the UE to wiretap the information signal. The blue shaded circular plane with radius $\mathcal{R}_T$ centered at the UE denotes the LEDs that act as the information transmitters, while the yellow annulus with inner radius $\mathcal{R}_{J_1}$ and outer radius $\mathcal{R}_{J_2}$ denotes the jammers. The white annulus indicates the LEDs that are silent.

4.4.1 Received Optical Power Density Analysis

In the continuum model, to deal with the infinite number of LEDs, we characterize the emitted optical power of LEDs by the optical power density per unit of LED

area P_T [W/m^2]. We assume that the information transmitter and the jammer emit signals with the same optical power density.

Firstly, the received optical power density of the data signal emitted by the information transmitters, i.e., the blue shaded plane, P_D [W/m^2] at $(r_{PE}, \theta_{PE}, 0)$ can be described by

$$\begin{aligned} P_D(r_{PE}, \theta_{PE}) &= \int_0^{\mathcal{R}_T} \int_0^{2\pi} P_T \frac{(m+1)}{2\pi l_{PE}^2} \left(\frac{H}{l_{PE}}\right)^{(m+1)} r \, \mathrm{d}\theta \, \mathrm{d}r \\ &\overset{(a)}{=} \frac{P_T}{2} \left(1 + \frac{\mathcal{R}_T^2 - H^2 - r_{PE}^2}{\sqrt{(H^2 + \mathcal{R}_T^2)^2 + 2r_{PE}^2(H^2 - \mathcal{R}_T^2) + r_{PE}^4}}\right) \end{aligned} \tag{4.18}$$

where $l_{PE} = \sqrt{r^2 + r_{PE}^2 - 2rr_{PE}\cos(\theta - \theta_{PE}) + H^2}$ is the distance between the differential transmitter and the point $(r_{PE}, \theta_{PE}, 0)$. Also, for equality (a) in (4.18) and the following analysis, we assume all of the LED transmitters have the perfect *Lambertian* emission pattern with $\phi_{1/2} = 60^\circ$ $(m = 1)$, which is the most commonly considered light source pattern to illuminate the entire room evenly as in [10, 18, 105]. Note that the value of $P_D(r_{PE}, \theta_{PE})$ is independent of θ_{PE}; thus we replace the notation of $P_D(r_{PE}, \theta_{PE})$ with $P_D(r_{PE})$.

In addition, the received optical power density of the jamming signal emitted by the jammers, i.e., the yellow annulus, P_J [W/m^2] at $(r_{PE}, \theta_{PE}, 0)$ can be described as

$$\begin{aligned} P_J(r_{PE}, \theta_{PE}) &= \int_{\mathcal{R}_{J_1}}^{\mathcal{R}_{J_2}} \int_0^{2\pi} P_T \frac{(m+1)}{2\pi l_{PE}^2} \left(\frac{H}{l_{PE}}\right)^{(m+1)} r \, \mathrm{d}\theta \, \mathrm{d}r \\ &= \frac{P_T}{2} \left(\frac{H^2 - \mathcal{R}_{J_1}^2 + r_{PE}^2}{\sqrt{H^4 + \left(\mathcal{R}_{J_1}^2 - r_{PE}^2\right)^2 + 2H^2\left(\mathcal{R}_{J_1}^2 + r_{PE}^2\right)}} \right. \\ &\qquad \left. - \frac{H^2 - \mathcal{R}_{J_2}^2 + r_{PE}^2}{\sqrt{H^4 + \left(\mathcal{R}_{J_2}^2 - r_{PE}^2\right)^2 + 2H^2\left(\mathcal{R}_{J_2}^2 + r_{PE}^2\right)}} \right). \end{aligned} \tag{4.19}$$

Similarly, we replace the notation of $P_J(r_{PE}, \theta_{PE})$ with $P_J(r_{PE})$.

4.4.2 SINR and Secrecy Rate Analysis

With the same simplifications assumed in (4.8), the received signals for U at the origin and PE at $(r_{PE}, \theta_{PE}, 0)$ with the ternary scheme can be rewritten as

$$y_U(t) = \zeta_U P_D(0)\hat{x} + \zeta_U P_J(0)\hat{j} + n_U, \tag{4.20a}$$

$$y_{PE}(t) = \zeta_{PE} P_D(r_{PE})\hat{x} + \zeta_{PE} P_J(r_{PE})\hat{j} + n_{PE} \tag{4.20b}$$

respectively, where $\zeta_k = \alpha A_{\mathrm{PD},k} \kappa_k^2 R_{\mathrm{rsp.},k} T_k / \sin^2(\Psi_k)$ ($\mathrm{m}^2 \cdot \mathrm{V/W}$) for $k \in \{U, PE\}$, and $\hat{x} = x/(1[\mathrm{A}])$ and $\hat{j} = j/(1[\mathrm{A}])$ signifies the normalized (dimensionless) versions of x and j, respectively. Also, the secrecy rate expression under the ternary scheme in (4.9) can be rewritten with the continuum model as

$$\begin{aligned} R_{s,\mathrm{cont.}}(r_{PE}) = \max \Bigg\{ & \frac{1}{2} \log \left(\frac{e^{2\eta}(P_D^2(0) + P_J^2(0)) + D}{\varphi P_J^2(0) + D} \right) \\ & - \frac{1}{2} \log \left(\frac{\varphi(P_D^2(r_{PE}) + P_J^2(r_{PE}))}{e^{2\eta} P_J^2(r_{PE})} \right), 0 \Bigg\} \end{aligned} \tag{4.21}$$

where $D = \sigma^2 / \sigma_T^2 \zeta_U^2$.

4.4.3 Optimization Based on Average Secrecy Rate

Since the location of the ED is unknown at the transmitters, with only its statistical information being available, we can numerically calculate the *average* secrecy rate as

$$\begin{aligned} \overline{R}_{s,\mathrm{cont.}} &= \int_{\mathcal{R}_{E_1}}^{\mathcal{R}_{E_2}} f_{r_{PE}}(r) R_{s,\mathrm{cont.}}(r)\, \mathrm{d}r \\ &= \int_{\mathcal{R}_{E_1}}^{\mathcal{R}_{E_2}} \frac{2r}{\mathcal{R}_{E_2}^2 - \mathcal{R}_{E_1}^2} R_{s,\mathrm{cont.}}(r)\, \mathrm{d}r \end{aligned} \tag{4.22}$$

where $f_{r_{PE}}(r) = 2r/(\mathcal{R}_{E_2}^2 - \mathcal{R}_{E_1}^2)$ denotes the PDF of the ED location. The problem of maximizing the average secrecy rate (4.23) can be formulated as

$$\overline{R}_{s,\text{cont.}}^{\star} = \max_{\mathcal{R}_T, \mathcal{R}_{J_1}, \mathcal{R}_{J_2}} \overline{R}_{s,\text{cont.}} \tag{4.23}$$
$$\text{s.t.} \quad 0 \leq \mathcal{R}_T \leq \mathcal{R}_{J_1} \leq \mathcal{R}_{J_2}.$$

Note that the optimization problem (4.23) is also a non-convex problem, and the objective function includes the integration to be solved numerically. However, the continuum model significantly reduces the problem from finding the optimal beamforming and jamming vectors consisting of $2N$ elements in the discrete model to finding only three variables, i.e., $\mathcal{R}_T$, $\mathcal{R}_{J_1}$ and $\mathcal{R}_{J_2}$. Moreover, $\overline{R}_{s,\text{cont.}}^{\star}$ includes only a one-dimensional integral. In practice, finding the optimal solutions of the three parameters via the SQP algorithm can be executed in a second on a standard PC (Intel i7, 3.4 GHz) using MATLAB.

4.4.4 Link Between the Continuum and Discrete Cases

In this subsection, we provide guidelines on how to apply the three parameters $\mathcal{R}_T$, $\mathcal{R}_{J_1}$ and $\mathcal{R}_{J_2}$ obtained from the continuum model to a real VLC system, that is, the discrete model. To transform the continuous model to the discrete model in a straightforward manner, we set the roles of the discrete transmitters in minimizing the sum of the distances between the continuous and discrete transmitters. More specifically, assuming that the UE is located at the origin of our coordinate system and N LED transmitters are uniformly distributed over the entire room, selecting the jammers is executed as

$$\mathcal{J}^* = \min_{\mathcal{J}} \sum_{i \in \mathcal{J}} d_{J,i}$$

$$\text{s. t.} \, |\mathcal{J}| = N_J \tag{4.24}$$

where $N_J = \left\lfloor \pi(\mathcal{R}_{J_2}^2 - \mathcal{R}_{J_1}^2) P_T / (I_{DC}\eta) \right\rceil$ denotes the number of the jammers and $\mathcal{J} = \{j_1, j_2, ..., j_{N_J}\}$ for $j_i \in \{1, 2, ..., N\}$ denotes the index set of the jammers. Also, $d_{J,i}$ denotes the shortest distances between the discrete transmitters and the continuous set of the jammers, which can be defined as

$$d_{J,i} = \begin{cases} \mathcal{R}_{J_1} - \sqrt{x_i^2 + y_i^2} & \text{for} \quad 0 \le \sqrt{x_i^2 + y_i^2} < \mathcal{R}_{J_1}, \\ 0 & \text{for} \quad \mathcal{R}_{J_1} \le \sqrt{x_i^2 + y_i^2} < \mathcal{R}_{J_2}, \\ \sqrt{x_i^2 + y_i^2} - \mathcal{R}_{J_2} & \text{for} \quad \mathcal{R}_{J_2} \le \sqrt{x_i^2 + y_i^2} \end{cases} \tag{4.25}$$

where $\{x_i, y_i\}$ for $i \in \{1, 2, ..., N\}$ denotes the coordinates of the transmitters.

In addition, selecting the information transmitters can be similarly executed as

$$\begin{aligned} \mathcal{T}^* &= \min_{\mathcal{T}} \sum_{i \in \mathcal{T}} d_{T,i} \\ &\text{s. t.} \, |\mathcal{T}| = N_T \end{aligned} \tag{4.26}$$

where $N_T = \left\lfloor \pi \mathcal{R}_T^2 P_T / (I_{DC}\eta) \right\rceil$ denotes the number of the information transmitters and $\mathcal{T} = \{t_1, t_2, ..., t_{N_T}\}$ for $t_i \in \{1, 2, ..., N\}$ denotes the index set of the transmitters. $d_{T,i}$ denotes the shortest distances between the discrete transmitters and the continuous set of transmitters, which can be defined as

$$d_{T,i} = \begin{cases} 0 & \text{for} \quad 0 \le \sqrt{x_i^2 + y_i^2} < \mathcal{R}_T, \\ \sqrt{x_i^2 + y_i^2} - \mathcal{R}_T & \text{for} \quad \mathcal{R}_T \le \sqrt{x_i^2 + y_i^2}. \end{cases} \tag{4.27}$$

Figure 4.6 shows an example of mapping the continuous transmitter to the discrete transmitters minimizing the sum of the distances, where the 20×20 LEDs are distributed on a square lattice.

Once the mapping is finalized, the secrecy rate with the selected discrete infor-

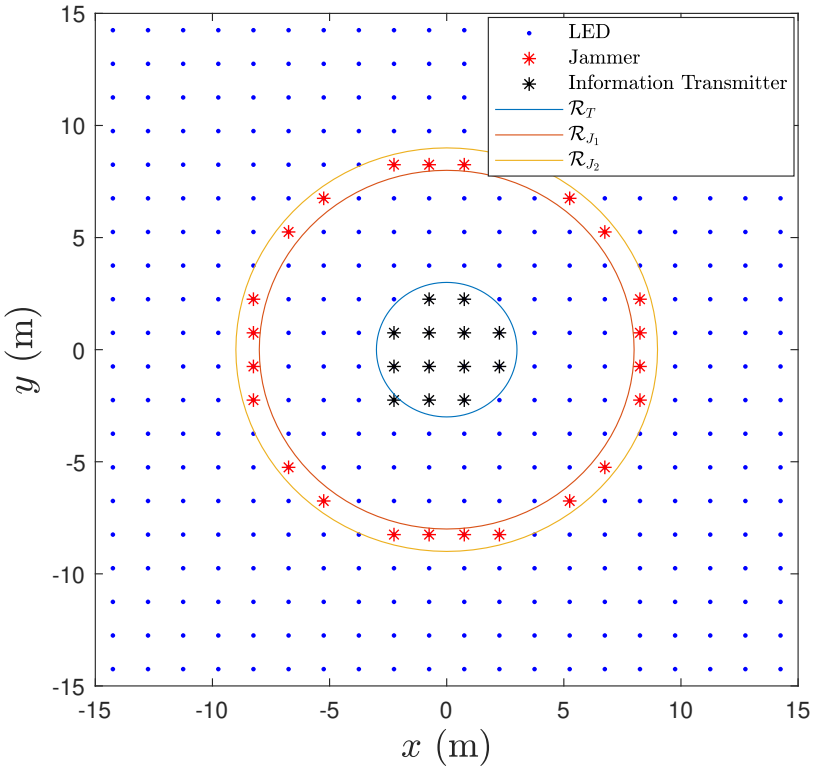


Figure 4.6. An example of the role selection of the discrete transmitters. For the continuum model, $\mathcal{R}_T = 3$ m, $\mathcal{R}_{J_1} = 8$ m and $\mathcal{R}_{J_2} = 9$ m are assumed. For the discrete model, the 20×20 discrete LED transmitters are assumed to be uniformly distributed on a square lattice in the 30×30 m^2 room.

mation transmitters and jammers given the location of PE, whose coordinate in the work plane is (r_{PE}, θ_{PE}), can be calculated as

$$R_{s,\text{disc.}}(r_{PE}, \theta_{PE}) = \max \left\{ \frac{1}{2} \log \left(\frac{e^{2\eta} \left(\mathbf{e}_{\mathcal{T}}^T \mathbf{H}_U \mathbf{e}_{\mathcal{T}} + \mathbf{e}_{\mathcal{J}}^T \mathbf{H}_U \mathbf{e}_{\mathcal{J}} \right) + C}{\varphi \mathbf{e}_{\mathcal{J}}^T \mathbf{H}_U \mathbf{e}_{\mathcal{J}} + C} \right) \right.$$
$$\left. - \frac{1}{2} \log \left(\frac{\varphi \left(\mathbf{e}_{\mathcal{T}}^T \mathbf{H}_{PE} \mathbf{e}_{\mathcal{T}} + \mathbf{e}_{\mathcal{J}}^T \mathbf{H}_{PE} \mathbf{e}_{\mathcal{J}} \right)}{e^{2\eta} \mathbf{e}_{\mathcal{J}}^T \mathbf{H}_{PE} \mathbf{e}_{\mathcal{J}}} \right), 0 \right\} \tag{4.28}$$

where $\mathbf{e}_{\mathcal{T}}$ and $\mathbf{e}_{\mathcal{J}}$ are the column vectors whose ith and jth entries for $i \in \mathcal{T}$ and $j \in \mathcal{J}$ are all 1's and the others are all 0's, respectively. Finally, the optimal average secrecy rate, which is obtained by mapping the continuum model to the discrete model, can

Table 4.1. Simulation Parameters

Room configuration	
Length (L) × Width (W)	30×30 m^2
Height from the work plane (H)	2.2 m
Number of light fixtures	36
Number of LEDs per fixture	25
Locations of transmitters	$\{\pm 2.5, \pm 7.5 \pm 12.5\}$
LED electrical and optical characteristics	
Average optical power per LED	2 W
Current-to-light conversion efficiency η	1 W/A
Nominal half-intensity angle $\Phi_{1/2}$	60°
Modulation index α	0.4
Optical receiver characteristics	
Photodetector's responsivity $R_{\text{rsp.}}$	0.54 mA/mW
Lens refractive index κ	1.5
Noise power σ^2	−98.33 dBm
Field of View Ψ_c	90°
Transimpedance amplifier gain T	50 V/A

be calculated by numerically evaluating

$$\begin{aligned} \overline{R}^{\star}_{s,\text{disc.}} &= \int_{\mathcal{R}_{E_1}}^{\mathcal{R}_{E_2}} \int_0^{2\pi} f_{rPE}(r) R_{s,\text{disc.}}(r,\theta) r \, \mathrm{d}\theta \, \mathrm{d}r \\ &= \int_{\mathcal{R}_{E_1}}^{\mathcal{R}_{E_2}} \int_0^{2\pi} \frac{2r^2}{\mathcal{R}_{E_2}^2 - \mathcal{R}_{E_1}^2} R_{s,\text{disc.}}(r,\theta) \, \mathrm{d}\theta \, \mathrm{d}r. \end{aligned} \tag{4.29}$$

4.5 Numerical Results

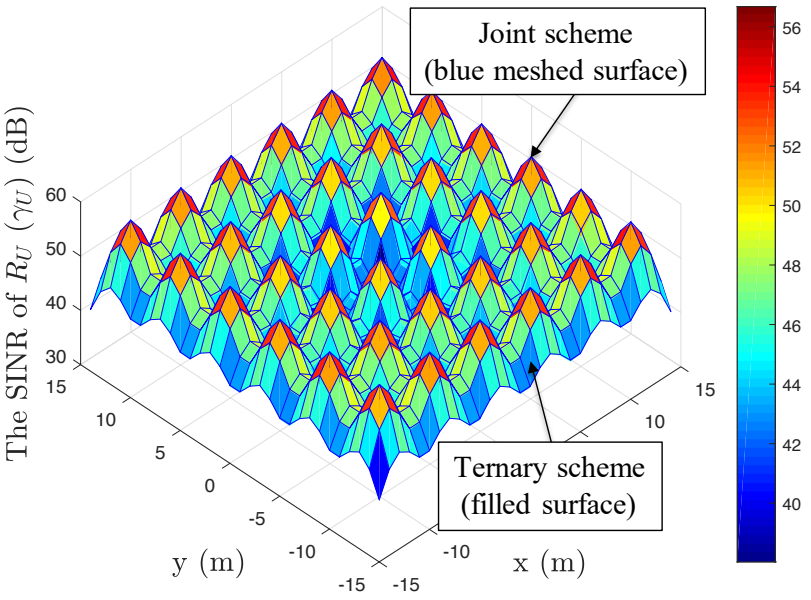
In this section, we provide numerical results to verify the performances of the proposed joint strategies. The room configuration and simulation parameters are provided in Table 4.1. Here, we utilize the characteristics of the LED transmitters and receivers employed in [10], which considered a typical office room and common lightening devices. In addition, emitted light is assumed to be "warm-white," i.e., color temperature is between 2700 and 3000 K, with luminous efficiency 284 lm/W [85, Table 3.2]. Based on this assumption, we adjust the number of light fixtures and the

number of LEDs per fixture such that the considered LED arrangement satisfies the lighting standards, e.g., from 400 to l000 lx for a typical office [86]. According to the Lumen method [87], the considered configuration yields the light level of 410 lx in the room. We use the Cartesian coordinate system to identify positions of transmitters and receivers, where the center of the room is located at the origin.

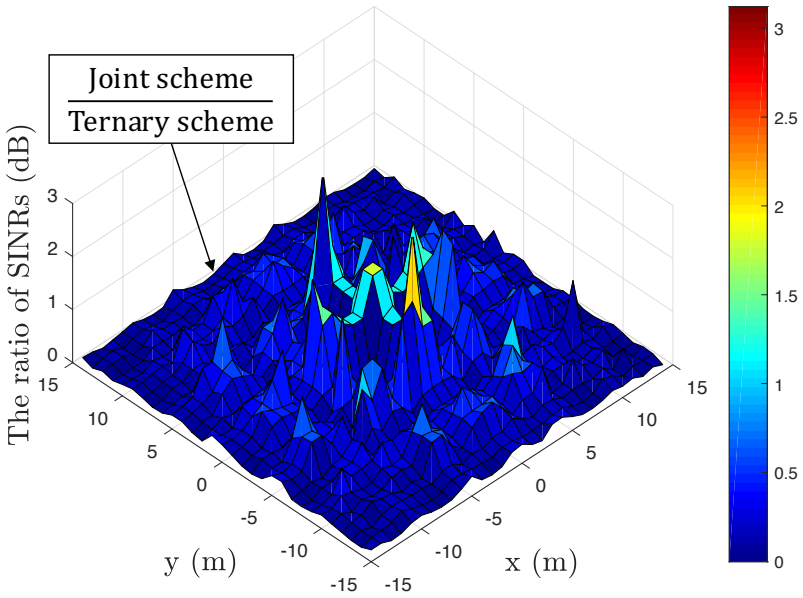
4.5.1 Signal-to-Interference-plus-Noise Ratio

Figure 4.7 shows the comparison of the SINR of the UE for the joint scheme and the ternary scheme according to the location of the UE. The optimal beamforming weight and jamming intensity vectors for the given location of the UE are obtained by solving the optimization problems (4.13) and (4.17), respectively, and the SINRs of the UE are plotted according to the locations of the UE in Figure 4.7(a). In the figure, there are two very similar surfaces, where the top blue meshed surface corresponds to the joint scheme denoted by $\boldsymbol{\gamma}_U^{\text{jnt.}}$, while the bottom filled surface relates to the ternary scheme denoted by $\boldsymbol{\gamma}_U^{\text{ter.}}$. As seen in the figure, the performances of the joint scheme and the ternary scheme with respect to $\boldsymbol{\gamma}_U$ are so similar that it is difficult to observe their difference. To clarify the gap between the two surfaces, the ratio of SINRs is plotted on a dB scale, i.e., $10 \times \log_{10}(\boldsymbol{\gamma}_U^{\text{jnt.}}/\boldsymbol{\gamma}_U^{\text{ter.}})$, according to location of the UE in Figure 4.7(b). The figure shows that the two proposed schemes yield a similar performance in most of the area, while the joint scheme shows slightly better performance at the center of the room. Considering that the complexity in solving the optimization problem for the joint scheme (4.13) is much higher than that of the ternary scheme (4.17), the small performance gap indicates that the ternary scheme may be preferred in practice.

Figure 4.8 shows the SINRs of ***PE*** with the joint scheme and the beamforming, respectively, as a function of the ED locations. The beamforming scheme in **Chapter 3** is given as a benchmark in which the beamforming vector (without jamming)

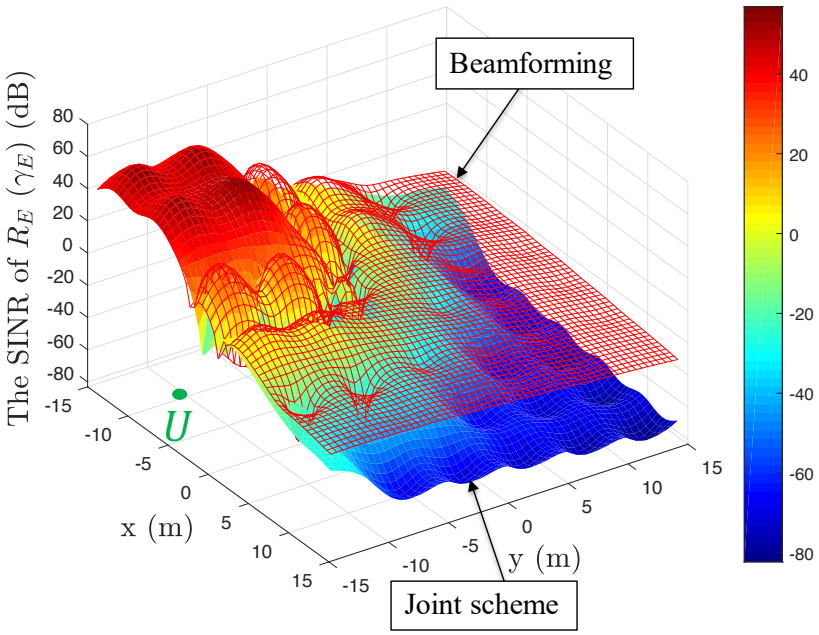


(a) The SINRs of the UE with the joint scheme and the ternary scheme, respectively, according to the different locations of the UE.

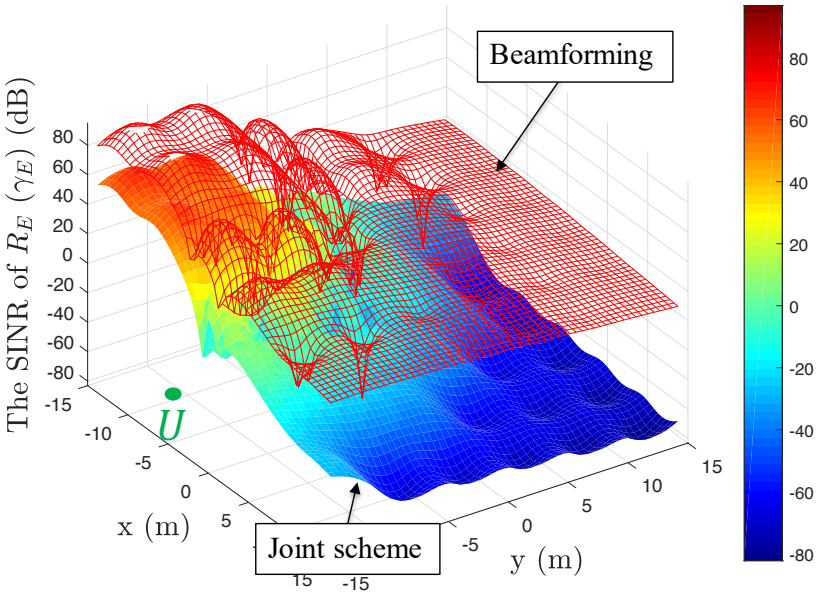


(b) The ratio of SINRs of the joint scheme and the ternary scheme, i.e., $10 \times \log_{10}(\gamma_U^{\text{int.}}/\gamma_U^{\text{ter.}})$

Figure 4.7. The comparison of the SINRs of the UE between the joint strategy and the ternary strategy. $\overline{\rho}_{PE} = 0.3$ is used for the optimizations.



(a) The SINR of *PE* being equipped with $A_{\mathrm{PD},E} = 1$ cm^2.



(b) The SINR of *PE* being equipped with $A_{\mathrm{PD},E} = 100$ cm^2.

Figure 4.8. The comparison for the SINRs of *PE* between the joint strategy and the beamforming according to the different locations of *PE*. In both figures, *U* is equipped with $A_{\mathrm{PD},U} = 1$ cm^2, while *PE* has a larger PD $A_{\mathrm{PD},E} = 100$ cm^2 in (b).

can be calculated without the knowledge on the locations or CSI of the ED like the proposed joint scheme. In the figure, there are two surfaces, where the top meshed surface is for the beamforming-only method, while the bottom filled surface is for the joint scheme. Here, U is located at $(-10.5, -10.5)$. For a fair comparison, $\gamma_U = 46$ dB is set for both the joint scheme and the beamforming-only approach. As follows from Figure 4.8(a), for both the schemes, the SINR of PE is very high when PE is close to the the UE location, but it decreases very quickly as PE moves away from U because the channel gain decays like $l^{(m+3)}$. However, at the faraway locations from the UE, γ_{PE} with the joint scheme is much lower than that with the beamforming-only technique due to the presence of the jammers there.

On the other hand, the fact that γ_{PE} at a distant location is much lower than γ_U with both schemes might evoke a thought that the beamforming scheme itself is enough to ensure a secure connection unless PE is located near to U. However, in reality, the possible eavesdropping scenario in VLC systems can include the ED with dominant receiver front-end specifications that are much better than those of the UE, such as a larger physical PD area, a higher PD responsivity, a higher refractive index, etc. Moreover, in our earlier work [106], it was shown that the collusion of multiple EDs could achieve a high diversity gain to improve the SNR of the EDs, which results in the increase of the SOP. Thus, due to these facts, lowering the ED's SINR as much as possible would be essential for securing the transmission even when the SINR of a UE is higher than that of an ED with the same specification of receiver device.

From this perspective, Figure 4.8(b) shows how effectively the proposed joint scheme reduces the SINR of PE being equipped with a larger PD[3]. In Figure 4.8(b), the physical area of the PD of PE ($A_{\mathrm{PD},E} = 100$ cm^2) is set much larger than that of the UE ($A_{\mathrm{PD},E} = 1$ cm^2). For the beamforming scheme, it is shown that PE is able to significantly improve its SINR up to 40 dB over the entire room by increasing the

[3]Considering the channel model in (2.1), other better specifications of the ED can be considered in the same way.

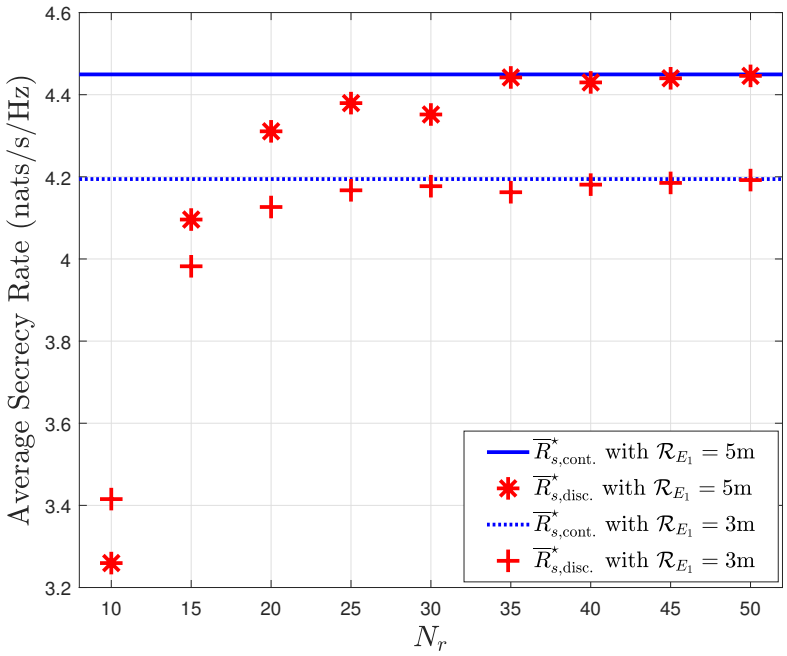


Figure 4.9. The optimized average secrecy rates of the continuum model and its corresponding discrete model for the different number of transmitters $N = N_r \times N_r$. $\overline{R}^{\star}_{s,\text{cont.}}$ and $\overline{R}^{\star}_{s,\text{disc.}}$ correspond to (4.23) and (4.29), respectively.

PD size, compared to Figure 4.8(a). However, for the joint scheme, it is shown that γ_{PE} slightly increases near the location of the UE, while it remains almost unchanged in the distant area. This is because PE receives more of the jamming signals as well as the information signals through the larger PD; it cannot increase its SINR just by increasing the PD size. In addition, the probability of the secrecy connectivity [93], which can be defined as $P_{sc} = \mathbb{P}(\gamma_U > \gamma_{PE})$, decreases from 0.94 to 0.75 with the beamforming scheme, while it slightly changes from 0.93 to 0.90 with the joint scheme.

4.5.2 Secrecy Rate with the Continuum Model

Figure 4.9 shows the optimized average secrecy rate of the continuum model and its corresponding discrete model according to different numbers of transmitters in order to demonstrate the validity of the continuum model. In order to maintain the light level of 410 lx in the room as the previous subchapter, we use $P_T = 2$ W/m^2

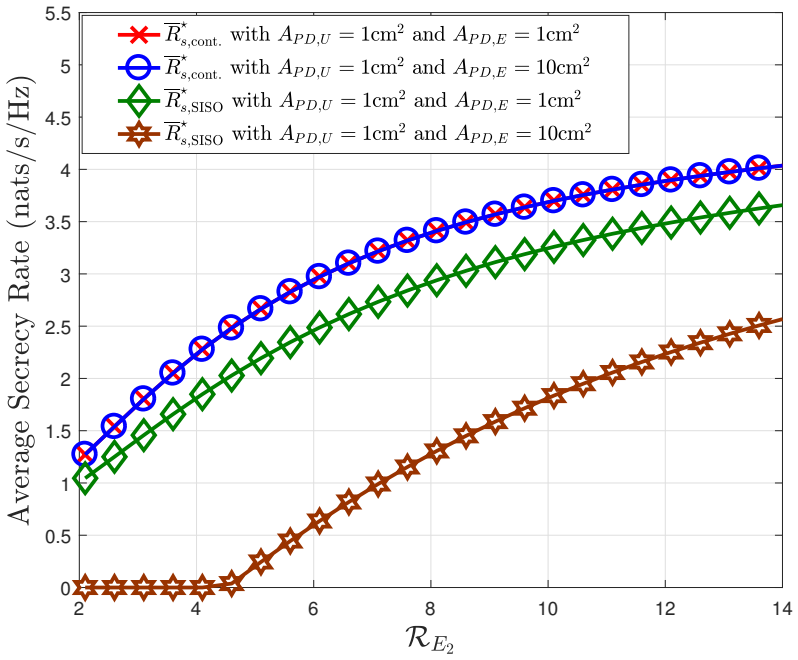


Figure 4.10. The optimized average secrecy rate $\overline{R}^{\star}_{s}$ for the different sizes of PD.

for the continuum model and adequately adjust the average optical power per LED according to the number of transmitters in the discrete model. For the discrete model, the UE is assumed to be located at $(0, 0)$ in 30×30 m^2 room and PE is assumed to be uniformly and randomly located in the annulus centered at $(0, 0)$ with inner radius $\mathcal{R}_{E_1}$ and outer radius $\mathcal{R}_{E_2} = 15$ m. $\sigma_T = 0.62$ is used. As the number of transmitters $N = N_r \times N_r$ increases, it is shown that the average secrecy rate of the discrete model converges to that of the continuum model. More specifically, when the 10×10 discrete LEDs are present in a 30×30 m^2 area, the gap between $\overline{R}^{\star}_{s,\text{cont.}}$ and $\overline{R}^{\star}_{s,\text{disc.}}$ is 0.78 nats/s/Hz for $\mathcal{R}_{E_1} = 3$m. However, when the number of transmitters is larger than 20×20, the gap rapidly decreases to less than 0.07 nats/s/Hz. This result verifies that the continuum model approximates well the real VLC systems that have an adequately large number of LEDs.

Figure 4.10 shows the performance of the ternary scheme in terms of the average secrecy rate. Here, PE is assumed to be uniformly and randomly located in the gray

annulus with inner radius $\mathcal{R}_{E_1} = 2$ m and outer radius $\mathcal{R}_{E_2}$. $\sigma_T = 0.62$ is used. For comparison, the SISO transmission [10] is given as a benchmark, whose secrecy rate expression with the continuum model and assuming that the input signal follows the truncated Gaussian distribution is given by

$$R_{s,\mathrm{SISO}} = \frac{1}{2}\log\left(\frac{\sigma_T^2\zeta_U^2 P_D^2(0)e^{2\eta} + \sigma^2}{\sigma_T^2\zeta_{PE}^2 P_D^2(r_{PE})\varphi + \sigma^2}\right). \tag{4.30}$$

See Appendix 4.A.2 for the proof. Then, we numerically solve the optimization problem maximizing the average secrecy rate for the SISO transmission, i.e.,

$$\overline{R}^{\star}_{s,\mathrm{SISO}} = \max_{\mathcal{R}_T} \overline{R}_{s,\mathrm{SISO}} \tag{4.31}$$

where

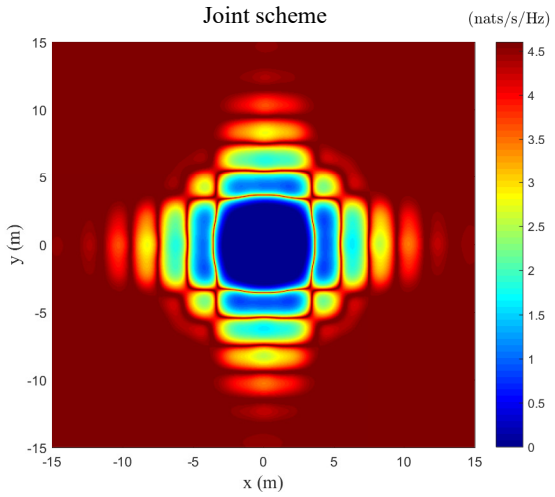
$$\overline{R}_{s,\mathrm{SISO}} = \int_{\mathcal{R}_{E_1}}^{\mathcal{R}_{E_2}} \frac{2r}{\mathcal{R}_{E_2}^2 - \mathcal{R}_{E_1}^2} R_{s,\mathrm{SISO}}(r)\,\mathrm{d}r. \tag{4.32}$$

In Figure 4.10, it is shown that the ternary scheme slightly outperforms the SISO transmission over the entire region of $\mathcal{R}_{E_2}$ when the physical areas of PD for U and PE are identically 1 cm^2. More specifically, when $\mathcal{R}_{E_2}$ is small, in which case PE is likely to be located nearer to the UE, the gap between $\overline{R}^{\star}_{s,\mathrm{cont.}}$ and $\overline{R}^{\star}_{s,\mathrm{SISO}}$ is small. This is because the jamming signals emitted from the near jammers would not be beneficial since the jamming signals would hamper even the information transmission from the LEDs to the UE. On the other hand, when $\mathcal{R}_{E_2}$ is large; thus PE is likely to be located at distant positions from the UE, PE cannot wiretap the information signal even without the jamming signals present because the channel gain in VLC systems decays very quickly according to the distance from the LEDs to the receiver. Therefore, the secrecy rate with the SISO transmission is similar to, but slightly less than, the ternary scheme. However, when the PD size of PE increases to 10 cm^2, it is shown that the gap between $\overline{R}^{\star}_{s,\mathrm{cont.}}$ and $\overline{R}^{\star}_{s,\mathrm{SISO}}$ becomes significant, because PE

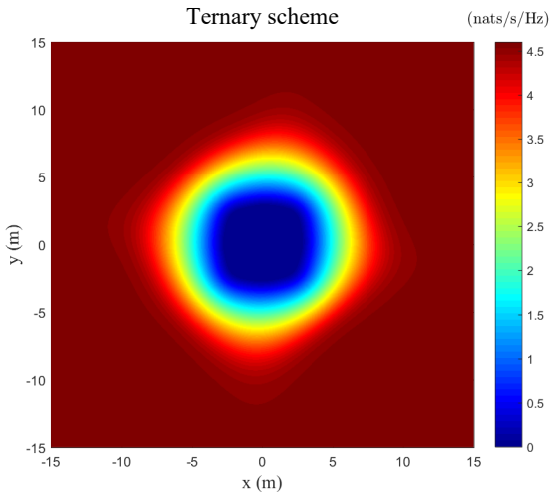
being equipped with a large PD is able to more effectively eavesdrop the information signal even at distant locations under the SISO transmission. However, under the ternary scheme, $\boldsymbol{PE}$ cannot increase its eavesdropping ability by increasing its PD size; thus the average secrecy rate remains unchanged. This result verifies that $\boldsymbol{PE}$ cannot increase its SINR just by increasing the PD size since $\boldsymbol{PE}$ receives more of the jamming signals as well as the information signals through the larger PD.

Figures 4.11(a), (b) and (c) show the secrecy rate performance as a function of $\boldsymbol{PE}$ locations for the three proposed schemes, i.e., the joint scheme, the ternary scheme and the continuum model (but transformed to the discrete model by utilizing the method described in Section 4.4.4), respectively. Here, the UE is located at $(0, 0)$ and 15×15 LEDs are uniformly distributed on a square lattice in a 30×30 m^2 room. Here, we consider a larger number of LEDs, compared to Figures 4.7 and 4.8, to reduce the performance gap when the continuum model is translated to the discrete model. In addition, for the continuum model, $\mathcal{R}_{E_1} = 0$ m and $\mathcal{R}_{E_1} = 15$ m are used. In (a) and (b), as we mentioned in Section 4.2.2, the two schemes perform in the way that the near LEDs act as the information transmitters, while all of the other distant LEDs act as the jammers. In (c), the continuum model performs in a similar way, except that the locations of jammers are slightly nearer to the UE than (a) and (b), reducing the low secrecy rate region (e.g., less than 3 nats/s/Hz). Although the beamforming and jamming vectors for the first two schemes are obtained from the suboptimal optimization problems maximizing the SINR of the UE, it is shown that these schemes also perform well in terms of maximizing the secrecy rate. Under the assumption that $\boldsymbol{PE}$ is randomly located in a circle with radius 15 m centered at the UE, the average secrecy rates for the joint scheme and the ternary scheme are 3.85 nats/s/Hz and 3.83 nats/s/Hz, respectively, while the continuum model yields 3.91 nats/s/Hz.

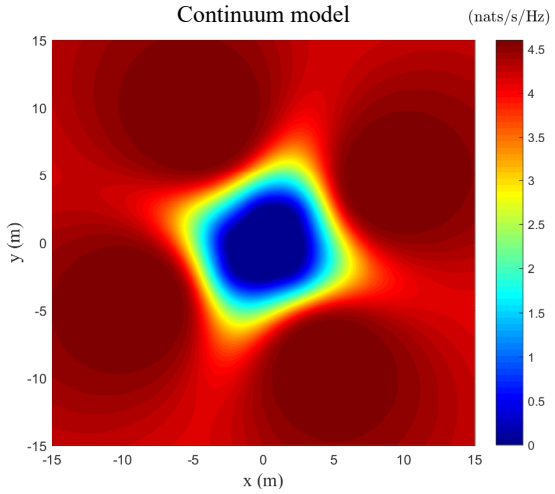
In addition, to compare the proposed joint scheme with the existing jamming



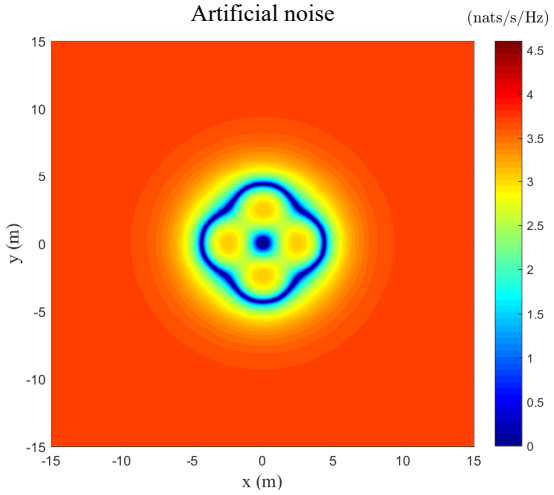
(a) Secrecy rate with the joint scheme (4.13).



(b) Secrecy rate with the ternary scheme (4.17).

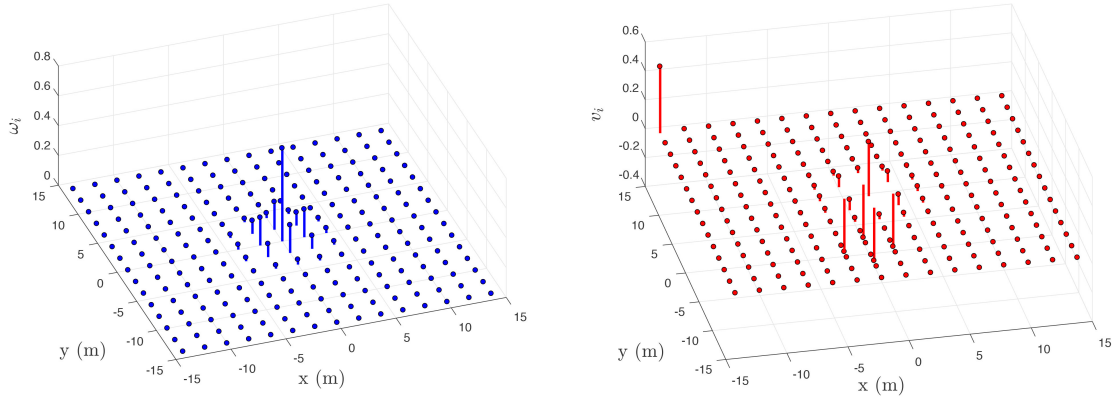


(c) Secrecy rate with the continuum model transformed to the discrete model using the procedure in Section 4.4.4.



(d) Secrecy rate with the artificial noise. $\rho = 0.5$ is used.

Figure 4.11. The comparison of secrecy rates under the different proposed schemes, the joint scheme, the ternary scheme, the continuum model, and the artificial noise transmission according to the location of PE.



(a) The beamforming weight ω_i. (b) The jamming intensity ν_i.

Figure 4.12. The beamforming and jamming vectors with the artificial noise. the UE is located at $(0, 0, 0)$. The 15×15 LED transmitters are uniformly distributed on a square lattice in the 30×30 m^2 room. $H = 2.2$ m, $\phi_{1/2} = 60°$ and $\rho = 0.5$ are used.

scheme that does not require knowledge of the location of an ED, the secrecy rate under the artificial noise scheme [11] is given in Figure 4.11(d). The beamforming and jamming vectors for the artificial noise can be obtained as

$$\mathbf{w}_{\mathrm{AN}} = k\rho\alpha I_{DC}\hat{\mathbf{h}}_U, \quad \mathbf{v}_{\mathrm{AN}} = k\alpha I_{DC}\frac{1-\rho}{N-1}\sum_{i=1}^{N-1}\hat{\varphi}_{\mathrm{B}_i}$$

respectively, where $\hat{\mathbf{h}}_U = \mathbf{h}_U/||\mathbf{h}_U||_1$, and $\hat{\varphi}_{\mathrm{B}_i} \in \mathbb{R}^N$ for $i \in \{1, 2, ..., N-1\}$ constitute a basis for the nullspace of $\mathbf{h}_U^T$ and are normalized such that $||\hat{\varphi}_{\mathrm{B}_i}||_1 = 1, \forall i \in \{1, 2, ..., N-1\}$. k is a constant such that the peak constraint

$$k\left(\rho|\hat{\mathbf{h}}_B| + \frac{1-\rho}{N-1}\sum_{i=1}^{N-1}|\hat{\varphi}_{B_i}|\right) \preceq \mathbb{1}$$

is satisfied. Also, ρ is the parameter that determines the optical power fraction devoted to a data signal, while $1-\rho$ is for jamming signals. In Figure 4.11(d), it is shown that the secrecy rate with the artificial noise is less than the continuum model in Figure 4.11(c) at the outer area of the room, while higher near around the UE. This result shows that transmitting the artificial noise (jamming) signals towards

the nullspace of the UE yields a higher secrecy performance at the small area near to the UE by not causing the interference at the UE site, but it does not perform in a way that maximizes the secrecy performance. Under the assumption that PE is randomly located in the room, the average secrecy rate for the artificial noise is 3.50 nats/s/Hz, while the continuum model yields 4.01 nats/s/Hz. The reason can be better understood by observing the beamforming and jamming vectors $\mathbf{w}_{\mathrm{AN}}, \mathbf{v}_{\mathrm{AN}}$ in Figure 4.12. It is noted that the beamforming weight of the nearest LED to the UE is $\omega_{\mathrm{nrst.}} = 0.62$, not 1, because the fraction $1 - \rho$, i.e., $\nu_{\mathrm{nrst.}} = 0.38$, is allocated to suppress the interference at the UE site. Since the channel gain largely depends on the distance between transmitter and receiver, the power allocation of the nearest LED for the jamming signals would significantly reduce the received optical power of the information signal at the UE site. In general, the decrease of the information reception at the UE would result in the degradation of the average secrecy performance, instead, it would be better to allow a small amount of interference at the UE site and allocate the whole power of the nearest LED to transmit the information signal as our proposed schemes behave. Moreover, although the jamming signal precoded by $\mathbf{v}_{\mathrm{AN}}$ does not cause interference at the UE site, almost all the jamming intensities at faraway locations from the UE are almost zero. In this case, the artificial noise scheme cannot take advantage of the jamming signals at the large outer area. Considering a practical scenario that the ED equipped with a powerful receiver would like to be located not too near to the intended user to escape the vigilance of the UE, the proposed joint scheme may be preferred. On the other hand, it is worth noting that finding $\mathbf{w}_{\mathrm{AN}}$ and $\mathbf{v}_{\mathrm{AN}}$ is deterministic and less complicated than solving the optimal solutions of the proposed joint or ternary strategy; thus, it may be more sensible to consider the artificial noise scheme of [11] when engineering PLS for small size rooms.

Figure 4.13 shows the SOP for the three proposed schemes, the artificial noise transmission [11], and the SISO transmission [10] with the same room configuration

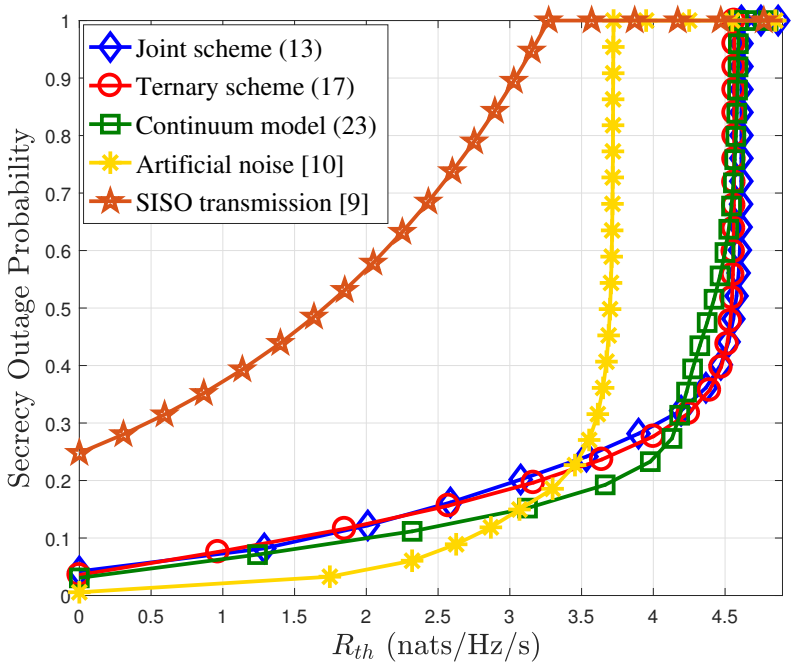


Figure 4.13. The secrecy outage probability under the different proposed schemes, such as the joint scheme, the ternary scheme, the continuum model, and the artificial noise transmission. the UE is located at $(0, 0)$ and 15×15 LEDs are uniformly distributed on a square lattice in 30×30 m^2 room. $A_{\mathrm{PD},E} = 10$ cm^2 is used.

of Figure 4.11, where the SOPs of the last two schemes are given as benchmarks. PE is assumed to be randomly located in a circle with radius 15 m centered at the UE. The SOP is defined as the probability that the secrecy capacity C_s is less than a threshold secrecy capacity C_{th}, i.e., $P_{\mathrm{SO}} = \mathbb{P}(C_s < C_{th})$ [107]. However, since the closed-form of the secrecy capacity with the input amplitude constraint is not readily available, we employ the secrecy rate in (4.9) to determine the secrecy outage; thus the SOP can be defined as $P_{\mathrm{SO}} = \mathbb{P}(R_s < R_{th})$, where R_{th} denotes the threshold secrecy rate. Figure 4.13 shows that all the proposed joint schemes and the artificial noise scheme outperform the SISO transmission, i.e., they have much lower SOPs over the entire region. Also, the SOPs of the joint and ternary schemes are similar to each other, while the continuum model has slightly lower SOP than the two schemes at the region up to 4.1 nats/s/Hz. In contrast, the artificial noise yields the lowest SOP among the four schemes at the region up to 3 nats/s/Hz, while it radically increases after 3.6

nats/s/Hz. This result shows that the proposed three schemes have better secrecy performance, i.e., lower SOP than the artificial noise transmission at the region of high R_{th}. Note that an ED generally prefers to stay at the outer area of the room, where the secrecy rate appears high, escaping the vigilance of the UE.

4.6 Summary

In this chapter, we studied simultaneous beamforming and jamming strategies when an ED is randomly located; thus its location or the CSI is not available at the transmitter. First, we formulated the optimization problem of maximizing the SINR of the intended user while constraining the SINR of the ED, and we then solved it by utilizing the CCP heuristic method. Then, we proposed a simpler ternary scheme that is much less complicated and obtained its solution by using TS. The numerical results verified that the ternary scheme provides an excellent practical solution to enhancing the secrecy performance without incurring a high computation complexity. Moreover, by utilizing a continuous LED model, the maximization of the average secrecy rate under the ternary scheme was investigated.

4.A Appendices

4.A.1 Secrecy Rate with the Joint Technique of Beamforming and Jamming

A lower bound on the secrecy rate of (4.6) can be obtained as follows

$$\begin{aligned} C_s &= \max_{p_S, p_J} \left(\mathbb{I}(S;Y_U) - \mathbb{I}(S;Y_{PE})\right) \\ &\overset{(a)}{\geq} \mathbb{I}(S;Y_U) - \mathbb{I}(S;Y_{PE}) \\ &\overset{(b)}{\geq} \mathbb{I}(S;Y_U) - \mathbb{I}(S;V_{PE}) \\ &= \mathbb{h}(Y_U) - \mathbb{h}(Y_U|S) - \mathbb{h}(V_{PE}) + \mathbb{h}(V_{PE}|S) \end{aligned} \tag{4.33}$$

where $\mathbb{h}(\cdot)$ denotes differential entropy and $V_{PE} = \alpha I_{DC} \mathbf{h}_{PE}^T \mathbf{w} S + \alpha I_{DC} \mathbf{h}_{PE}^T \mathbf{v} J$. (a) follows from dropping the maximization by choosing a truncated Gaussian distribution on p_S and p_J, and (b) follows from the data-processing inequality, i.e., $Y_{PE} = g(V_{PE}) = V_{PE} + N_{PE}$. Firstly, we lower-bound $\mathbb{h}(Y_U)$ by using the entropy-power inequality as

$$\begin{aligned} \mathbb{h}(Y_U) &\geq \frac{1}{2} \log \left(e^{2\mathbb{h}(\alpha I_{DC} \mathbf{h}_U^T \mathbf{w} S)} + e^{2\mathbb{h}(\alpha I_{DC} \mathbf{h}_U^T \mathbf{v} J)} + e^{2\mathbb{h}(N_U)} \right) \\ &= \frac{1}{2} \log \left(2\pi e \left(\sigma_T^2 \alpha^2 I_{DC}^2 (\mathbf{w}^T \mathbf{H}_U \mathbf{w} + \mathbf{v}^T \mathbf{H}_U \mathbf{v}) e^{2\eta} + \sigma^2 \right) \right) \end{aligned} \tag{4.34}$$

where (4.34) follows from the facts that

$$\mathbb{h}\left(\alpha I_{DC} \mathbf{h}_U^T \mathbf{w} S\right) = \log\left(\left|\alpha I_{DC} \mathbf{h}_U^T \mathbf{w}\right|\right) + \frac{1}{2} \log\left(2\pi e \sigma_T^2\right) + \eta, \tag{4.35a}$$

$$\mathbb{h}\left(\alpha I_{DC} \mathbf{h}_U^T \mathbf{v} J\right) = \log\left(\left|\alpha I_{DC} \mathbf{h}_U^T \mathbf{v}\right|\right) + \frac{1}{2} \log\left(2\pi e \sigma_T^2\right) + \eta, \tag{4.35b}$$

$$\mathbb{h}\left(N_U\right) = \frac{1}{2} \log 2\pi e \sigma^2. \tag{4.35c}$$

Then, we upper-bound $\mathbb{h}(Y_U|S)$ and $\mathbb{h}(V_{PE})$ as

$$\begin{aligned}\mathbb{h}\left(Y_U|S\right) &= \mathbb{h}\left(Y_U - \alpha I_{DC}\mathbf{h}_U^T\mathbf{w}S|S\right) = \mathbb{h}\left(\alpha I_{DC}\mathbf{h}_U^T\mathbf{v}J + N_U\right) \\ &\leq \frac{1}{2}\log 2\pi e\left(\sigma_T^2\alpha^2 I_{DC}^2\mathbf{v}^T\mathbf{H}_U\mathbf{v}\varphi + \sigma^2\right) \qquad (4.36) \\ \mathbb{h}\left(V_{PE}\right) &= \mathbb{h}\left(\alpha I_{DC}\mathbf{h}_{PE}^T\mathbf{w}S + \alpha I_{DC}\mathbf{h}_{PE}^T\mathbf{v}J\right) \\ &\leq \frac{1}{2}\log 2\pi e\left(\sigma_T^2\alpha^2 I_{DC}^2(\mathbf{w}^T\mathbf{H}_{PE}\mathbf{w} + \mathbf{v}^T\mathbf{H}_{PE}\mathbf{v})\varphi\right) \qquad (4.37)\end{aligned}$$

by using the differential entropy of Gaussian random variables with variances $\mathbb{V}\mathrm{ar}\{\alpha I_{DC}\mathbf{h}_U^T\mathbf{v}J + N_U\}$ and $\mathbb{V}\mathrm{ar}\{\alpha I_{DC}\mathbf{h}_{PE}^T\mathbf{w}S + \alpha I_{DC}\mathbf{h}_{PE}^T\mathbf{v}J\}$, respectively. Lastly, we have

$$\begin{aligned}\mathbb{h}\left(V_{PE}|S\right) &= \mathbb{h}\left(V_{PE} - \alpha I_{DC}\mathbf{h}_{PE}^T\mathbf{w}S|S\right) = \mathbb{h}\left(\alpha I_{DC}\mathbf{h}_{PE}^T\mathbf{v}J\right) \\ &= \frac{1}{2}\log\left(2\pi e\alpha^2 I_{DC}^2\mathbf{v}^T\mathbf{H}_{PE}\mathbf{v}\sigma_T^2\right) + \eta. \qquad (4.38)\end{aligned}$$

Plugging (4.34), (4.36), (4.37) and (4.38) into (4.33) yields the secrecy rate for the joint technique in (4.9).

4.A.2 Secrecy Rate with the SISO channel

With the SISO transmission under the continuum model, the received signals for U and PE are given by

$$y_U(t) = \zeta_U P_D(0)\hat{x} + n_U, \qquad (4.39a)$$

$$y_{PE}(t) = \zeta_{PE}P_D(r_{PE})\hat{x} + n_{PE}. \qquad (4.39b)$$

Then, a lower bound on the secrecy rate of (4.39) can be obtained as follows

$$\begin{aligned}C_s &= \max_{p_S}\left(\mathbb{I}(S;Y_U) - \mathbb{I}(S;Y_{PE})\right) \\ &\overset{(a)}{\geq} \mathbb{I}(S;Y_U) - \mathbb{I}(S;Y_{PE})\end{aligned}$$

$$
\begin{aligned}
&= \mathbb{h}(Y_U) - \mathbb{h}(Y_U|S) - \mathbb{h}(Y_{PE}) + \mathbb{h}(Y_{PE}|S) \\
&= \mathbb{h}(Y_U) - \mathbb{h}(N_U) - \mathbb{h}(Y_{PE}) + \mathbb{h}(N_{PE}) = \mathbb{h}(Y_U) - \mathbb{h}(Y_{PE}) \\
&\overset{(b)}{\geq} \frac{1}{2}\log\left(e^{2\mathbb{h}(\zeta_U P_D(0)S)} + e^{2\mathbb{h}(N_U)}\right) - \frac{1}{2}\log 2\pi e\,\mathbb{V}\mathrm{ar}\{Y_{PE}\} \\
&= \frac{1}{2}\log\left(2\pi e(\sigma_T^2\zeta_U^2 P_D^2(0)e^{2\eta} + \sigma^2)\right) \\
&\quad - \frac{1}{2}\log\left(2\pi e(\sigma_T^2\zeta_{PE}^2 P_D^2(r_{PE})\varphi + \sigma^2)\right) \\
&= \frac{1}{2}\log\left(\frac{\sigma_T^2\zeta_U^2 P_D^2(0)e^{2\eta} + \sigma^2}{\sigma_T^2\zeta_{PE}^2 P_D^2(r_{PE})\varphi + \sigma^2}\right)
\end{aligned}
\tag{4.40}
$$

where, similarly, (a) follows from dropping the maximization by choosing a truncated Gaussian distribution on p_S, and (b) follows by lower-bounding $\mathbb{h}(Y_U)$ using the entropy-power inequality and upper-bounding $\mathbb{h}(Y_{PE})$ using the differential entropy of a Gaussian random variable with variance $\mathbb{V}\mathrm{ar}\{\zeta_{PE}P_D(r_{PE})\hat{x} + n_{PE}\}$.

Chapter 5

Zero-Forcing Beamforming for Active and Passive Eavesdroppers Mitigation

Many existing PLS methods for VLC systems [10–18, 67, 108], as well as the proposed beamforming techniques in the previous chapters, are based on the assumption that either active or passive EDs are present, but not both simultaneously. The difference between active and passive EDs in VLC systems lies with the availability of the CSI of the EDs at the transmitter sites. In reality, it may be the case that EDs try to escape the vigilance of a UE or a network manager; thus, it would be challenging to obtain information about the types, locations, and numbers of the EDs. When it is assumed that only active EDs (AEDs) are present, which is a common assumption on EDs except for the works in this thesis, the objective of PLS schemes is generally to suppress the signal received at the AEDs' sites by steering a transmission beam to the null space of the AEDs' channels [11, 17, 108]. However, if unknown passive EDs (PEDs) are concurrently present, these PLS schemes may yield opportunities for eavesdropping at the PEDs' sites.

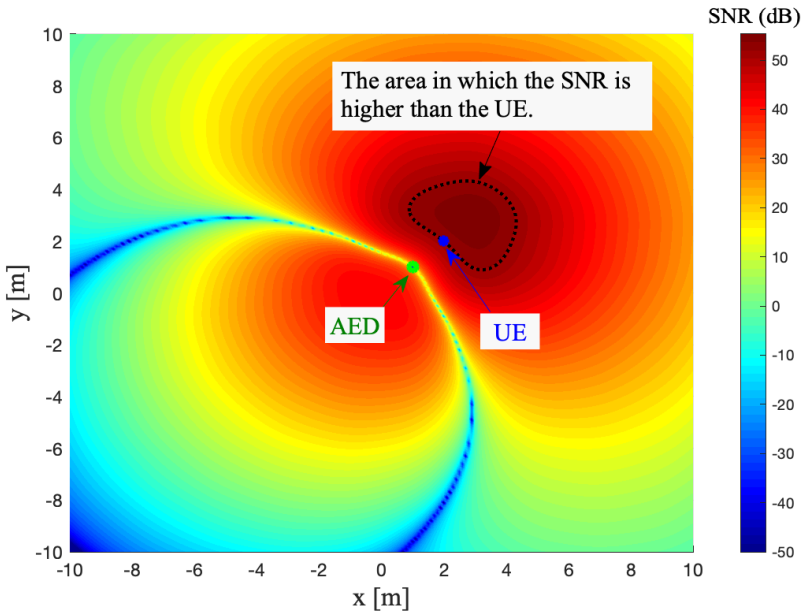


Figure 5.1. The SNR according to the receiver locations when ZF precoding is utilized. The UE and the AED are located at (2, 2) and (1, 1), respectively.

In order to clearly explain the vulnerability of existing PLS schemes, an exemplary result corresponding to a ZF scheme [11] is provided in Figure 5.1. The figure shows the SNRs according to measurement locations when the ZF strategy is adopted. The detailed room geometry and system parameters are given in Table 5.1 in Section 5.4. The ZF beamformer obtained by (11) in [11] in a deterministic way can eliminate information reception by an unintended user (i.e., an AED) by designing the precoding matrix such that the transmitted signal lies in the null space of the AED's channel. One UE and one AED are assumed to be present; however, any PEDs that may reside in the neighborhood of the transmission are ignored. The UE and the AED are marked with blue and green dots, respectively, in the figure.

In Figure 5.1, we note that even when the AED is located close to the UE, the ZF beamformer effectively minimizes the information reception at the AED site. From this result, the ZF strategy appears to secure the transmission. However, from the perspective of any passive devices that may exist in the region, it is possible to achieve a higher SNR than the UE. Note that if any PED is located in the black contoured

area in Figure 5.1, it can achieve a higher SNR than the UE, which results in a secrecy outage. Compared to the beamforming and LED selection schemes in **Chapter 3** devised for transmission in the presence of PEDs, for which the UE is very likely to retain the highest SNR, the ZF precoder designed for the nearby AED expands the contour area where the SNR is higher than that of the UE. This more spacious area would yield more opportunities for PEDs to be located in the contour area and retain a higher SNR than the UE, which results in a higher SOP. This vulnerability originates from the fact that the ZF design purely aims at forcing the AED's SNR to zero without consideration for SNRs of other unknown receivers in the area. In contrast, since the previous PLS schemes devised for only PEDs in **Chapter 3 and 4** have not considered AEDs, which can be regarded as more apparent security threats than PEDs, the PLS schemes need to be further improved to cope with any types of EDs.

Hence, the purpose of this chapter is to propose a novel ZF beamforming strategy that can deal with both active and passive EDs. In order to take the unknown (passive) ED locations into account for the beamforming, we utilize tools from stochastic geometry as in the previous chapters. This chapter begins by proposing a ZF beamforming strategy that suppresses the SNRs of the AEDs to zero while maximizing the SNR of the UE and constraining the average SNR of the PEDs. An optimization problem is formulated to find a beamforming vector that lies in the null space of the AEDs, satisfying the requirements and constraints for the UE and the PEDs. The proposed beamforming strategy directs the transmission along a particular eigenmode related to the null space of the active ED channels and the intensity of the passive ED point process. An inverse free preconditioned Krylov subspace projection method [29] is adopted to find the eigenmode. The numerical results show that the proposed ZF beamforming strategy can effectively secure the VLC transmission against active and passive EDs.

On the other hand, in some cases, especially when the number of LED transmitters is small and the location of the UE is not favorable from the secrecy perspective, the strict condition that the SNRs of the AEDs must be zero makes the proposed ZF beamforming strategy unable to cope with the PEDs effectively. Thus, an alternative solution is proposed to relax the constraint on the SNRs of the AEDs and more rigorously suppress the SNRs of PEDs. Thus, we call this the *relaxed ZF beamforming* scheme. Accordingly, we formulate an optimization problem with the objective to minimize the SOP by reducing the area in which the SNR is higher than that of the UE, thus reducing the likelihood that PEDs will achieve a higher SNR than the UE. To simplify the calculation of the area, we adopt an approach of considering the SNRs measured at discrete points obtained by the Lloyd algorithm [109]. The optimization also has constraints that regulate both the SNRs of the UE and the AEDs.

5.1 System Framework

5.1.1 Data Transmission

We consider the downlink of a VLC system as shown in Figure 5.2, where W, L, and H denote the width, the length, and the height of the ceiling relative to the work plane, respectively. N LED transmitters are attached to the ceiling of the room. Each transmitter – i.e., an LED fixture consisting of multiple individual LEDs – is assumed to be capable of communicating independently of other transmitters. We assume that one UE and N_{A} AEDs are present in the work plane of the room. Multiple PEDs are assumed to be randomly distributed according to a homogeneous PPP $\mathbf{\Phi}_{PE}$ with density λ_{PE}. Note that the homogeneous PPP of the PEDs means that their locations and CSI are completely random and unknown, which is the worst case from the secrecy viewpoint [22]. On the other hand, the CSI of the UE and the AEDs are known to the LED transmitters. The UE, the AEDs, and the PEDs are denoted by

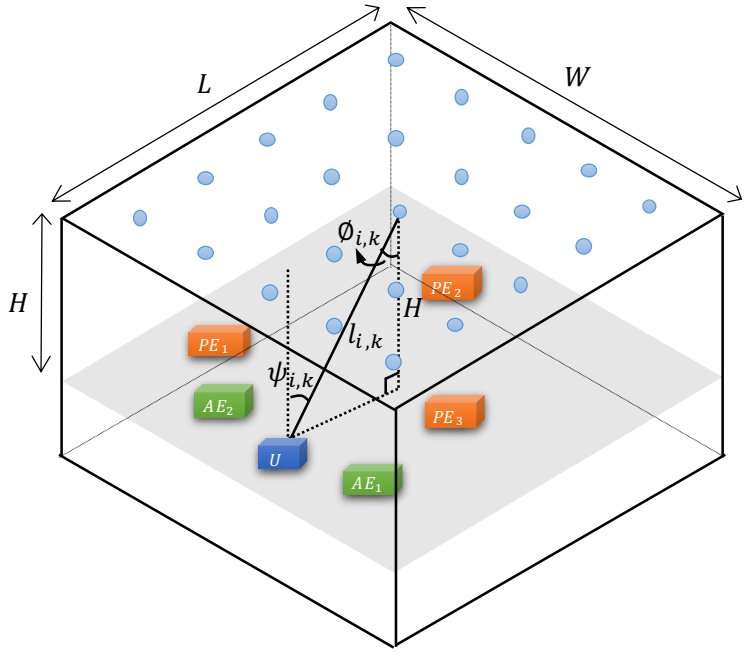


Figure 5.2. Rectangular room configuration for VLC systems.

U, AE_p for $p \in \{1, 2, ..., N_{\mathrm{A}}\}$, and PE_q for $q \in \Phi_E$, respectively. Also, we assume that EDs act independently of one another, i.e., there is no collusion.

A DC biased PAM VLC scheme depicted in Figure 2.2 is considered. The data signal $s_i(t) \in \mathbb{R}$ for the ith transmitter in time slot t is superimposed on a fixed bias current $I_{DC} \in \mathbb{R}_+$. The current I_{DC} is used for the purpose of illumination. Thus, the ith transmitter's modulated signal $x_i(t)$ corresponding to $s_i(t)$ is a zero-mean current signal that can be expressed as $x_i(t) = \alpha I_{DC} s_i(t)$, where $\alpha \in [0, 1]$ is the modulation index. To maintain linear current-to-light conversion, the amplitude of $x_i(t)$ is constrained such that $|x_i(t)| \leq \alpha I_{DC}$. Also, $\mathbb{E}[x_i(t)] = 0$ is assumed; thus the data signal does not affect illumination.

The channel gain $h_{i,k} \in \mathbb{R}_+$ from the ith transmitter to receiver $k \in \{U, AE_p, PE_q\}$ in a VLC system corresponding to an LED with a generalized Lambertian emission pattern is given in (2.1). Moreover, by assuming that a receiver's PD faces up normal to the work plane, i.e., assuming $\phi_{i,k} = \psi_{i,k}$, we can rewrite the channel gain as $h_{i,k} = K l_{i,k}^{-(m+3)}$, where $K = \left(\eta(m+1) A_{\mathrm{PD},k} H^{m+1} \kappa_k^2 R_{\mathrm{rsp.},k} T_k\right) / \left(2\pi \sin^2(\Psi_c)\right)$.

As described in Figure 2.5, a MISO beamforming vector $\mathbf{w} = [\omega_1, \omega_2, ..., \omega_N]^T$ can be defined, where $\omega_i \in \mathbb{R}$ for $i \in \{1, 2, ..., N\}$ is a weight for the ith transmitter and $|\omega_i| \leq 1$. The ith LED transmitter multiplies the modulated data signal $x_i(t)$ by ω_i before transmitting. In the considered MISO VLC system, the data signal $s_i(t)$ for the ith transmitter is assumed to be identically $s(t)$ for all transmitters as in [10]. Therefore, the signal at the receiver k in the MISO VLC system can be described as

$$y_k(t) = \alpha I_{DC} \mathbf{h}_k^T \mathbf{w} s(t) + n_k(t) \tag{5.1}$$

where $\mathbf{h}_k = [h_{1,k}, h_{2,k}, ..., h_{N,k}]^T \in \mathbb{R}^N$ denotes the channel gain vector. Also, n_k signifies a zero-mean AWGN random variable with variance σ^2 at receiver k. We assume that all the receivers retain an identical AWGN power variance σ^2. For notational convenience, the time index t is ignored for the remainder of the chapter.

5.1.2 Performance Measures

For Gaussian VLC MISO channels with an amplitude constraint, the peak SNR at receiver k with beamforming can be written as

$$\gamma_k = \frac{\alpha^2 I_{DC}^2 \mathbf{w}^T \mathbf{h}_k \mathbf{h}_k^T \mathbf{w}}{\sigma^2} = \varphi \mathbf{w}^T \mathbf{H}_k \mathbf{w} \tag{5.2}$$

where $\mathbf{H}_k = \mathbf{h}_k \mathbf{h}_k^T$ and $\varphi = \alpha^2 I_{DC}^2 / \sigma^2$. Similarly to the previous chapters, we use the term *SNR* to refer to the peak SNR throughout the chapter for brevity. The average SNR of a PED can be expressed as

$$\begin{aligned} \overline{\gamma}_{PE} &= \mathbb{E}[\varphi \mathbf{w}^T \mathbf{h}_{PE_q} \mathbf{h}_{PE_q}^T \mathbf{w}] \\ &= \varphi \mathbf{w}^T \mathbb{E}[\mathbf{h}_{PE_q} \mathbf{h}_{PE_q}^T] \mathbf{w} = \varphi \mathbf{w}^T \overline{\mathbf{H}}_{PE} \mathbf{w} \end{aligned}$$

where $\overline{\mathbf{H}}_{PE} = \mathbb{E}[\mathbf{h}_{PE_q}\mathbf{h}_{PE_q}^T]$ and its element in the ith row and jth column is given by

$$\overline{H}_{PE_{i,j}} = \frac{1}{N_{PE}} \int_{\frac{-L}{2}}^{\frac{L}{2}} \int_{\frac{-W}{2}}^{\frac{W}{2}} \frac{\lambda_{PE} K^2}{l_i^{m+3}(\mathbf{x}) l_j^{m+3}(\mathbf{x})} \, \mathrm{d}\mathbf{x}$$

where $l_i(\mathbf{x})$ denotes the distance between the ith transmitter and the point $\mathbf{x} \in \mathbb{R}^2$ in the work plane of the room (its origin is the center of the room). Also, N_{PE} denotes the average number of PEDs, which is given by

$$N_{PE} = \int_{\frac{-L}{2}}^{\frac{L}{2}} \int_{\frac{-W}{2}}^{\frac{W}{2}} \lambda_{PE} \, \mathrm{d}\mathbf{x}.$$

The SOP can be described by the equation

$$P_{SO} \overset{(a)}{=} \mathbb{P}(\gamma_U < \max_{l \in \Phi_{PE}} \gamma_{PE_q}) \overset{(b)}{=} 1 - \exp\left(-\iint_{\mathcal{A}} \lambda_{PE} \, \mathrm{d}\mathbf{x}\right) \tag{5.3}$$

where, for (a), we assume that secrecy outage only occurs when the maximum SNR observed by a PED is greater than the SNR of the UE, which is a justifiable assumption since the SNRs of the AEDs are effectively minimized by using the proposed beamforming design. For (b), we apply the void probability of a PPP [90]. Also, $\mathcal{A} = \{\mathbf{x} \mid \gamma(\mathbf{x}, \mathbf{w}) > \gamma_U\}$, where $\gamma(\mathbf{x}, \mathbf{w})$ denotes the SNR measured at the point $\mathbf{x}$, which can be expressed as

$$\gamma(\mathbf{x}, \mathbf{w}) = \varphi \mathbf{w}^T \mathbf{h}(\mathbf{x}) \mathbf{h}(\mathbf{x})^T \mathbf{w} \tag{5.4}$$

where $\mathbf{h}(\mathbf{x})$ denotes the channel gain vector at the point $\mathbf{x}$. Note that $\mathcal{A}$ denotes the black contour area in Figure 5.1.

5.2 Zero-Forcing Beamforming

To design the beamforming scheme that simultaneously copes with the AEDs and the PEDs, we exploit the traditional ZF scheme for VLC systems [11]. The traditional ZF beamformer for a single AED AE_1, where the PEDs are ignored, can be obtained by projecting the UE's channel onto the null space of the AED [78]. The corresponding ZF beamforming vector can be expressed as

$$\mathbf{w} = g\boldsymbol{\Psi}_{AE_1}\boldsymbol{\Psi}_{AE_1}^T\mathbf{h}_U. \tag{5.5}$$

Here, $\boldsymbol{\Psi}_{AE_1} \in \mathbb{R}^{N\times(N-1)}$ is a matrix whose $N-1$ columns constitute a basis for the null space of the AED's channel vector $\mathbf{h}_{AE_1}$, and g is a constant such that $|\mathbf{w}| \preceq \mathbb{1}$. Note that by constraining the beamforming vector to lie in the null space of the AED channel, the SNR of the AED γ_{AE_1} can be suppressed to zero. Based on this idea, in this section, we find a new ZF beamformer that lies in the null space of the AEDs' channels in order to suppress the SNRs of the AEDs to zero while simultaneously considering the SNRs of the UE and the PEDs.

5.2.1 Maximizing the Legitimate User's SNR

First, we formulate the optimization problem for the ZF beamforming vector $\mathbf{w}$ that maximizes the SNR of the UE while constraining the average SNR of the PEDs. Without knowledge of PED locations, considering the average SNR of the PEDs is a natural approach as in **Chapter 3 and 4**. In addition, it is worth noting that the secrecy outages caused by PEDs can also be reduced by maximizing the SNR of the UE given a constraint on the average SNR of the PEDs.

In a similar manner to (5.5), we constrain the beamforming vector $\mathbf{w}$ to lie in the null space of the AEDs' channel matrix $[\mathbf{h}_{AE_1}\ \mathbf{h}_{AE_2}\ \ldots\ \mathbf{h}_{AE_{N_A}}]^T$, which can be

expressed as

$$\mathbf{w} = \boldsymbol{\Psi}_{AE}\boldsymbol{\Psi}_{AE}^{T}\mathbf{a} \tag{5.6}$$

where $\boldsymbol{\Psi}_{AE} \in \mathbb{R}^{N\times(N-N_A)}$ is a matrix whose $N - N_A$ columns constitute a basis for the null space of the AEDs' channel matrix, and $\mathbf{a} \in \mathbb{R}^{N}$ is an arbitrary real vector. This condition ensures that the beamforming vector $\mathbf{w}$ derived from the projection makes the SNRs of the AEDs zero. Therefore, letting $\boldsymbol{\Theta} = \boldsymbol{\Psi}_{AE}\boldsymbol{\Psi}_{AE}^{T}$, i.e., $\mathbf{w} = \boldsymbol{\Theta}\mathbf{a}$, the optimization problem involving the vector $\mathbf{a}$ can be written as

$$\arg\max_{\mathbf{a}} \ \varphi\mathbf{a}^{T}\mathbf{H}_{U}^{\Theta}\mathbf{a} \tag{5.7a}$$

$$\text{s. t.} \begin{cases} \varphi\mathbf{a}^{T}\overline{\mathbf{H}}_{PE}^{\Theta}\mathbf{a} \preceq \overline{\rho}_{PE} \\ |\boldsymbol{\Theta}\mathbf{a}| \preceq \mathbb{1} \end{cases} \tag{5.7b}$$

where $\mathbf{H}_{U}^{\Theta} = \boldsymbol{\Theta}^{T}\mathbf{H}_{U}\boldsymbol{\Theta}$ and $\overline{\mathbf{H}}_{PE}^{\Theta} = \boldsymbol{\Theta}^{T}\overline{\mathbf{H}}_{PE}\boldsymbol{\Theta}$, and $\overline{\rho}_{PE}$ denotes the target constraint on the average SNR of a PED[1]. The Lagrangian for this problem is

$$\mathcal{L} = \varphi\mathbf{a}^{T}\mathbf{H}_{U}^{\Theta}\mathbf{a} - \lambda\left(\varphi\mathbf{a}^{T}\overline{\mathbf{H}}_{PE}^{\Theta}\mathbf{a} - \overline{\rho}_{PE}\right) + \mu_{-}^{T}(\boldsymbol{\Theta}\mathbf{a} + \mathbb{1}) - \mu_{+}^{T}(\boldsymbol{\Theta}\mathbf{a} - \mathbb{1}) \tag{5.8}$$

where $\lambda \in \mathbb{R}$ and $\mu_{-}, \mu_{+} \in \mathbb{R}^{N}$ are the Lagrange multipliers. For $\mathcal{L}$ to yield a non-trivial, analytic maximum with respect to $\mathbf{a}$, we assume the second constraint of (5.7b) is slack, i.e., any element of $\boldsymbol{\Theta}\mathbf{a}$ is strictly in between -1 and 1. Then, we have

$$\mu_{-} = \mu_{+} = \mathbb{0} \tag{5.9}$$

according to the local sensitivity analysis in [82]. The satisfaction of the condition stated in (5.9) depends upon $\overline{\rho}_{PE}$. If $\overline{\rho}_{PE}$ is small, no element of $\boldsymbol{\Theta}\mathbf{a}$ will reach ± 1, i.e., the second constraint is inactive.

[1]For PEDs distributed as a homogeneous PPP, considering the average SNR of a single PED $\overline{\gamma}_{PE}$ is identical to constraining the sum of the average SNRs of multiple PEDs since they obey the relation $\mathbb{E}_{\Phi_{PE}}\left[\sum_{l\in\Phi_{PE}}\gamma_{PE_l}\right] = \lambda_{PE}LW\overline{\gamma}_{PE}$ due to Campbell's theorem [75].

It is worth noting that $\overline{\rho}_{PE}$ is a system parameter to be appropriately chosen according to given VLC environments, such as a particular distribution of LED transmitters, the location of the UE, the LED transmit power, etc. For example, if $\overline{\rho}_{PE}$ is set too low, the LED transmitters should reduce the transmit power to satisfy the $\overline{\rho}_{PE}$ constraint, but the received signal power at the UE site would also be reduced in a commensurate manner. On the other hand, if the UE is located very close to one of the LED transmitters, the closest LED transmitter to the UE can increase its transmit power to increase the SNR of the UE while simultaneously satisfying the $\overline{\rho}_{PE}$ constraint. PLS theories suggest choosing the value of $\overline{\rho}_{PE}$ in a way that makes the SNR difference between the UE and the PEDs as large as possible [5].

Then, with assuming that (5.9) is satisfied, setting the partial derivative of $\mathcal{L}$ (with respect to $\mathbf{a}$) equal to zero leads to

$$\mathbf{H}_U^{\Theta}\mathbf{a} = \lambda\overline{\mathbf{H}}_{PE}^{\Theta}\mathbf{a}. \tag{5.10}$$

Here, $\overline{\mathbf{H}}_{PE}^{\Theta}$ is singular with rank less than or equal to $N - N_A$. Hence, we employ the inverse free preconditioned Krylov subspace projection method [29] to obtain the maximum eigenvalue $\lambda_{\max}$ and corresponding eigenvector $\mathbf{a}_{\max}$. In this method, an eigenvector estimate $\mathbf{a}_k$, where k denotes the iteration number, iteratively improves through the Rayleigh-Ritz projection onto the Krylov subspace

$$K_m\left(\mathbf{H}_U^{\Theta} - \rho_k\overline{\mathbf{H}}_{PE}^{\Theta}, \mathbf{a}_k\right) = \text{span}\left(\mathbf{a}_k, (\mathbf{H}_U^{\Theta} - \rho_k\overline{\mathbf{H}}_{PE}^{\Theta})\mathbf{a}_k, ..., (\mathbf{H}_U^{\Theta} - \rho_k\overline{\mathbf{H}}_{PE}^{\Theta})^m\mathbf{a}_k\right) \tag{5.11}$$

where $\rho_k = \mathbf{a}_k^T\mathbf{H}_U^{\Theta}\mathbf{a}_k / \mathbf{a}_k^T\overline{\mathbf{H}}_{PE}^{\Theta}\mathbf{a}_k$ denotes the Rayleigh quotient, and m is a parameter to be chosen. $\text{span}(\mathbf{v}_1, \mathbf{v}_2, ..., \mathbf{v}_N)$ denotes the set of all linear combinations of a collection of vectors $\mathbf{v}_1, \mathbf{v}_2, ..., \mathbf{v}_N$. In this chapter, we use the MATLAB program eigifp implemented in [110], which can carry out the whole procedure mentioned above by taking the two inputs, $\mathbf{H}_U^{\Theta}$ and $\overline{\mathbf{H}}_{PE}^{\Theta}$, and returning the maximum eigenvalue

Algorithm 3 CCP algorithms for solving (5.7)

given an initial feasible point $\mathbf{a}_0$
$k := 0$
repeat
1. *Convexify.* Form

$$g(\mathbf{a}; \mathbf{a}_k) \triangleq \varphi \mathbf{a}_k^T \mathbf{H}_U^\Theta \mathbf{a}_k + 2\varphi (\mathbf{H}_U^\Theta \mathbf{a}_k)^T (\mathbf{a} - \mathbf{a}_k)$$

2. *Solve.* Set the value of $\mathbf{a_{k+1}}$ to a solution of the convex problem

$$\arg\max_{\mathbf{a}} \; g(\mathbf{a}; \mathbf{a}_k) \tag{5.13a}$$

$$\text{s. t.} \begin{cases} \varphi \mathbf{a}^T \overline{\mathbf{H}}_{PE}^\Theta \mathbf{a} \le \overline{\rho}_{PE} \\ |\Theta \mathbf{a}| \preceq \mathbb{1} \end{cases} \tag{5.13b}$$

3. *Update iteration.* $k := k + 1$.

until stopping criterion is satisfied.

and corresponding eigenvector.

The solution of (5.10) satisfies

$$\rho_U = \varphi \mathbf{a}^T \mathbf{H}_U^\Theta \mathbf{a} = \varphi \lambda \mathbf{a}^T \overline{\mathbf{H}}_{PE}^\Theta \mathbf{a} \le \lambda_{\max} \overline{\rho}_{PE}. \tag{5.12}$$

Here, it is noted that the maximum SNR of the UE is proportional to $\lambda_{\max}$. Therefore, the optimal vector $\mathbf{a}^*$ can be obtained by scaling the eigenvector $\mathbf{a}_{\max}$ corresponding to $\lambda_{\max}$ such that $\varphi \mathbf{a}^{*T} \overline{\mathbf{H}}_{PE}^\Theta \mathbf{a}^* = \overline{\rho}_{PE}$. The optimal beamforming vector $\mathbf{w}^*$ is given by $\mathbf{w}^* = \Theta \mathbf{a}^*$. Lastly, the assumption that (5.9) is satisfied must be verified to confirm the feasibility of $\mathbf{w}^*$. If any element of $\mathbf{w}^*$ is strictly in between -1 and 1, (5.9) is satisfied; thus the acquired solution $\mathbf{w}^*$ is confirmed to be the optimal solution.

On the other hand, if this condition is *not* satisfied[2], the solution $\mathbf{a}^*$ can be numerically found with the concave-convex procedure (CCP) [26]. Given an initial feasible point $\mathbf{a}_0$, we transform the objective function (5.7a) into an affine function (i.e., convex) by applying the first-order Taylor approximation and solving the convex

[2]If any element of $\mathbf{w}^*$ obtained from the eigenmode of (5.10) is larger than 1 or less than -1, the second constraint in (5.7b) is not slack; (5.9) cannot be satisfied.

optimization problem by using a standard optimization programming method like the SQP algorithm [100]. Then, we set the solution to $\mathbf{a}_1$ and repeat the same procedure until the improvement in the objective value is less than some threshold ϵ. The detailed iterative algorithm is given in Algorithm 3.

5.2.2 Minimizing the Average SNR of Passive Eavesdroppers

We now investigate the problem of finding a ZF beamformer that minimizes the average SNR of the PEDs while satisfying the required SNR of the UE. Similar to the previous subsection, we can formulate the optimization problem in terms of $\mathbf{a}$:

$$\arg\min_{\mathbf{a}} \ \varphi \mathbf{a}^T \overline{\mathbf{H}}_{PE}^{\Theta} \mathbf{a} \tag{5.14a}$$

$$\text{s. t.} \begin{cases} \varphi \mathbf{a}^T \mathbf{H}_U^{\Theta} \mathbf{a} \geq \rho_U \\ |\Theta \mathbf{a}| \preceq \mathbb{1}. \end{cases} \tag{5.14b}$$

where ρ_U denotes the required SNR of the UE.

Following the same approach as above leads to an analogous result:

$$\mathbf{H}_U^{\Theta} \mathbf{a} = \eta \overline{\mathbf{H}}_{PE}^{\Theta} \mathbf{a} \tag{5.15}$$

where $\eta = 1/\lambda$. Similarly, the maximum eigenvalue $\eta_{\max}$ and corresponding eigenvector $\mathbf{a}_{\max}$ can be obtained through the inverse free preconditioned Krylov subspace projection method, and the solution satisfies

$$\overline{\gamma}_{PE} = \varphi \mathbf{a}^T \overline{\mathbf{H}}_{PE}^{\Theta} \mathbf{a} = \varphi \frac{1}{\eta} \mathbf{a}^T \mathbf{H}_U^{\Theta} \mathbf{a} \geq \frac{1}{\eta_{\max}} \rho_U. \tag{5.16}$$

From this, we deduce that the minimum $\overline{\gamma}_E$ is inversely proportional to the maximum eigenvalue of $\eta_{\max}$. Thus, the optimal vector $\mathbf{a}^*$ can be obtained by scaling the corresponding eigenvector $\mathbf{a}_{\max}$ such that $\varphi \mathbf{a}^{*T} \mathbf{H}_U^{\Theta} \mathbf{a}^* = \rho_U$. Finally, the optimal

beamforming vector $\mathbf{w}^*$ can be obtained as $\mathbf{w}^* = \boldsymbol{\Theta}\mathbf{a}^*$.

If the second constraint in (5.14b) is not slack, the optimal solution $\mathbf{a}^*$ should be solved by a numerical method similar to Algorithm 3, where the left term of the first constraint in (5.14b) needs to be transformed to an affine function (i.e., convex) by using a first-order Taylor approximation:

$$\varphi \mathbf{a}_k^T \mathbf{H}_U^{\Theta} \mathbf{a}_k + 2\varphi (\mathbf{H}_U^{\Theta} \mathbf{a}_k)^T (\mathbf{a} - \mathbf{a}_k). \tag{5.17}$$

We will verify the performances of the proposed ZF beamforming schemes in Section 5.4.

5.3 Relaxed Zero-Forcing Beamforming

In Section 5.2, we proposed a ZF beamforming scheme for suppressing the SNRs of the AEDs to zero, while simultaneously maximizing the SNR of the UE and constraining the average SNR of the PEDs. In that context, the ZF beamforming vector should always lie in the null space of the AEDs' channel matrix. However, this condition is sometimes so strict that it makes the ZF beamformer unable to cope with the PEDs effectively, especially when the number of LED transmitters is not high (i.e., the AED null space is small) or the UE is located at an unfavorable location, e.g., the middle of the LED transmitters. In these cases, the LED transmitters should considerably increase their information transmit power to allow an adequate received information power at the UE as well as simultaneously considering the AEDs. However, this will significantly expand the area in which the SNR is higher than at the UE, facilitating the PEDs to achieve a higher SNR than the UE. To resolve this situation, we devise an idea that more rigorously constraining the PEDs may be possible by relaxing the strict constraints on the AEDs of the ZF beamforming strategy.

Based on this idea, we propose an alternative approach, whose optimization goal

is to minimize the SOP caused by the PEDs while satisfying positive SNR constraints for the UE and the AEDs, respectively. The main characteristic of the alternative beamforming technique is that the constraints on the SNRs of the AEDs are relaxed, i.e., we let $\gamma_{AE_p} > 0$ to allow a larger subspace from which to choose feasible beamforming vectors. Thus, we call this strategy *relaxed ZF beamforming*.

Based on these design features, we formulate an optimization problem minimizing the SOP in (5.3):

$$\arg\min_{\mathbf{w}} \; 1 - \exp\left(-\iint_{\mathcal{A}} \lambda_{PE}\, \mathrm{d}\mathbf{x}\right) \tag{5.18a}$$

$$\text{s.t.} \begin{cases} \gamma_U \geq \rho_U \\ \gamma_{AE_p} \leq \rho_{AE}, \quad \forall p \in \{1, 2, ..., N_A\} \\ |\mathbf{w}| \preceq \mathbb{1} \end{cases} \tag{5.18b}$$

where the first and second constraints ensure that the SNRs of the UE and the AEDs satisfy the SNR requirement ρ_U and the SNR constraint ρ_{AE}, respectively. Without loss of generality, we assume that the same value of ρ_{AE} is set for all the AEDs. To guarantee the PLS of the VLC system, we let $\rho_U > \rho_{AE}$, which is consistent with assumption (a) in (5.3). Then, this optimization problem can be equivalently transformed to

$$\arg\min_{\mathbf{w}} \; |\mathcal{A}| \tag{5.19a}$$

$$\text{s.t.} \begin{cases} \gamma_U \geq \rho_U \\ \gamma_{AE_p} \leq \rho_{AE}, \quad \forall p \in \{1, 2, ..., N_A\} \\ |\mathbf{w}| \preceq \mathbb{1} \end{cases} \tag{5.19b}$$

where $|\mathcal{A}|$ denotes the area of the region $\mathcal{A}$.

Calculating $|\mathcal{A}|$ analytically is generally intractable. Hence, we employ an alternative approach by sampling the SNR space at points $\mathbf{x}_i \in \mathcal{X}$, where $\mathcal{X}$ signifies a set

of locations in the work plane of the room. An SNR surface according to the receiver locations like Figure 5.1 in VLC systems is generally continuous and smooth due to the properties of optical channels, which do not experience fading and largely depend on geometric factors related to indoor VLC environments [111]. Therefore, a small number of discrete points constituting $\mathcal{X}$ would be enough to describe the continuous SNR surface. This approach reduces computational complexity.

5.3.1 Sampling the SNR Space

First, we explain the practical procedure to generate the points $\mathbf{x}_i \in \mathcal{X}$ by utilizing Lloyd's algorithm [109]. The number and distribution of $\mathbf{x}_i$ affect the efficiency of the optimization; thus, carefully distributing the points is crucial. This is because the area that is likely to experience a high SNR is of primary interest, since the objective is to minimize the SOP by reducing the area $\mathcal{A}$ that retains the high SNR values. If most points are generated in the area in which the SNRs are low, the optimization problem cannot correctly recognize the high SNR region. Thus, we must sample the space more in the high SNR area.

Lloyd's method is an iterative algorithm that can be used to generate a centroidal Voronoi diagram. We can use the algorithm to generate the points $\mathbf{x}_i \in \mathcal{X}$ according to the SNR level. This can be achieved by replacing the density function for centroidal Voronoi diagrams with the SNR function $\gamma(\mathbf{x}, \mathbf{w})$ in (5.4). More specifically, Figure 5.3 shows a flow chart of the point generation procedure using the Lloyd method. Observing the figure, we first randomly generate a fixed number of points $\mathbf{x}_i$ in the work plane of the room. Then, we construct the Voronoi tessellation based on the sample points and calculate the centroid of each region in the tessellation using

$$\mathbf{C}_i = \frac{\int_{\mathcal{A}_{\mathbf{x}_i}} \mathbf{x}\, \gamma(\mathbf{x}, \mathbf{w})\, \mathrm{d}\mathcal{A}_{\mathbf{x}_i}}{\int_{\mathcal{A}_{\mathbf{x}_i}} \gamma(\mathbf{x}, \mathbf{w})\, \mathrm{d}\mathcal{A}_{\mathbf{x}_i}} \tag{5.20}$$

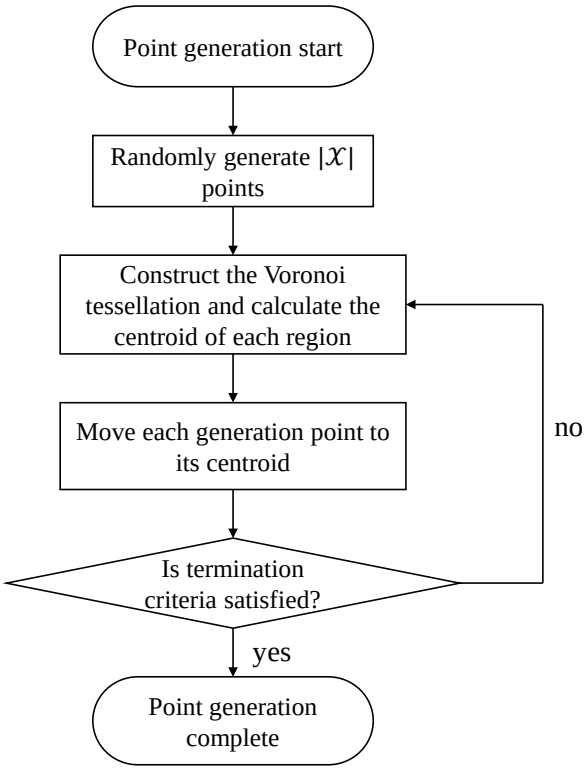


Figure 5.3. A flow chart of the point generation procedure using the Lloyd algorithm.

where $\mathcal{A}_{\mathbf{x}_i}$ denotes the tile region for the generated point $\mathbf{x}_i$. Next, we move each point $\mathbf{x}_i$ to its centroid $\mathbf{C}_i$ and then reconstruct the Voronoi tessellation and so on. The algorithm proceeds iteratively until a termination criterion is satisfied, e.g., the maximum distance moved in any region in an iteration falls below a certain threshold. Figure 5.4 shows the generated points (black dots) belonging to $\mathcal{X}$ that result from the proposed algorithm. Note that the points are densely and evenly distributed in the higher SNR area as intended.

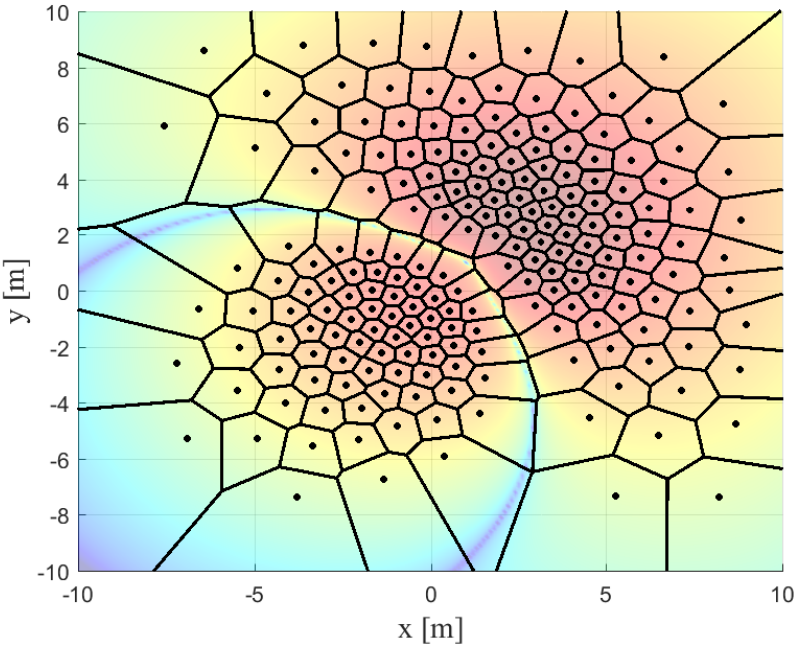


Figure 5.4. The points obtained using Lloyd's algorithm with $|\mathcal{X}| = 200$. $\gamma(\mathbf{x}, \mathbf{w})$ for Figure 5.1(a) is adopted.

5.3.2 Optimizing Over the Sampled Space

Returning to the problem described in (5.19), by using the points $\mathbf{x}_i$ generated by Lloyd's method, we can re-express (5.19) as

$$\arg\min_{\mathbf{w}} \sum_{\mathbf{x}_i \in \mathcal{X}} \max\{\gamma(\mathbf{x}_i, \mathbf{w}) - \gamma_U, 0\} \tag{5.21a}$$

$$\text{s. t.} \begin{cases} \gamma_U \geq \rho_U \\ \gamma_{AE_p} \leq \rho_{AE}, \quad \forall p \in \{1, 2, ..., N_A\} \\ \overline{\gamma}_{PE} \leq \overline{\rho}_{PE} \\ |\mathbf{w}| \preceq \mathbb{1}. \end{cases} \tag{5.21b}$$

Note that since the objective function in (5.21a) decreases when $\gamma(\mathbf{x}_i, \mathbf{w})$ is less than γ_U, the optimization problem aims to find the beamformer that makes the number of points $\mathbf{x_i}$ that retain a higher SNR than γ_U as few as possible, which naturally reduces $|\mathcal{A}|$ to make it as small as possible. In addition, although it can be seen

that the SNRs of PEDs are already taken into account in the objective function, we add the third constraint in (5.21b). This constraint restricts the average SNR of the PEDs $\overline{\gamma}_{PE}$ to $\overline{\rho}_{PE}$ in order to prevent the area far from the UE, where $\mathbf{x}_i$ may not exist, from retaining a very high SNR.

To deal with the function $\max\{\cdot\}$ in the objective, (5.21) can be equivalently transformed with an auxiliary variable t_i for $i \in \{1, 2, ..., |\mathcal{X}|\}$ to yield the problem

$$\arg\min_{\mathbf{w}, t_i \forall i} \sum_i t_i \tag{5.22a}$$

$$\text{s. t.} \begin{cases} t_i \geq \gamma(\mathbf{x}_i, \mathbf{w}) - \gamma_U, \quad \forall i \in \{1, 2, ..., |\mathcal{X}|\} \\ t_i \geq 0, \quad \forall i \in \{1, 2, ..., |\mathcal{X}|\} \\ \gamma_U \geq \rho_U \\ \gamma_{AE_p} \leq \rho_{AE}, \quad \forall p \in \{1, 2, ..., N_A\} \\ \overline{\gamma}_{PE} \leq \overline{\rho}_{PE} \\ |\mathbf{w}| \preceq \mathbb{1}. \end{cases} \tag{5.22b}$$

Substituting (5.2) into (5.22), the problem can be written as

$$\arg\min_{\mathbf{w}, t_i \forall i} \sum_i t_i \tag{5.23a}$$

$$\text{s. t.} \begin{cases} t_i \geq \gamma(\mathbf{x}_i, \mathbf{w}) - \varphi \mathbf{w}^T \mathbf{H}_U \mathbf{w}, \quad \forall i \in \{1, 2, ..., |\mathcal{X}|\} \\ t_i \geq 0, \quad \forall i \in \{1, 2, ..., |\mathcal{X}|\} \\ \varphi \mathbf{w}^T \mathbf{H}_U \mathbf{w} \geq \rho_U \\ \varphi \mathbf{w}^T \mathbf{H}_{AE_p} \mathbf{w} \leq \rho_{AE}, \quad \forall p \in \{1, 2, ..., N_A\} \\ \varphi \mathbf{w}^T \overline{\mathbf{H}}_{PE} \mathbf{w} \leq \overline{\rho}_{PE} \\ |\mathbf{w}| \preceq \mathbb{1}. \end{cases} \tag{5.23b}$$

Here, the difficulty of solving (5.23) arises from the fact that the second term on the right side of the first constraint and the left side of the third constraint yield non-

Algorithm 4 CCP algorithms for solving (5.23)

given initial feasible points $\mathbf{w}_0$ and $t_{i,0}$ $\forall i$, $k := 0$
Generate $\mathbf{x}_i \in \mathcal{X}$ by using Lloyd's method based on $\gamma(\mathbf{x}, \mathbf{w_0})$

repeat
Convexify. Form

$$g(\mathbf{w}; \mathbf{w}_k) \triangleq \varphi \mathbf{w}_k^T \mathbf{H}_U \mathbf{w}_k + 2\varphi(\mathbf{H}_U \mathbf{w}_k)^T(\mathbf{w} - \mathbf{w}_k) \tag{5.24}$$

Solve. Set the values of $\mathbf{w}_{k+1}$ and $t_{i,k+1}$ $\forall i$ to solutions of the convex problem

$$\min_{\mathbf{w}, t_i \forall i} \sum_i t_i \tag{5.25}$$

$$\text{s. t.} \begin{cases} t_i \geq \gamma(\mathbf{x}_i, \mathbf{w}) - g(\mathbf{w}; \mathbf{w}_k), \ \forall i \in \{1, 2, ..., |\mathcal{X}|\} \\ t_i \geq 0, \quad \forall i \in \{1, 2, ..., |\mathcal{X}|\} \\ g(\mathbf{w}; \mathbf{w}_k) \geq \rho_U \\ \varphi \mathbf{w}^T \mathbf{H}_{AE_p} \mathbf{w} \leq \rho_{AE}, \ \forall p \in \{1, 2, ..., N_A\} \\ \varphi \mathbf{w}^T \overline{\mathbf{H}}_{PE} \mathbf{w} \leq \overline{\rho}_{PE} \\ |\mathbf{w}| \preceq \mathbb{1}. \end{cases} \tag{5.26}$$

Update iteration. $k := k + 1$.
until stopping criterion is satisfied.

convex sets. Thus, once again, we apply the CCP approach [26]. Given initial feasible points $\mathbf{w}_0, t_{i,0}$ $\forall i$, we transform the non-convex functions into affine functions by calculating the first-order Taylor approximations. We then solve the convex optimization problem. Next, we set the solutions to $\mathbf{w}_1, t_{i,1}$ $\forall i$, and repeat the same procedure until the improvement in the objective value is less than a predefined threshold ϵ. The details of this iterative algorithm are given in Algorithm 4. Since the CCP works in a heuristic manner, the final solution depends on the initial points $\mathbf{w}_0, t_{i,0}$ $\forall i$. Therefore, it is wise to start the algorithm with several initial points and take as the final choice, denoted by $\mathbf{w}^*, t_i^*$ $\forall i$, that minimizes the objective function.

On the other hand, it is worth mentioning that the CCP has features and advantages that it takes an initial point that significantly affects the final point and that it can retain more information in each of the iterates than other heuristic algorithms since the CCP reserves the information from all the convex components

Table 5.1. Simulation parameters.

Room configuration	
Length (L) × Width (W)	20×20 m^2
Height from the work plane (H)	2.2 m
Number of LEDs per fixture	16
LED electrical and optical characteristics	
Average optical power per LED	0.5 W
Current-to-light conversion efficiency η	5 W/A
Nominal half-intensity angle $\phi_{1/2}$	60°
Modulation index α	0.4
Optical receiver characteristics	
Photodetector's responsivity $R_{\text{rsp.}}$	0.54 mA/mW
Photodetector's physical area A_{PD}	1 cm^2
Lens refractive index κ_k	1.5
Noise power σ^2	−98.33 dBm
Field of View Ψ_c	90°
Transimpedance amplifier gain T	50 V/A

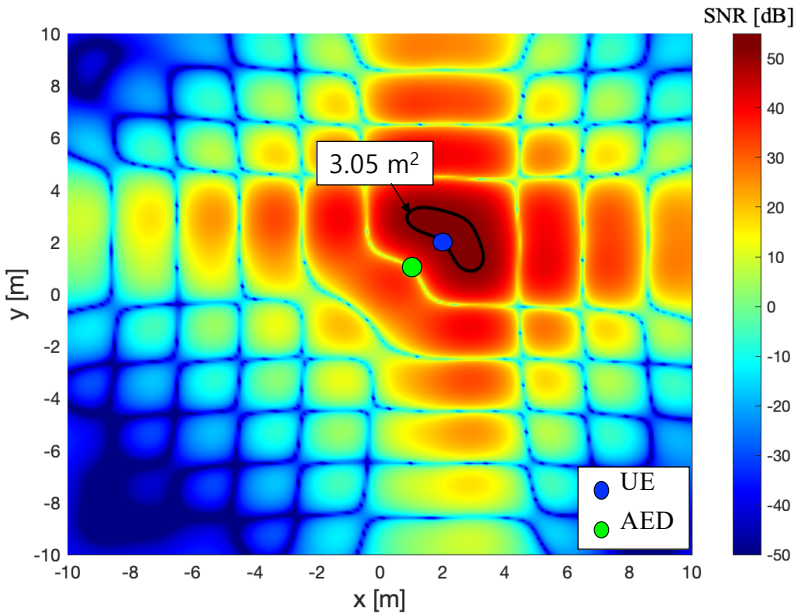
and only linearizes the concave portions [26]. In other words, if the CCP takes an initial point that is feasible and seems close to the optimal point, it is likely to yield a moderately near-optimal performance. In this sense, using the ZF beamforming vector obtained from (5.7) to generate the initial point $\mathbf{w}_0$ is a practical approach, since the ZF beamformer can initially satisfy the conditions of (5.23) for reasonable values of ρ_U, ρ_{AE}, and $\overline{\rho}_{PE}$ and seems close to the optimal point. With this initial point, the optimization procedure (5.23) gradually changes the ZF beamforming vector into the optimal beamformer $\mathbf{w}^*$ of the relaxed ZF beamforming method as the CCP algorithm iterates, thus minimizing the area that the SNR is higher than that of the UE while satisfying all the requirements for the UE, AED, and PED as stated in the constraints.

5.4 Numerical Results

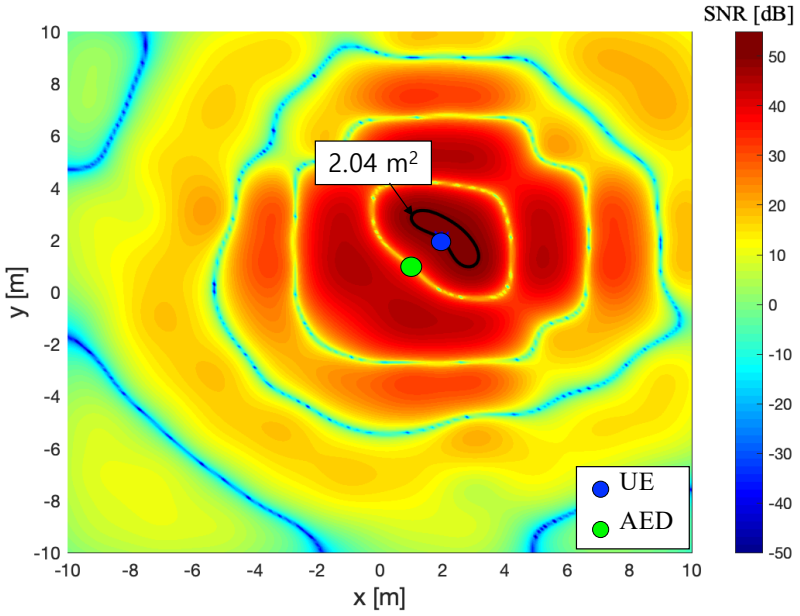
In this section, numerical results are provided to verify the performances of the proposed ZF beamforming and relaxed ZF beamforming schemes. The room configura-

tion and simulation parameters are given in Table 5.1. Here, we utilize the characteristics of the LED transmitters and receivers employed in [10], which considered a typical office room and common lightening devices. In addition, emitted light is assumed to be "warm-white," i.e., color temperature is between 2700 and 3000 K, with luminous efficiency 284 lm/W [85, Table 3.2]. In addition, emitted light is assumed to be "warm-white," i.e., color temperature is between 2700 and 3000 K, with luminous efficiency 284 lm/W [85, Table 3.2]. Based on this assumption, we adjust the number of light fixtures and the number of LEDs per fixture such that the considered LED arrangement satisfies the lighting standards, e.g., from 400 to l000 lx for a typical office [86]. The 10×10 transmitter array consists of LEDs that are uniformly distributed on a square lattice in a 20×20 m^2 room. The locations of the LED transmitters are given by $(x_T, y_T, 2.2)$, where $x_T,\ y_T \in \{\pm 1, \pm 3, \pm 5, \pm 7, \pm 9\}$. According to the Lumen method [87], the considered configuration yields the light level of 410 lx in the room.

Figures 5.5(a) and (b) show the SNR values according to receiver locations when the proposed ZF beamforming and the relaxed ZF beamforming strategies are adopted. Also, the SNRs corresponding to traditional ZF beamforming [11] are given in Figure 5.1. For all of these results, the UE and the AED are located at $(2, 2)$ and $(1, 1)$, which are marked by blue and green markers, respectively. Also, the black contours denote the areas in which the SNR is higher than that of the UE. To aid presentation, the figures show the SNR down to -50 dB, although the SNRs at the AED sites with the traditional ZF beamforming and proposed ZF beamforming schemes are less than this value. The figures show that the contour areas with the proposed ZF beamforming and the relaxed ZF beamforming schemes are 3.05 m^2 and 2.04 m^2, respectively, which are much smaller than that of the traditional ZF beamforming (7.9 m^2). These results verify that the proposed two ZF beamforming schemes can reduce the area in which the PEDs can achieve a higher SNR than the UE while suppressing the SNR of the AED to zero, or at least smaller than the constraint ρ_{AE}



(a) The ZF beamforming of (5.7).



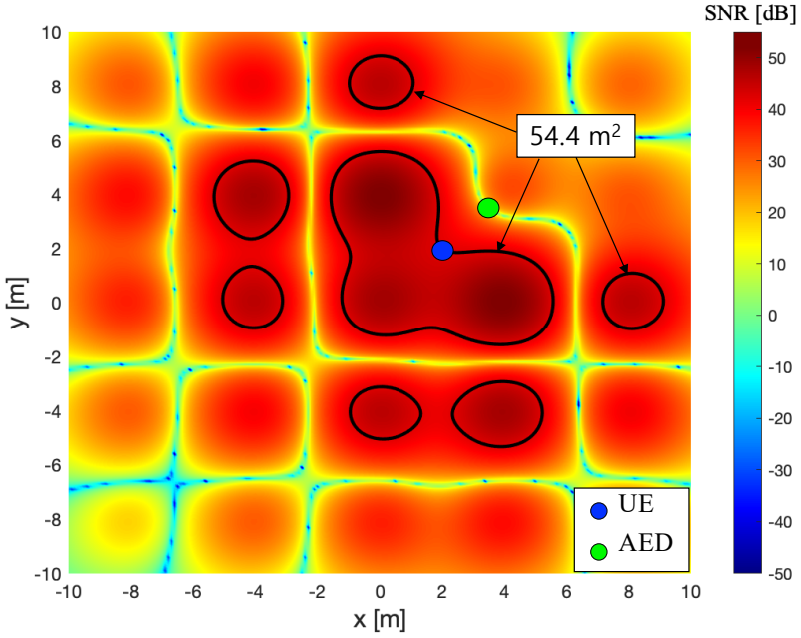
(b) The relaxed ZF beamforming of (5.18).

Figure 5.5. The SNR according to the receiver locations. The 10×10 LEDs are uniformly distributed on a square lattice. The locations of the UE and the AED are $(2, 2)$ and $(1, 1)$, respectively. $\rho_U = 50$ dB, $\rho_{AE} = 10$ dB, $\overline{\rho}_{PE} = 35$ dB, and $|\mathcal{X}| = 100$ are used.

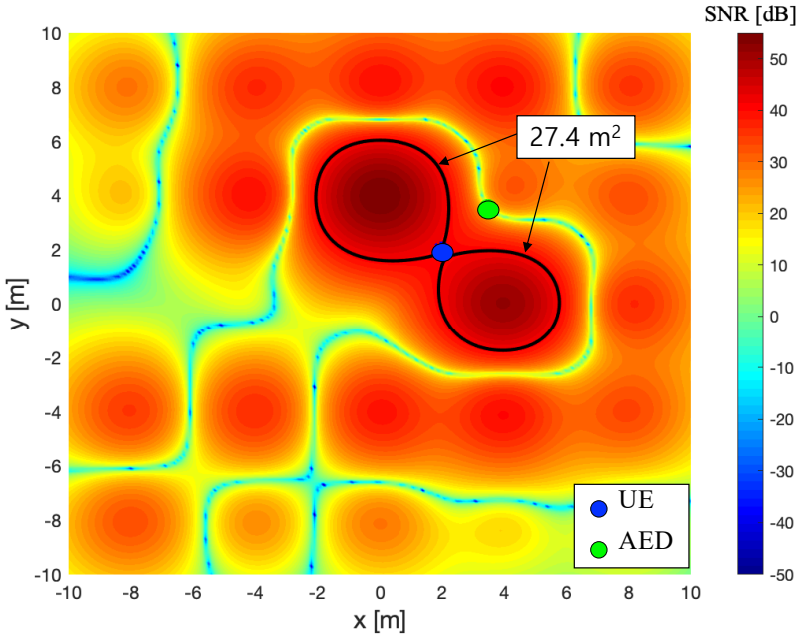
in the relaxed case. On the other hand, it is observed that the contour area with the relaxed ZF beamforming in Figure 5.5(b) is slightly smaller than that corresponding to the ZF beamforming method shown in Figure 5.5(a). As discussed in Section 5.3, by relaxing the constraint on the SNR of the AED, i.e., from $\rho_{AE} = 0$ to $\rho_{AE} = 10$ dB, the relaxed ZF beamformer can make the contour area smaller than that of the ZF beamforming, accordingly reducing the likelihood of a secrecy outage occuring.

Figures 5.6(a) and (b) more clearly show the performance difference between the ZF beamforming and the relaxed beamforming schemes. Here, a smaller number of LEDs, i.e., $N = 5 \times 5$, are located at $(x_T, y_T, 2.2)$, where $x_T, y_T \in \{0, \pm 4, \pm 8\}$. Also, the UE is located at $(2, 2)$, i.e., the center of four LED transmitters, which is an unfavorable location from the secrecy perspective. Indeed, since the channel gain in (2.1) largely depends on the distance between the LED and the receiver, the LED transmitters should sufficiently increase the transmit power by adjusting their beamforming weights up to ± 1 in order to ensure a high SNR at the UE site. However, the increased transmit power would also raise the possibility of being wiretapped by EDs. Also, the condition that the SNR of the AED must be zero in the ZF beamforming scheme reduces the size of the subspace that the beamforming vector can lie within. Therefore, as seen in Fig 5.6(a), the ZF beamforming scheme yields an extensive contour area (54.4 m^2) for this unfavorable secrecy environment, which would result in a high SOP. In contrast, as shown in Figure 5.6(b), the relaxed ZF beamforming can somewhat resolve this problem by relaxing the constraint on the SNR of the AED from $\rho_{AE} = 0$ to $\rho_{AE} = 10$ dB and reduce the contour area to 27.4 m^2, which is much smaller than that obtained by ZF beamforming.

Figures 5.7(a) and (b) show the SNRs according to the receiver locations when two AEDs are present. Even for multiple AEDs, it is noted that the ZF beamforming scheme in Figure 5.7(a) can suppress the SNRs of the two AEDs to zero by aligning the beamforming vectors with the null space of AEDs' channel matrix while maximizing

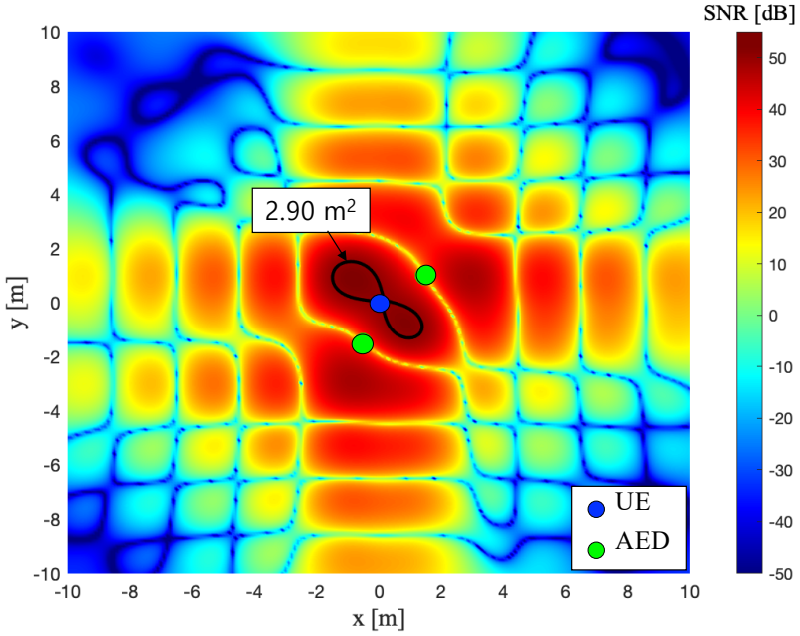


(a) The ZF beamforming of (5.7).

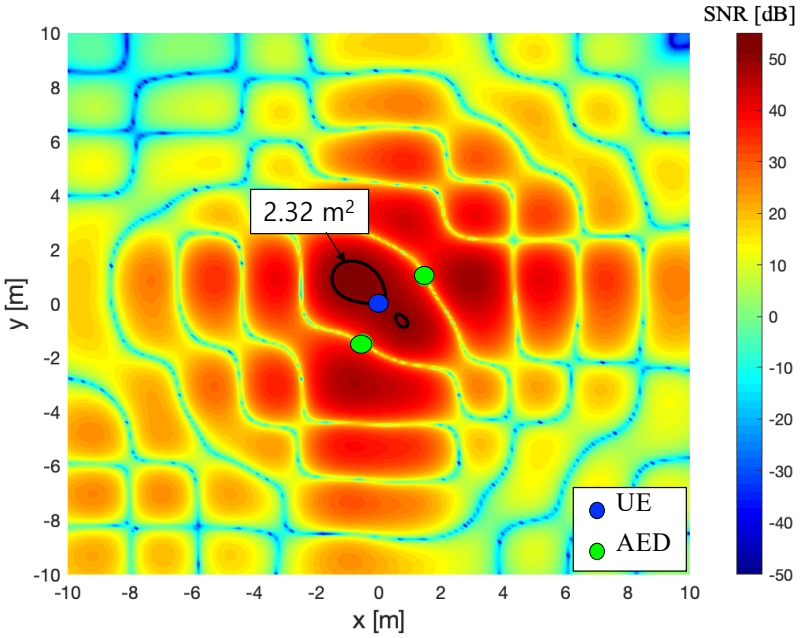


(b) The relaxed ZF beamforming of (5.18).

Figure 5.6. The SNR according to the receiver locations when a smaller number of LEDs, i.e., $N = 5 \times 5$, are present. The locations of the UE and the AED are $(2, 2)$ and $(3.5, 3.5)$, respectively. $\rho_U = 40$ dB, $\rho_{AE} = 10$ dB, $\overline{\rho}_{PE} = 35$ dB, and $|\mathcal{X}| = 100$ are used.



(a) The ZF beamforming of (5.7).



(b) The relaxed ZF beamforming of (5.18).

Figure 5.7. The SNR according to the receiver locations when two AEDs are present. The 10×10 LEDs are uniformly distributed on a square lattice. The locations of the UE and the two AEDs are $(0, 0)$, $(1, 1.5)$, and, $(-1.5, -0.5)$ respectively. $\rho_U = 50$ dB, $\rho_{AE} = 10$ dB, $\overline{\rho}_{PE} = 35$ dB, and $|\mathcal{X}| = 100$ are used.

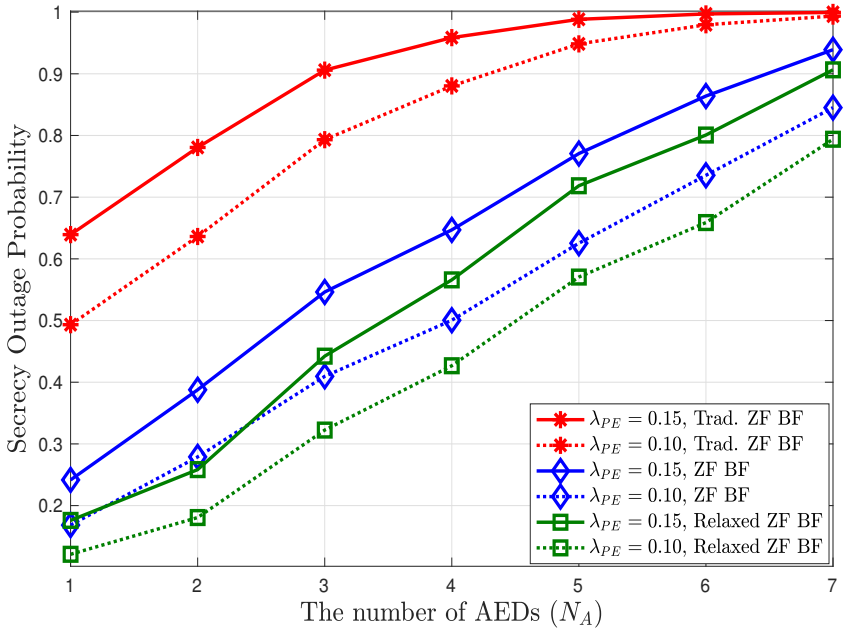


Figure 5.8. The SOP plotted as a function of the number of AEDs N_A. The location of the UE is $(0, 0)$, while N_A AEDs are randomly located in a circle with radius 3 m centered at the UE. For ZF beamforming, $\overline{\rho}_{PE} = 25$ dB is used. For relaxed ZF beamforming, ρ_U is set to be similar to the maximum ρ_U obtained by ZF beamforming for each simulation trial, and $\rho_{AE} = 10$ dB, $\overline{\rho}_{PE} = 25$ dB, and $|\mathcal{X}| = 100$ are used.

the SNR of the UE. Similarly, the relaxed ZF beamforming scheme restricts the SNRs of the multiple AEDs to lower than $\rho_{AE} = 10$ dB while minimizing the contour area in which the PEDs can cause a secrecy outage.

Figure 5.8 shows the SOP obtained by Monte Carlo simulation with 10^4 trials for different densities of PEDs λ_{PE} when different numbers of AEDs N_A are randomly located around the UE. The UE is located at $(0, 0)$, and N_A AEDs are randomly located within a circle with radius 3 m centered at the UE. Also, the SOP corresponding to traditional ZF beamforming [11] is provided as a benchmark. Since [11] considered a single AED, we adopt the ZF beamforming vector $\mathbf{w} = g\boldsymbol{\Psi}_{AE}\boldsymbol{\Psi}_{AE}^T\mathbf{h}_U$ as in [78] to manage multiple AEDs. The figure shows that the proposed ZF and relaxed ZF beamforming schemes yield much lower SOPs than traditional ZF beamforming. By taking the presence of PEDs into account in designing the beamforming vector

optimization, the proposed two schemes effectively prevent the unknown PEDs from retaining a higher SNR than the UE, which results in lower SOPs. Moreover, the relaxed beamforming scheme is shown to yield lower SOPs than the proposed ZF scheme regardless of the number of AEDs, verifying that the relaxed ZF beamforming can deal with PEDs better than the proposed ZF beamforming. On the other hand, for all the beamforming schemes, it is noted that the SOP increases as N_A increases. For the proposed ZF beamforming, this is because the rank of the null space of the AEDs' channel matrix decreases as more AEDs exist; thus, the subspace that the optimal beamforming vector of (5.7) maximizing the UE's SNR can lie within also shrinks. Hence, the maximum SNR of the UE achieved by the optimal beamformer is limited, which yields a more extensive contour area resulting in a higher SOP. Besides, for the relaxed ZF beamforming approach, a larger number of AEDs impose additional constraints to the optimization problem (5.18), which contracts the possible vector space for the achievable ZF beamformers minimizing the contour area.

Figure 5.9 shows the SOPs obtained by Monte Carlo simulation with 10^4 trials according to different radii of the circle in which two AEDs are randomly located. The circle is centered at the UE, which is located at $(0, 0)$. It is shown that the proposed ZF and relaxed ZF beamforming methods yield lower SOPs than traditional ZF over all investigated parameters. This result verifies that traditional ZF aims only to lower the AEDs' SNRs without consideration for PEDs; thus, the SOPs with the traditional ZF beamforming approach are shown to be high, especially when the AEDs are likely to be close to the UE. On the other hand, the proposed beamforming schemes can effectively reduce the area in which the SNR is higher than the UE, which results in a lower SOP and suppresses the SNRs of the AEDs.

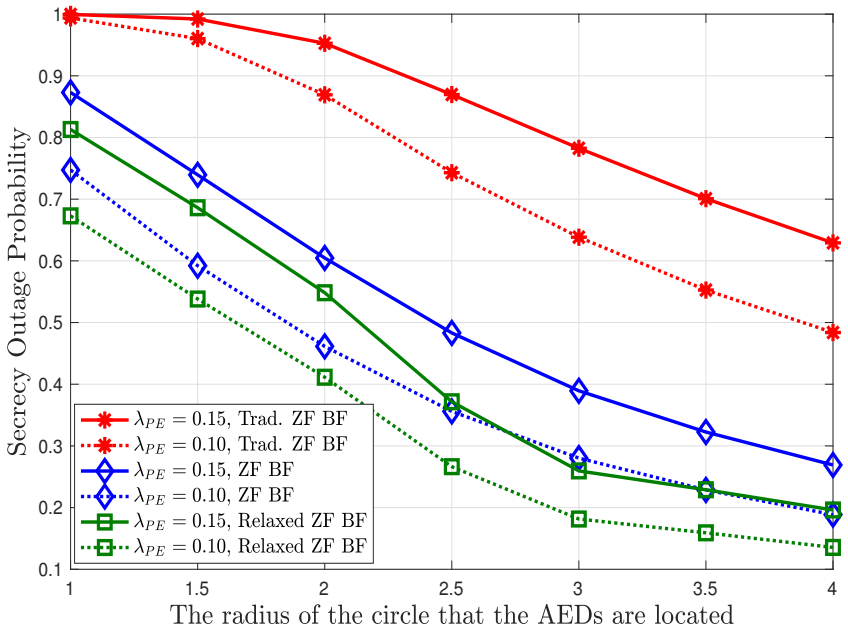


Figure 5.9. The SOP plotted as a function of the radius of the circle in which two AEDs are randomly located. The location of the UE is $(0, 0)$, and the circle is centered at the UE. For ZF beamforming, $\overline{\rho}_{PE} = 25$ dB is used. For relaxed ZF beamforming, ρ_U is set to be similar to the maximum ρ_U obtained by ZF beamforming for each simulation trial, and $\rho_{AE} = 10$ dB, $\overline{\rho}_{PE} = 25$ dB, and $|\mathcal{X}| = 100$ are used.

5.5 Summary

This chapter proposed ZF beamforming schemes for secure VLC systems. Unlike traditional beamforming schemes, which can cope with either AEDs or PEDs, but not both, the proposed ZF beamforming and relaxed ZF beamforming schemes can secure VLC transmissions against AEDs and PEDs simultaneously. With the ZF beamforming scheme, we can design a beamforming vector that lies in the null space of the AEDs' channel matrix, so that the SNRs of AEDs can be completely suppressed in theory while maximizing the SNR of the UE. On the other hand, the relaxed ZF beamforming approach is capable of taking the possible existence of PEDs into account, relaxing the constraint on the SNRs of the AEDs. To reduce the complexity of the relaxed approach, Lloyd's algorithm was used to sample the SNR space, and it was shown through numerical experiments that the new ZF beamforming methods

significantly outperform the traditional approach. Given that both PEDs and AEDs may be present in reality, it can be concluded that the proposed beamforming schemes provide practical approaches for engineering secure VLC systems.

Chapter 6

Conclusion

6.1 Thesis Summary

In this thesis, we proposed three MISO beamforming and jamming strategies for VLC systems in the presence of randomly located EDs. Unlike existing VLC PLS schemes, which require the knowledge of the locations or CSI of the passive EDs, our proposed PLS techniques need only statistical information on the passive ED locations, which can be effectively obtained by analyzing the user behavior characteristics and the layout of the room. Stochastic geometry tools, BPP and PPP, were utilized to model the random locations of passive EDs and measure the average secrecy performance metrics, such as the average secrecy capacity and the secrecy outage probability.

More specifically, in **Chapter 3**, the first MISO beamforming strategy was proposed. The optimization problem was formulated to determine the optimal beamformer that can minimize the average SNR of passive EDs and maximize the SNR of the UE. Then, an LED selection scheme, less complicated than beamforming, was proposed, and the SOP under the selection scheme was analytically studied. Although the LED selection scheme is not superior to the beamformer, LED selection could provide a practical way of enhancing the security of VLC systems by lowering

computational complexity.

In **Chapter 4**, we proposed a joint strategy of beamforming and jamming to cope with a realistic scenario in which the ED, equipped with a high-quality receiver architecture, tries to wiretap information signals. As in the first beamforming scheme, this joint scheme was also feasible without the knowledge of the location and CSI of the ED. First, the optimization problem for the beamforming and jamming vectors that maximize the SINR of a UE while suppressing the SINR of an ED was formulated, and then solved by employing the heuristic method called the CCP. Then, to alleviate the high computational complexity of the joint scheme, a simpler version, called the ternary scheme, was designed; we adopted the TS method to solve the related assignment optimization problem. In addition, we investigated the problem of maximizing the average secrecy rate by utilizing a continuous LED model. The numerical and simulation results proved that these proposed schemes could secure the VLC systems effectively, even in the presence of an ED with receiver front-end specifications that are much better than those of the UE.

In the following, **Chapter 5** proposed new ZF beamforming techniques to cope with active and passive EDs simultaneously. Given that both PEDs and AEDs may be present in reality, this novel ZF scheme, designed to combat any type of ED, could be regarded as a more practical approach for engineering secure VLC systems. The proposed ZF beamforming scheme lays the optimal beamformer in the null space of the AEDs' channel matrix so that the SNRs of AEDs can be entirely suppressed in theory, while maximizing the SNR of the UE. Also, we developed the relaxed ZF beamforming approach, which is capable of flexibly taking the possible existence of PEDs into account, while relaxing the constraint on the SNRs of the AEDs.

The analyses and methodologies presented in the thesis provide useful insights and analytic tools that can be used to increase security in VLC systems, and provide a solid basis for further study.

6.2 Future Directions

In this thesis, we have proposed and studied three MISO beamforming and jamming schemes, which are practical in that they do not require knowledge of the EDs' exact locations. However, in order to more effectively and practically secure the VLC systems, there still exist a few challenges that we have to take into account. In this section, we present some vulnerabilities of PLS in VLC systems and briefly provide some potential (although not perfect) solutions, with a view to stimulating discourse in the research community.

6.2.1 Enhanced Jamming

Our three proposed PLS transmission schemes, as well as other existing PLS techniques for VLC systems, have assumed that an ED behaves similarly to the UE when communicating with the LED transmitters; for example, the ED would receive all the optical signals emitted from the LEDs within the ED's FoV. With this assumption, beamforming and jamming strategies are designed to create a destructive superposition of information signals and cause interference at the ED site, thereby allowing only a low signal reception there. However, EDs in VLC systems can avoid beamforming and jamming interference due to two intrinsic properties of VLC systems. The first is that the multiple LED transmitters must be spatially distributed to illuminate the entire room evenly within the lighting standards, and the second is that the channel gain in VLC systems largely depends on the distance between the transmitter and the receiver. These two properties lead the beamforming and jamming strategies to perform in a way that the LEDs near to the intended user emit the information, while the distant LEDs are silent or emit the jamming signals, as we discussed in the previous chapters. In other words, unlike RF systems, the ED anticipates which LED performs as either an information transmitter or a jammer, and selectively receives

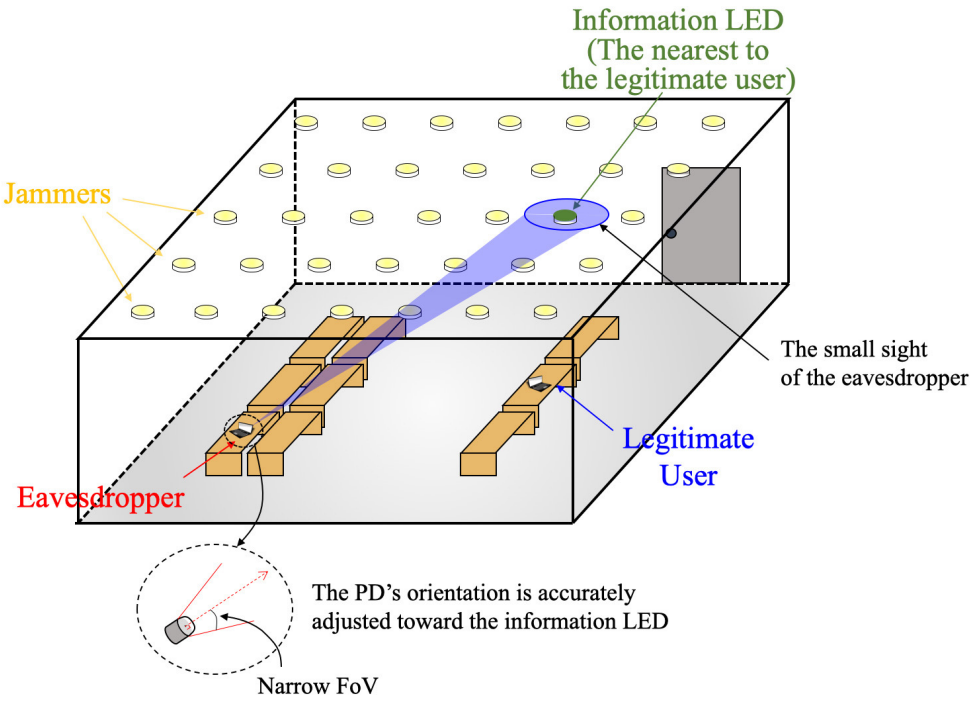


Figure 6.1. An example of VLC systems with a jamming strategy, where the ED is equipped with a narrow FoV PD, oriented directly toward the information LED transmitter.

only the information signal by narrowing the receiver FoV and accurately aligning the receiver's orientation toward the target LED transmitter, as depicted in Figure 6.1.

In order to combat such augmented EDs, jamming is still an advantageous approach since the EDs, even with powerful receiver architectures, cannot extract only the information component from the received signal in the presence of randomized jamming signals. In contrast, jamming signals can be designed such that they lie in the null space of the UE's channel and therefore do not disturb information reception. As a result, improving the traditional and proposed jamming strategies, to transmit both the information and jamming signals at very closely located LEDs or by randomly choosing the information transmitter and jammers, disregarding the location of the UE, is also a possible strategy.

The first approach can be further improved by forcing both information and jamming signals to be emitted from a single LED by splitting its transmitting power into two components. However, this would sacrifice the SINR of the UE. Besides, with

the latter approach, i.e., transmitter hopping, the information reception at the UE may be weakened due to the increase in the distances from the information LEDs; thus, appropriate beamforming strategies with multiple LEDs should supplement the signal strength at the UE. In addition, in order to allow even the LED transmitters close to the UE to emit the jamming components as well as the information signals, optimizing the jamming intensity vector (as defined in **Chapter 4**) along the eigenmode related to the null space of the UE channel and the average channel of the random EDs to maximize the degree of interference at EDs' sites would be a possible approach.

6.2.2 Reduced Complexity

In this thesis, we proposed PLS transmission techniques along with an attempt to reduce the computational complexity by employing various approximation and simplification methods. However, in practice, some of these need to reduce the computational complexity to serve multiple VLC users at required transmission rates and latencies. Thus, as a universal solution, it would be interesting to study how the quantization of beamforming vectors in practice would reduce the computational complexity while maintaining secrecy performance as similar as possible to the unquantized case. This quantization study would require building a proper mechanism to find the optimal quantized solution and finding an optimal quantization level to minimize the secrecy performance sacrificed. Besides, the quantization approach can be further improved and simplified by tailoring the beamforming codebook design devised for RF systems [112, 113] to VLC systems. In this method, the transmitters can reduce complexity and overhead by evaluating a limited number of codewords chosen from a pre-defined codebook. Because the channel gain in VLC systems largely depends on the distance between the transmitter and receiver, it would be possible to create an efficient beamforming codebook enhancing VLC systems' security based on the

geometric factors of VLC systems.

In addition, the PLS techniques would be required more for large open spaces, such as libraries, open-plan offices, conference halls, etc., since these large spaces would provide the EDs with more opportunities for concealment. Also, one of the important advantages of VLC is the provision of dense spatial re-use, which would be wanted more in a situation in which many concurrent users exist, i.e., large open spaces. In such rooms, there also would be a large number of LED transmitters evenly distributed to illuminate the entire room and serve many users at the same time. On the other hand, a large number of LED transmitters and receivers would accompany many beamforming optimization variables as well, resulting in high computation complexity in optimizing the beamforming and jamming vectors. In order to alleviate the complexity, it would be worthwhile considering strategies that sectorize the large room into several small areas and make only the LED transmitters in each sector participate in the PLS beamforming transmission to serve a particular user being located in the corresponding sector. This idea is based on the characteristic of VLC that the channel gain largely depends on the distance between the LED transmitter and the receiver; thus, far-off LED transmitters cannot significantly impact users in other sectors. Developing this mechanism would require an investigation of how to optimally sectorize a room and minimize interference and information leakage between sectors.

6.3 Conclusions

This thesis investigated the PLS techniques for VLC systems, proposing and developing new three beamforming and jamming strategies that do not require the knowledge of locations of EDs. In terms of their practicalities, simplicities, and performances, we believe that these proposed methods can present a feasible resolution to enhance

VLC systems' secrecy at the physical layer.

However, it is worth mentioning that VLC still faces various challenges in order to be implemented and commercialized in practice, such as mobility support, narrow modulation bandwidth, full-directional communication, etc. [114]. Thus, VLC needs continuous improvements and modifications in transceiver hardware and communication techniques. Undoubtedly, its security environments and conditions will also change, which would necessitate PLS technologies of VLC to react to the advancements of VLC. For example, a VLC system that uses only the LoS channel may suffer from the likelihood of blockage by, e.g., the human body and office partitions, which may cause severe fluctuations in the received SNR. Consequently, to provide consumers with a seamless communication service, VLC may need to utilize an optical signal reflected by a wall and window. This would require a significant modification of mathematical models and optimization approaches for designing PLS techniques to reflect the actual channel characteristics. With the continuous development of VLC systems, the existing PLS technologies, even those proposed in this thesis, will have to be improved and modified to keep face with VLC technology's advancement.

In addition, VLC is viewed as a complementary technology to other RF wireless communication technologies, such as Wi-Fi, mobile networks, mmWave communications, etc., rather than a replacement of the role of RF. Hence, both technologies are likely to be combined in a single device to meet the demand for future wireless applications. In this sense, the combination of VLC and RF may significantly enhance secrecy performances by exploiting the inherently different characteristics of RF and VLC channels. More specifically, VLC may promise a very high secrecy capacity when employing an appropriate transmission scheme, while it is entirely subject to a favorable location of a UE concerning an ED. On the other hand, regardless of the receiver locations, RF may not ensure a required secrecy capacity in indoor environments due to shadowing and multipath fading, while it can facilitate uncorrelated

transmissions. Utilizing the intrinsically different VLC and RF channels may enable finding an optimal solution that can always provide consumers with an adequate secrecy performance. For example, based on a given communication configuration, it would be possible to alternatively make an optimal choice between transmitting a secrecy key by using a keyless PLS scheme of VLC and generating and distributing a secret key by utilizing the distinct channel characteristics of the transmitter's and UE's reciprocal RF channel.

Security, in the real world, is a never-ending cycle between attacker and defender. Consequently, we cannot conclude that the VLC can be entirely secured by PLS methods, even by the proposed schemes in this thesis. However, we believe that the analyses and methodologies presented in the thesis will be an essential starting point to facilitate the security model and design for future VLC networks.

Bibliography

[1] P. Yang, Y. Xiao, M. Xiao, and S. Li, "6G wireless communications: Vision and potential techniques," *IEEE Netw.*, vol. 33, pp. 70–75, July 2019.

[2] Z. Zhang, Y. Xiao, Z. Ma, M. Xiao, Z. Ding, X. Lei, G. K. Karagiannidis, and P. Fan, "6G wireless networks: Vision, requirements, architecture, and key technologies," *IEEE Trans. Veh. Technol.*, vol. 14, pp. 28–41, Sep. 2019.

[3] L. U. Khan, "Visible light communication: Applications, architecture, standardization and research challenges," *Digital Commun. Netw.*, vol. 3, no. 2, pp. 78 – 88, 2017.

[4] H. Haas, L. Yin, Y. Wang, and C. Chen, "What is LiFi?," *J. Lightw. Technol.*, vol. 34, pp. 1533–1544, Mar. 2016.

[5] M. Bloch and J. Barros, *Physical-Layer Security: From Information Theory to Security Engineering.* New York, NY, USA: Cambridge University Press, 1st ed., 2011.

[6] A. D. Wyner, "The wire-tap channel," *Bell Syst. Tech. J.*, vol. 54, pp. 1355–1387, Jan. 1975.

[7] D. W. K. Ng, E. S. Lo, and R. Schober, "Robust beamforming for secure communication in systems with wireless information and power transfer," *IEEE Trans. Wireless Commun.*, vol. 13, pp. 4599–4615, Aug. 2014.

[8] G. Chen, J. P. Coon, and M. D. Renzo, "Secrecy outage analysis for downlink transmissions in the presence of randomly located eavesdroppers," *IEEE Trans. Inf. Forens. Security*, vol. 12, pp. 1195–1206, May 2017.

[9] J. Zhu, R. Schober, and V. K. Bhargava, "Linear precoding of data and artificial noise in secure massive MIMO systems," *IEEE Trans. Wireless Commun.*, vol. 15, pp. 2245–2261, Mar. 2016.

[10] A. Mostafa and L. Lampe, "Physical-layer security for MISO visible light communication channels," *IEEE J. Sel. Areas Commun.*, vol. 33, pp. 1806–1818, Sep. 2015.

[11] A. Mostafa and L. Lampe, "Physical-layer security for indoor visible light communications," in *IEEE ICC in Sydney, Australia*, pp. 3342–3347, June 2014.

[12] A. Mostafa and L. Lampe, "Securing visible light communications via friendly jamming," in *IEEE Globecom Workshops in Austin, USA*, pp. 524–529, Dec. 2014.

[13] A. Mostafa and L. Lampe, "Pattern synthesis of massive LED arrays for secure visible light communication links," in *IEEE ICCW in London, U.K.*, pp. 1350–1355, June 2015.

[14] A. Mostafa and L. Lampe, "Optimal and robust beamforming for secure transmission in MISO visible-light communication links," *IEEE Trans. Signal Process.*, vol. 64, pp. 6501–6516, Dec. 2016.

[15] H. Zaid, Z. Rezki, A. Chaaban, and M. S. Alouini, "Improved achievable secrecy rate of visible light communication with cooperative jamming," in *IEEE GlobalSIP in Orlando, U.S.A.*, pp. 1165–1169, Dec. 2015.

[16] M. A. Arfaoui, Z. Rezki, A. Ghrayeb, and M. S. Alouini, "On the secrecy capacity of MISO visible light communication channels," in *IEEE Globecom in Washington D.C., USA*, pp. 1–7, Dec. 2016.

[17] T. V. Pham and A. T. Pham, "On the secrecy sum-rate of MU-VLC broadcast systems with confidential messages," in *2016 CSNDSP in Prague, Czech Republic*, pp. 1–6, July 2016.

[18] T. V. Pham, T. Hayashi, and A. T. Pham, "Artificial-noise-aided precoding design for multi-user visible light communication channels," *IEEE Access*, vol. 7, pp. 3767–3777, 2019.

[19] M. Haenggi, "The secrecy graph and some of its properties," in *IEEE ISIT in Toronto, Canada*, pp. 539–543, July 2008.

[20] P. C. Pinto, J. Barros, and M. Z. Win, "Physical-layer security in stochastic wireless networks," in *IEEE ICCS in Guangzhou, China*, Nov. 2008.

[21] X. Zhou, R. K. Ganti, J. G. Andrews, and A. Hjorungnes, "On the throughput cost of physical layer security in decentralized wireless networks," *IEEE Trans. Wireless Commun.*, vol. 10, pp. 2764–2775, Aug. 2011.

[22] G. Geraci, S. Singh, J. G. Andrews, J. Yuan, and I. B. Collings, "Secrecy rates in broadcast channels with confidential messages and external eavesdroppers," *IEEE Trans. Wireless Commun.*, vol. 13, pp. 2931–2943, May 2014.

[23] T. X. Zheng, H. M. Wang, and Q. Yin, "On transmission secrecy outage of a multi-antenna system with randomly located eavesdroppers," *IEEE Commun. Lett.*, vol. 18, pp. 1299–1302, Aug. 2014.

[24] S. Cho, G. Chen, and J. P. Coon, "Securing visible light communication systems by beamforming in the presence of randomly distributed eavesdroppers," *IEEE Trans. Wireless Commun.*, vol. 17, pp. 2918–2931, May 2018.

[25] S. Cho, G. Chen, and J. P. Coon, "Secrecy analysis in visible light communication systems with randomly located eavesdroppers," in *IEEE ICC Workshops in Paris, France*, pp. 475–480, May 2017.

[26] T. Lipp and S. Boyd, "Variations and extension of the convex–concave procedure," *Optimization and Engineering*, vol. 17, pp. 263–287, June 2016.

[27] S. Cho, G. Chen, and J. P. Coon, "Enhancement of physical layer security with simultaneous beamforming and jamming for visible light communication systems," *IEEE Trans. Inf. Forens. Security*, vol. 14, pp. 2633–2648, Oct. 2019.

[28] S. Cho, G. Chen, and J. P. Coon, "Securing visible light communications with spatial jamming," in *IEEE ICC in Shanghai, China*, pp. 1–6, May 2019.

[29] G. H. Golub and Q. Ye, "An inverse free preconditioned Krylov subspace method for symmetric generalized eigenvalue problems," *SIAM J. Sci. Comput.*, vol. 24, no. 1, pp. 312–334, 2002.

[30] S. Cho, G. Chen, and J. P. Coon, "Zero-forcing beamforming for active and passive eavesdropper mitigation in visible light communication systems," *IEEE Trans. Inf. Forens. Security*, vol. 16, pp. 1495–1505, 2021.

[31] S. Cho, G. Chen, and J. P. Coon, "Enhancing security in VLC systems through beamforming," in *IEEE GLOBECOM in Taipei, Taiwan*, pp. 1–6, Dec. 2020.

[32] L. E. M. Matheus, A. B. Vieira, L. F. M. Vieira, M. A. M. Vieira, and O. Gnawali, "Visible light communication: Concepts, applications and challenges," *IEEE Commun. Surveys Tuts.*, vol. 21, no. 4, pp. 3204–3237, 2019.

[33] A. Jovicic, J. Li, and T. Richardson, "Visible light communication: opportunities, challenges and the path to market," *IEEE Commun. Mag.*, vol. 51, no. 12, pp. 26–32, 2013.

[34] A. T. Hussein and J. M. H. Elmirghani, "Mobile multi-gigabit visible light communication system in realistic indoor environment," *J. Lightw. Technol.*, vol. 33, pp. 3293–3307, Aug. 2015.

[35] D. Karunatilaka, F. Zafar, V. Kalavally, and R. Parthiban, "LED based indoor visible light communications: State of the art," *IEEE Commun. Surveys Tuts.*, vol. 17, no. 3, pp. 1649–1678, 2015.

[36] "IEEE standard for local and metropolitan area networks–part 15.7: Short-range optical wireless communications," *IEEE Std 802.15.7-2018 (Revision of IEEE Std 802.15.7-2011)*, pp. 1–407, 2019.

[37] A. M. Khalid, G. Cossu, R. Corsini, P. Choudhury, and E. Ciaramella, "1-Gb/s transmission over a phosphorescent white LED by using rate-adaptive discrete multitone modulation," *IEEE Photon. J.*, vol. 4, no. 5, pp. 1465–1473, 2012.

[38] M. S. Islim, R. X. Ferreira, X. He, E. Xie, S. Videv, S. Viola, S. Watson, N. Bamiedakis, R. V. Penty, I. H. White, A. E. Kelly, E. Gu, H. Haas, and M. D. Dawson, "Towards 10 gb/s orthogonal frequency division multiplexing-based visible light communication using a GaN violet micro-LED," *Photon. Res.*, vol. 5, pp. A35–A43, Apr. 2017.

[39] L. Zeng, D. C. O'Brien, H. L. Minh, G. E. Faulkner, K. Lee, D. Jung, Y. Oh, and E. T. Won, "High data rate multiple input multiple output (MIMO) optical wireless communications using white led lighting," *IEEE J. Sel. Areas Commun.*, vol. 27, pp. 1654–1662, Dec. 2009.

[40] H. L. Minh, D. O'Brien, G. Faulkner, L. Zeng, K. Lee, D. Jung, Y. Oh, and E. T. Won, "100-Mb/s NRZ visible light communications using a postequalized white LED," *IEEE Photon. Technol. Lett.*, vol. 21, pp. 1063–1065, Aug. 2009.

[41] A. H. Azhar, T. A. Tran, and D. O'Brien, "A gigabit/s indoor wireless transmission using MIMO-OFDM visible-light communications," *IEEE Photon. Technol. Lett.*, vol. 25, pp. 171–174, Jan. 2013.

[42] D. Tsonev, H. Chun, S. Rajbhandari, J. J. D. McKendry, S. Videv, E. Gu, M. Haji, S. Watson, A. E. Kelly, G. Faulkner, M. D. Dawson, H. Haas, and D. O'Brien, "A 3-Gb/s single-LED OFDM-based wireless VLC link using a gallium nitride μled," *IEEE Photon. Technol. Lett.*, vol. 26, pp. 637–640, Apr. 2014.

[43] Q. Wang, Z. Wang, and L. Dai, "Multiuser MIMO-OFDM for visible light communications," *IEEE Photon. J.*, vol. 7, pp. 1–11, Dec. 2015.

[44] S. Dimitrov, S. Sinanovic, and H. Haas, "Clipping noise in ofdm-based optical wireless communication systems," *IEEE Trans. Commun.*, vol. 60, pp. 1072–1081, Apr. 2012.

[45] H. Burchardt, N. Serafimovski, D. Tsonev, S. Videv, and H. Haas, "Vlc: Beyond point-to-point communication," *IEEE Commun. Mag.*, vol. 52, no. 7, pp. 98–105, 2014.

[46] S. Shao, A. Khreishah, M. B. Rahaim, H. Elgala, M. Ayyash, T. D. C. Little, and J. Wu, "An indoor hybrid WiFi-VLC internet access system," in *IEEE MASS in Philadelphia, USA*, pp. 569–574, Oct. 2014.

[47] X. Li, R. Zhang, and L. Hanzo, "Cooperative load balancing in hybrid visible light communications and WiFi," *IEEE Trans. Commun.*, vol. 63, pp. 1319–1329, Apr. 2015.

[48] T. Rakia, H. C. Yang, F. Gebali, and M. S. Alouini, "Optimal design of dual-hop VLC/RF communication system with energy harvesting," *IEEE Commun. Lett.*, vol. 20, pp. 1979–1982, Oct. 2016.

[49] P. Hu, P. H. Pathak, A. K. Das, Z. Yang, and P. Mohapatra, "PLiFi: Hybrid WiFi-VLC networking using power lines," in *ACM Workshop on VLCS in New York City, NY, USA*, pp. 31–36, 2016.

[50] S. Schmid, L. Arquint, and T. R. Gross, "Using smartphones as continuous receivers in a visible light communication system," in *ACM Workshop on VLCS in New York City, NY, USA*, pp. 61–66, 2016.

[51] A. T. Hussein and J. M. H. Elmirghani, "Mobile Multi-Gigabit Visible Light Communication System in Realistic Indoor Environment," *J. Lightw. Technol.*, vol. 33, no. 15, pp. 3293–3307, 2015.

[52] D. Tsonev, S. Videv, and H. Haas, "Light fidelity (Li-Fi): towards all-optical networking," in *SPIE OPTO in San Francisco, CA, USA*, vol. 9007, pp. 1 – 10, 2014.

[53] T. Komine and M. Nakagawa, "Fundamental analysis for visible-light communication system using LED lights," *IEEE Trans. Consum. Electron*, vol. 50, pp. 100–107, Feb. 2004.

[54] H. Elgala, R. Mesleh, and H. Haas, "Predistortion in optical wireless transmission using OFDM," in *IEEE HIS in Shenyang, China*, vol. 2, pp. 184–189, 2009.

[55] C. E. Shannon, "A mathematical theory of communication," *Bell Syst. Tech. J.*, vol. 27, pp. 379–423, 1948.

[56] J. G. Smith, *On the Information Capacity of Peak and Average Power Constrained Gaussian Channels*. Ph.D. dissertation, Department of Electrical Engineering, University of California, Berkeley, California, 1969.

[57] J. G. Smith, "The information capacity of amplitude- and variance-constrained scalar gaussian channels," *J. of Inf. Control*, vol. 18, pp. 203–219, 1971.

[58] A. Lapidoth, S. Moser, and M. Wigger, "On the capacity of free-space optical intensity channels," *IEEE Trans. Inf. Theory*, vol. 55, no. 10, pp. 4449–4461, Oct. 2009.

[59] A. D. Wyner, "The wire-tap channel," *Bell Syst. Tech. J.*, vol. 54, pp. 1355–1387, Jan. 1975.

[60] Y. Liang, H. V. Poor, and S. Shamai (Shitz), "Information theoretic security," *Found. Trends Commun. Inf. Theory*, vol. 5, Apr. 2009.

[61] L. Wang, N. Yang, M. Elkashlan, P. L. Yeoh, and J. Yuan, "Physical layer security of maximal ratio combining in two-wave with diffuse power fading channels," *IEEE Trans. Inf. Forens. Security*, vol. 9, pp. 247–258, Feb. 2014.

[62] T. Zheng, H. Wang, and Q. Yin, "On transmission secrecy outage of a multi-antenna system with randomly located eavesdroppers," *IEEE Commun. Letters*, vol. 18, no. 8, pp. 1299–1302, 2014.

[63] M. Ghogho and A. Swami, "Physical-layer secrecy of mimo communications in the presence of a poisson random field of eavesdroppers," in *IEEE ICC Workshops in Kyoto, Japan*, pp. 1–5, 2011.

[64] G. Chen, Y. Gong, P. Xiao, and J. A. Chambers, "Dual antenna selection in secure cognitive radio networks," *IEEE Trans. Veh. Technol.*, vol. 65, pp. 7993–8002, Oct. 2016.

[65] T. Zheng, H. Wang, J. Yuan, D. Towsley, and M. H. Lee, "Multi-antenna transmission with artificial noise against randomly distributed eavesdroppers," *IEEE Trans. Commun.*, vol. 63, no. 11, pp. 4347–4362, 2015.

[66] J. Yang, I. Kim, and D. I. Kim, "Optimal cooperative jamming for multiuser broadcast channel with multiple eavesdroppers," *IEEE Trans. Wireless Commun.*, vol. 12, pp. 2840–2852, June 2013.

[67] J. Wang, H. Ge, M. Lin, J. Wang, J. Dai, and M. Alouini, "On the secrecy rate of spatial modulation-based indoor visible light communications," *IEEE J. Sel. Areas Commun*, vol. 37, no. 9, pp. 2087–2101, 2019.

[68] M. A. Arfaoui, A. Ghrayeb, and C. M. Assi, "Secrecy performance of multi-user MISO VLC broadcast channels with confidential messages," *IEEE Trans. Wireless Commun.*, vol. 17, pp. 7789–7800, Nov. 2018.

[69] O. Ozel, E. Ekrem, and S. Ulukus, "Gaussian wiretap channel with an amplitude constraint," in *IEEE ITW in Lausanne, Switzerland*, Sep. 2012.

[70] Z. Rezki and M. Alouini, "Secret-key agreement with public discussion over multi-antenna transmitters with amplitude constraints," in *IEEE ISIT*, pp. 1534–1538, Jun. 2017.

[71] F. Baccelli and B. Błaszczyszyn, "Stochastic geometry and wireless networks: Volume i theory," *Foundations and Trends in Networking*, vol. 3, no. 3–4, pp. 249–449, 2010.

[72] F. Baccelli and B. Błaszczyszyn, "Stochastic geometry and wireless networks: Volume ii applications," *Foundations and Trends in Networking*, vol. 3, no. 3–4, pp. 249–449, 2010.

[73] H. ElSawy, E. Hossain, and M. Haenggi, "Stochastic geometry for modeling, analysis, and design of multi-tier and cognitive cellular wireless networks: A survey," *IEEE Commun. Surveys Tuts.*, vol. 15, pp. 996–1019, Third 2013.

[74] A. Baddeley, *Spatial Point Processes and their Applications*, vol. 1892, pp. 1–75. Springer, 2007.

[75] S. N. Chiu, D. Stoyan, W. S. Kendall, and J. Mecke, *Stochastic geometry and its applications; 3rd ed.* Wiley Series in Probability and Statistics, Hoboken, NJ: Wiley, 2013.

[76] J. G. Andrews, S. Buzzi, W. Choi, S. V. Hanly, A. Lozano, A. C. K. Soong, and J. C. Zhang, "What will 5G be?," *IEEE J. Sel. Areas Commun.*, vol. 32, pp. 1065–1082, June 2014.

[77] C. Chen, D. Basnayaka, and H. Haas, "Downlink SINR statistics in OFDM-based optical attocell networks with a poisson point process network model," in *IEEE GLOBECOM in San Diego, USA*, pp. 1–6, Dec. 2015.

[78] A. Khisti and G. W. Wornell, "Secure transmission with multiple antennas I: The MISOME wiretap channel," *IEEE Trans. Inf. Theory*, vol. 56, pp. 3088–3104, July 2010.

[79] S. M. Moser, M. Mylonakis, L. Wang, and M. Wigger, "Asymptotic capacity results for MIMO wireless optical communication," in *IEEE ISIT*, pp. 536–540, Jun. 2017.

[80] I. Krikidis, J. S. Thompson, and S. Mclaughlin, "Relay selection for secure cooperative networks with jamming," *IEEE Trans. Wireless Commun.*, vol. 8, pp. 5003–5011, Oct. 2009.

[81] H. Hui, A. L. Swindlehurst, G. Li, and J. Liang, "Secure relay and jammer selection for physical layer security," *IEEE Signal Process. Lett.*, vol. 22, pp. 1147–1151, Aug. 2015.

[82] S. Boyd and L. Vandenberghe, *Convex Optimization*. New York, NY, USA: Cambridge University Press, 2004.

[83] J. Grubor, S. Randel, K. D. Langer, and J. W. Walewski, "Bandwidth-efficient indoor optical wireless communications with white light-emitting diodes," in *CSNDSP in Graz, Austria*, pp. 165–169, Jul. 2008.

[84] I. S. Gradshteyn and I. M. Ryzhik, *Table of integrals, series, and products*. Elsevier/Academic Press, seventh ed., 2007.

[85] R. Lenk and C. Lenk, *Practical Lighting Design with LEDs*. Wiley, 2011.

[86] *Lighting of Indoor Work Places,* European Stand. EN 12464-1, 2003.

[87] M. Rea and I. E. S. of North America, *The IESNA Lighting Handbook: Reference & Application*. Illuminating Engineering Society of North America, 2000.

[88] D. Tse and P. Viswanath, *Fundamentals of Wireless Communication*. New York, NY, USA: Cambridge University Press, 2005.

[89] E. Wong, *Active-Set Methods for Quadratic Programming*. PhD thesis, Department of Mathematics, University of California, San Diego, June 2011.

[90] A. Baddeley, E. Rubak, and R. Turner, *Spatial point patterns: methodology and applications with* R. CRC Press, 2015.

[91] I. Marin-Garcia, V. Guerra, and R. Perez-Jimenez, "Study and Validation of Eavesdropping Scenarios over a Visible Light Communication Channel," *Sensors*, vol. 17, no. 12, p. 2687, 2017.

[92] H. Shen, Y. Deng, W. Xu, and C. Zhao, "Secrecy-oriented transmitter optimization for visible light communication systems," *IEEE Photon. J*, vol. 8, no. 5, 2016.

[93] P. C. Pinto, J. Barros, and M. Z. Win, "Secure communication in stochastic wireless networks—Part I: Connectivity," *IEEE Trans. Inf. Forens. Security*, vol. 7, pp. 125–138, Feb. 2012.

[94] A. Lapidoth, S. M. Moser, and M. A. Wigger, "On the capacity of free-space optical intensity channels," *IEEE Trans. Inf. Theory*, vol. 55, pp. 4449–4461, Oct. 2009.

[95] J. Wang, C. Liu, J. Wanga, Y. Wu, M. Lin, and J. Cheng, "Physical-layer security for indoor visible light communications: Secrecy capacity analysis," *IEEE Trans. Commun.*, pp. 1–1, 2018.

[96] H. Wang, X. Zhou, and M. C. Reed, "Physical layer security in cellular networks: A stochastic geometry approach," *IEEE Trans. Wireless Commun.*, vol. 12, no. 6, pp. 2776–2787, 2013.

[97] G. Pan, J. Ye, and Z. Ding, "On secure VLC systems with spatially random terminals," *IEEE Commun. Lett.*, vol. PP, no. 99, pp. 1–1, 2016.

[98] I. Csiszar and J. Korner, "Broadcast channels with confidential messages," *IEEE Trans. Inf. Theory*, vol. 24, no. 3, pp. 339–348, 1978.

[99] A. Charnes and W. W. Cooper, "Programming with linear fractional functionals," *Naval Research Logistics Quarterly*, vol. 9, no. 3-4, pp. 181–186, 1962.

[100] P. T. Boggs and J. W. Tolle, "Sequential quadratic programming," *Acta Numerica*, vol. 4, pp. 1–51, 1995.

[101] F. Glover and M. Laguna, *Tabu Search*. Norwell, MA, USA: Kluwer Academic Publishers, 1997.

[102] C. Blum and A. Roli, "Metaheuristics in combinatorial optimization: Overview and conceptual comparison," *ACM Comput. Surv.*, vol. 35, p. 268–308, Sept. 2003.

[103] M. R. Garey and D. S. Johnson, *Computers and Intractability; A Guide to the Theory of NP-Completeness*. New York, NY, USA: W. H. Freeman & Co., 1990.

[104] "Preface," in *Nature-Inspired Optimization Algorithms* (X.-S. Yang, ed.), pp. xi – xii, Oxford: Elsevier, 2014.

[105] H. Chun, C. Chiang, and D. C. O'Brien, "Visible light communication using OLEDs: Illumination and channel modeling," in *2012 IWOW in Pisa, Italy*, pp. 1–3, 2012.

[106] S. Cho, G. Chen, and J. P. Coon, "Physical layer security in visible light communication systems with randomly located colluding eavesdroppers," *IEEE Wireless Commun. Lett.*, vol. 7, pp. 768–771, Oct. 2018.

[107] M. Bloch, J. Barros, M. R. D. Rodrigues, and S. W. McLaughlin, "Wireless information-theoretic security," *IEEE Trans. Inf. Theory*, vol. 54, pp. 2515–2534, June 2008.

[108] T. V. Pham, H. Le-Minh, and A. T. Pham, "Multi-user visible light communication broadcast channels with zero-forcing precoding," *IEEE Trans. Commun.*, vol. 65, pp. 2509–2521, June 2017.

[109] A. Okabe, B. Boots, and K. Sugihara, *Spatial Tessellations: Concepts and Applications of Voronoi Diagrams*. New York, NY, USA: John Wiley & Sons, Inc., 1992.

[110] J. Money and Q. Ye, "Algorithm 845: EIGIFP: a MATLAB program for solving large symmetric generalized eigenvalue problems," *ACM Trans. Math. Softw.*, vol. 31, pp. 270–279, 01 2005.

[111] J. M. Kahn and J. R. Barry, "Wireless infrared communications," *Proceedings of the IEEE*, vol. 85, pp. 265–298, Feb. 1997.

[112] Pengfei Xia and G. B. Giannakis, "Design and analysis of transmit-beamforming based on limited-rate feedback," *IEEE Trans. Signal Process.*, vol. 54, no. 5, pp. 1853–1863, 2006.

[113] S. Kutty and D. Sen, "Beamforming for millimeter wave communications: An inclusive survey," *IEEE Commun. Surveys Tuts.*, vol. 18, no. 2, pp. 949–973, 2016.

[114] M. A. Arfaoui, M. D. Soltani, I. Tavakkolnia, A. Ghrayeb, M. Safari, C. Assi, and H. Haas, "Physical layer security for visible light communication systems: A survey," *IEEE Commun. Surveys Tuts.*, pp. 1–1, 2020.